Real-time Awareness and Fast Reconfiguration Capabilities for Agile Optical Networks

Atiyah Sayyidah Ahsan

ABSTRACT

Real-time Awareness and Fast Reconfiguration Capabilities
for Agile Optical Networks

Atiyah Sayyidah Ahsan

Ever-growing demand for speed and bandwidth coupled with increasing energy consumption in current networks are driving the need for intelligent, next-generation networking architectures that can overcome fundamental spectral and energy limitations. Metro-only internet traffic in particular is experiencing unprecedented growth rates and increasing twice as fast as long-haul traffic. The current quasi-static peak capacity provisioned network is ill-equipped to support this rise of unpredictable, high bandwidth but short-duration traffic flows.

A promising solution to address the emerging networking challenges is agile optical networking. Agile optical networking leverages novel photonic devices and multi-layer switching capabilities along with network awareness and intelligence to allocate resources in accordance to changing traffic demands and network conditions. However, *network agility requires changing the wavelength configuration in the optical layer in real-time to match the traffic demands.* Rapidly changing the wavelength loading conditions in optical amplifiers result in debilitating power fluctuations that propagate through the network and can lead to network instability, a problem that is avoided in current networks by using long reconfiguration times encompassing many small adjustments.

An agile optical network, once successfully implemented, will be characterized by unpredictable transmission impairments. Power levels along any path in an agile network is constantly fluctuating due to the continuously changing wavelength configuration; consequently, power dependent transmission impairments are also constantly fluctuating. *Real-time knowledge of the state of the physical layer is thus critical for managing signal quality and reliability in an agile optical network, requiring the development of cost-effective, energy-efficient monitoring solutions that can support advanced*

modulation formats.

This dissertation focuses on developing solutions for the two key requirements for a stable agile optical network. Techniques that allow wavelength reconfiguration on the order of seconds while maintaining stable network operation and minimal data loss are presented. Functionality of an existing advanced optical performance monitor is extended to include autonomous monitoring of both single and multiple channel systems, so that it can be used in agile optical network for real-time introspection of the physical layer.

Contents

List of Figures

Glossary

AGC	Automatic Gain Controlled
ARPANET	Advanced Research Projects Agency Network
ASE	Amplified Spontaneous Emission
AWG	Arbitrary Waveform Generator
BER	Bit Error Rate
BV	Bandwidth Variable
CAGR	Compound Annual Growth Rate
CD	Chromatic Dispersion
CDC	Cloud Data Center
CW	Continuous Wavelength
DAC	Digital-to-Analog Converter
DD-QPSK	Double Differential Quadrature Phase Shift Keying
DLI	Delay-Line-Interferometer
DPSK	Differential Phase Shift Keying
DSB	Double Side Band
DTR	Dwell Time Ratio
EDFA	Erbium Doped Fiber Amplifier
FC	Filter Concatenation
FEC	Forward Error Correction
FWM	Four Wave Mixing
ICT	Information and Communication Technology
IFFT	Inverse Fast Fourier Transform
IMDD	Intensity Modulation and Direct Detection

IP	Internet Protocol
ISI	Inter Symbol Interference
ITU	International Telecommunication Union
MCM	Multi Carrier Modulation
MZM	Mach-Zehnder Modulator
OFDM	Orthogonal Frequency Division Multiplexing
OSA	Optical Spectrum Analyser
OSNR	Optical-Signal-to-Noise-Ratio
PDL	Polarization Dependent Loss
PL	Physical Layer
PLI	Physical Layer Impairments
PMD	Polarization Mode Dispersion
PT	Pilot Tone
QoT	Quality of Transmission
QPSK	Quadrature Phase Shift Keying
ROADM	Reconfigurable Optical Add Drop Multiplexer
SBS	Stimulated Brillouin Scattering
SC	Single Carrier
SDN	Software Defined Networking
SG-DBR	Sampled Grating-Distributed Bragg Reflector
SNR	Signal-to-Noise-Ratio
SPM	Self Phase Modulation
SRS	Stimulated Raman Scattering
SSMF	Standard Single Mode Fiber
TDM	Time Division Multiplexing
UCP	Unified Control Plane
VOA	Variable Optical Attenuator
WDM	Wavelength Division Multiplexing
WSS	Wavelength Selective Switch
XPM	Cross Phase Modulation
XT	Crosstalk

Acknowledgements

I would like to express my deepest gratitude to the following persons for supporting me throughout the graduate school process and making this dissertation possible.

Dr. Keren Bergman, my advisor, for giving me the opportunity to be a member of her laboratory and enabling my graduate studies. I thank her for providing not only unerring guidance and vision but also immense academic freedom that allowed me to become a self-sufficient and independent researcher. Her success and work ethic have been and will continue to be constant sources of inspiration for me.

Dr. Daniel Kilper, my mentor, for always making the time to help me with whatever issue I was grappling with, be it a paper review or unpredictable behavior in an experimental set-up. I thank him for always asking the hard questions and sharing his invaluable lab experience, thereby helping me become a better experimentalist.

Dr. Gil Zussman, dissertation committee member, for the many discussions throughout the years on the CIAN research topics.

Dr. John Wissinger, dissertation committee member, for the numerous collaborations at the TOAN test-bed in Arizona and all the career support.

Dr. Debasis Mitra, dissertation committee member, for chairing my thesis defense.

Dr. Alan Wilner, Dr. Michal Lipson, Dr. Milorad Cvijetic, Dr. Bahram Jalali, & **Dr. Liam Barry**, principal investigators of research groups associated with CIAN, for encouraging and providing resources for research collaborations.

Cathy Chen, Robert Margolies, and Lee Zhu, my office-mates, for the the amazing work environment and all the shared graduate school milestones: studying for quals, paper deadlines, conference travel and, even defending on the same day.

Elsa Sanchez, Lydia Reyes, & **the Electrical Engineering Department staff**, for all instances of their support for the past five years.

LRL members, past and present, for their friendship and support and the many stimulating discussions.

Dr. Jeffrey Hopwood, my undergraduate thesis advisor, for getting me started on research and steering me towards graduate school.

Ali Qadri, my college friend, for proof-reading my graduate school applications (all eight of them!) and providing me with much-needed critical feedback.

Doris Tabassum & **Nur-Taz Rahman**, my childhood friends whose academic careers mirror mine, for treading the same path as me and sharing the same triumphs and tribulations.

The Alam family, my adoptive family in the U.S., for all their support throughout the years.

Amira Ahsan & **Arifa Ahsan**, my sisters, for always being there for me.

Md. Ali Ahsan & **Shamima Chowdhury**, my parents, for their unconditional love and support and numerous sacrifices to ensure that I had the best education possible. I would not be at this point of success today if it were not for them.

To...

My parents.

Thank you for teaching me to love lifelong learning.

Chapter 1

Introduction

The Internet has evolved considerably from its humble beginning as the Advanced Research Projects Agency Network (ARPANET)(Fig. 1.1); it originated as a four node connection between academic institutions in the United States and grew into network used by 3.2 billion people worldwide [11, 12]. This evolution has been primarily driven by the insatiable consumer demand for speed and bandwidth. As traffic continues to grow exponentially, the underlying fiber optical network is rapidly approaching the Shannon limit, the fundamental capacity limit [13]. Historically, network growth has been achieved through packet switching while the optical layer has been used a passive, over-provisioned transmission medium. However, given emerging traffic patterns and the physical capacity limits, it is no longer sustainable to just increase network capacity. Versatile new networking paradigms have to be developed that make more efficient use

(a)

(b)
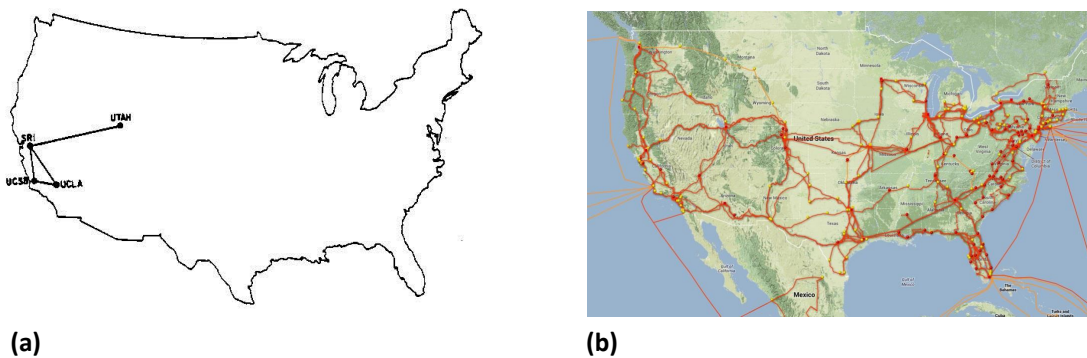
Figure 1.1: (a) ARPANET in 1969 (b) Level 3s North America internet backbone (adapted from [1])

of network resources for a scalable, energy-efficient next-generation Internet.

1.1 Agile Optical Networks

A. Existing Network Layered Architecture
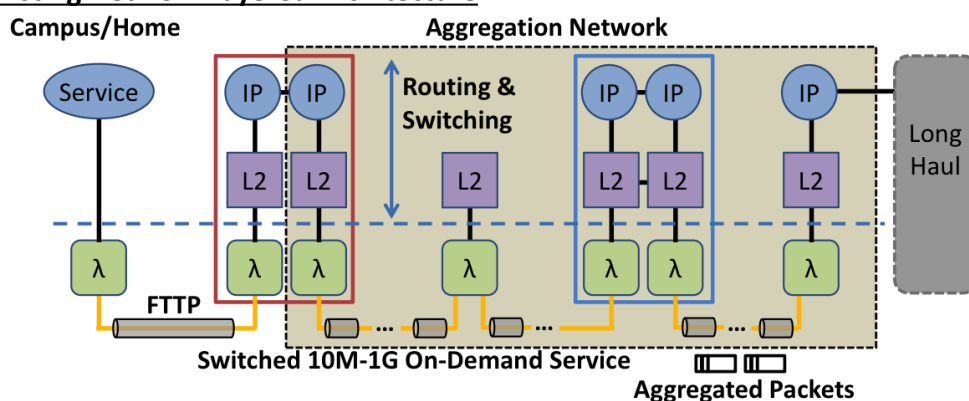
B. Agile Cross-Layer Architecture
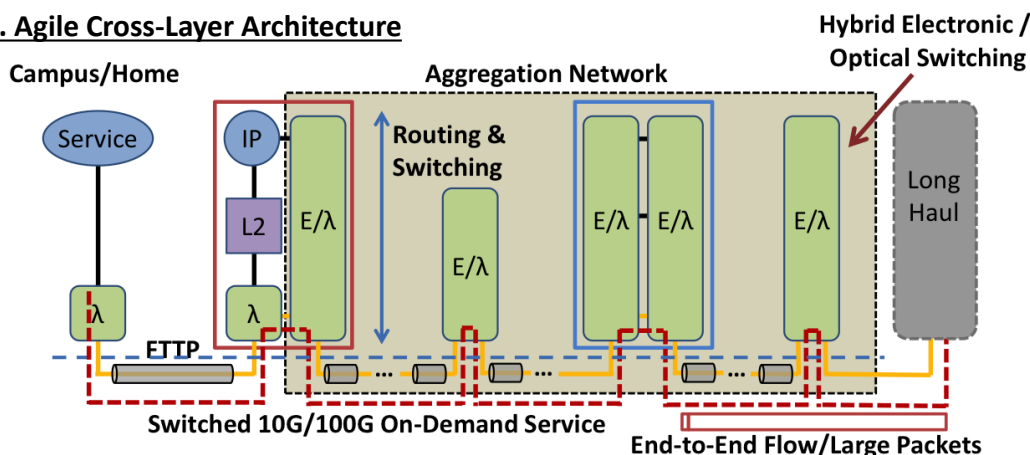
Figure 1.2: (a) Detailed current state of the art commercial network node. Data is delivered as short packets that are aggregated and repetitively processed in multi-tiered electronic switching and routing fabrics. (b) Agile optical network node with hybrid electronic and optical switching to minimize the electronic processing and set up end to end data flows to deliver data on demand. (adapted from [2])

The current Internet infrastructure consists of a quasi-static optical transmission network (λ) and separate layers of electronic switching (L2) and routing (IP). The optical layer serves mostly as 'fat, dumb pipes' connecting large electronic circuit and packet switches, where majority of the processing is performed. Fig. 1.2 (a) illustrates the

current network architecture. Data is broken into many packets and electronic processing is performed at each node to determine routing and service dependent functions such as quality of service (QoS) handling, firewalling, and protection. Even for services involving large bursts of data, the data is still broken down into many packets with multiple layers of headers and repetitive electronic processing along the path. Optical switching capabilities at reconfigurable optical add-drop multiplexers (ROADM) are used predominantly for provisioning and restoring signals. Optical channel capacity in a network is fixed and provisioned based on peak traffic demand, with additional capacity margins to allow for back-up paths for network protection. Once a wavelength channel is set-up, a process that can take up to days because of debilitating amplifier dynamics (detailed in section 2.1), it is typically not changed during the life of the system. Given the networking challenges outlined in section 1.2, this approach of a static, heavily over-provisioned optical layer is not scalable and agile optical networking has been proposed as an alternative solution [2, 4, 7, 14, 15, 16]. Agile optical networking aims to achieve a more intelligent, active optical layer by moving the higher layer switching functions down into the optical layer where photonic devices can be used to efficiently switch and aggregate traffic (Fig. 1.2 (b)). Network agility allows optical channel capacity to be provisioned in real-time in accordance to traffic demand, resulting in tighter margins and improved network efficiency.

1.2 Drivers for Agile Optical Networks

1.2.1 Emerging Traffic Patterns
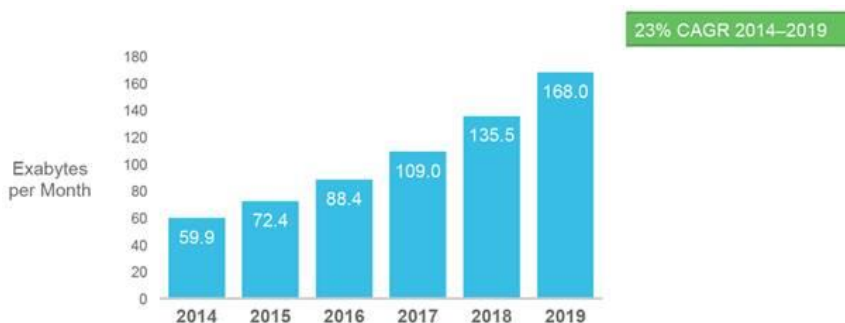
Figure 1.3: IP traffic growth showing a compound annual growth rate (CAGR) of 23% from 2014 to 2019 (adapted from [3])

Network traffic is increasing at near exponential rates due to increased penetration of broadband internet and an expanding variety of high bandwidth applications. IP traffic is projected to grow at a compound annual growth rate (CAGR) of 23% from 2014 to 2019 (Fig. 1.3) and will pass the zettabyte (1000 exabytes) threshold by the end of 2016 [3]. This traffic growth is driven by consumer demand for bandwidth-hungry applications such as on-demand video, social media, cloud services etc. In addition to traffic demand rising, the traffic itself is becoming increasingly heterogenous. With the advent of the Internet of Things (IoT), the number of data-intensive devices connected to the Internet is projected to reach 50 Billion – more than 6.5 times the world population – by 2020 (Fig. 1.4) [4]. Machine-to-machine (M2M) communication, where connected devices communicate directly with other devices, is expected to exceed 84 trillion events per year by 2022. IoT, consumer demand for cloud services and rise of big data have resulted in tremendous growth in the number of cloud data centers (CDC). As can be seen from Fig. 1.5 , CDC workload is growing at a CAGR of 24%of while that of traditional data centers is declining at a CAGR of −2%. By 2018, 78% of workload will be processed at cloud data centers [5]. Bulk data transfer between across geographically distributed CDCs is very common as it provides improved end-to-end performance and ensures high reliability under failures. Currently most CDCs perform bulk data transfer among three or more data centers and this transport requirement is projected to triple by 2018. As a result, inter-data center communication over the
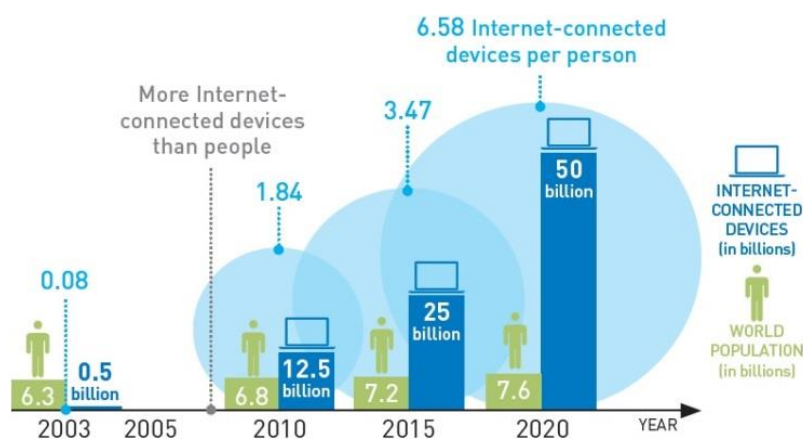
Figure 1.4: Growth in the number of data-intensive devices connected to the Internet(adapted from [4])

4

Figure 1.5: Cloud Data Center (CDC) workload is increasing driven by IoT, consumer demand for cloud services and rise of big data (adapted from [5])
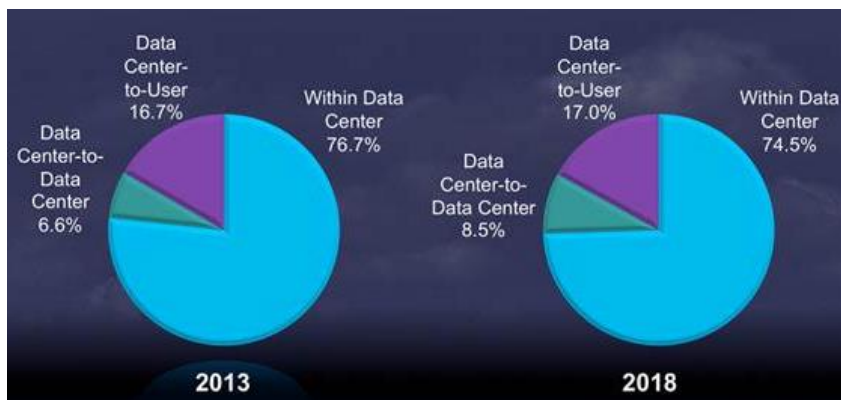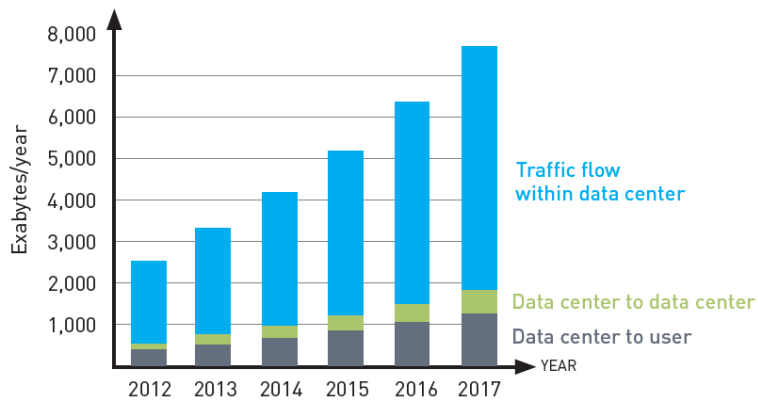
Figure 1.6: Inter-data center traffic over commodity Internet on the rise. It is growing faster than either data center-to-user traffic or intra-data center traffic (adapted from [4, 5])

5

commodity Internet is on the rise (Fig. 1.6) and is growing faster than either traffic to end-users or traffic within the data center. This inter-data center traffic is very bursty, with the amount of data transferred ranging from several terabytes to petabytes [5, 17]. Another significant contributor to the high volume of less aggregated, bursty network traffic is metro traffic, which is which is growing 2 times faster than long haul traffic and will exceed it in 2017 (Fig. 1.7 (a)). Consumer demand for video and cloud services have resulted in an increase in the number of DCs and content caches within the metro-network. Due to this increased concentration of traffic sources within the metro network, traffic that originates and terminates within the metro-network itself is on the rise as well (Fig. 1.7 (b)). The consequence of this rise in bursty traffic is illustrated in Fig. 1.8, which shows that the discrepancy between busy hour and
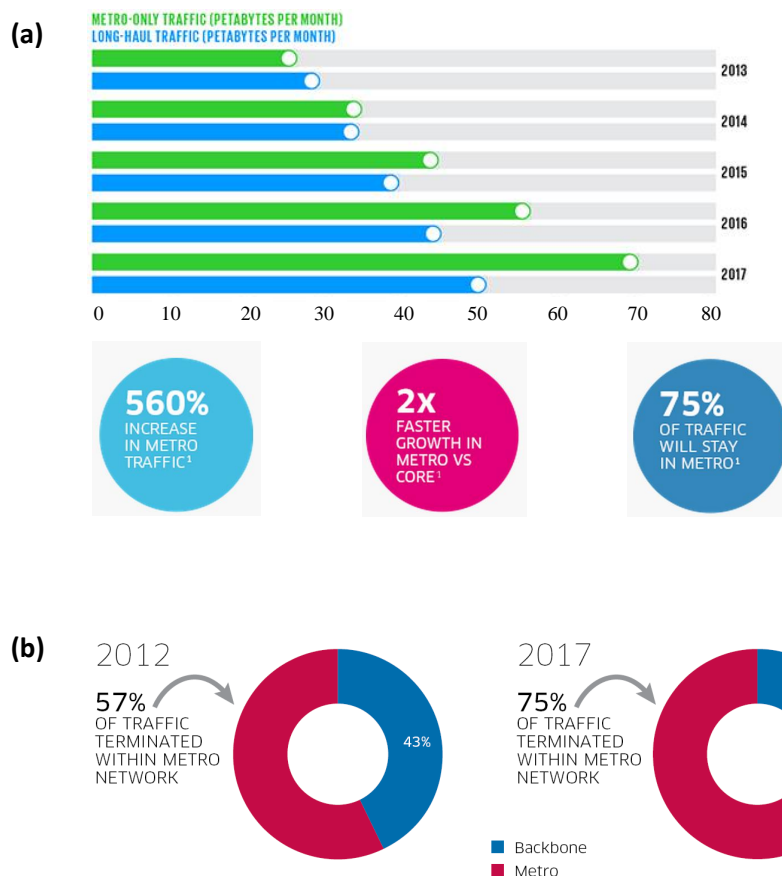
Figure 1.7: (a) Growth in metro-traffic which will surpass long-haul traffic in 2017. (b) The changing distribution of traffic between metro and backbone (adapted from [6])

average hour is increasing over time. Since current methods allocate resources based on busy hour traffic, resources will remain idle most of the time leading to network inefficiency. Agile optical networking capabilities thus become increasingly desirable to enable next-generation networks to support such unpredictable, high-bandwidth but short-lived traffic flows

Figure 1.8: Discrepancy between busy hour and average hour is increasing over time due to rising number of unpredictable, high-bandwidth but short-lived traffic flows(adapted from [3])

1.2.2 Fundamental Limits and Energy Constraints

The fiber optic network has been able to cost-effectively support the exponential traffic growth so far due to innovations – low-loss, single-mode transmission fiber, erbium-doped fiber amplifiers (EDFAs), wavelength division multiplexing (WDM), high spectral efficiency coding – that have increased its transmission capacity (Fig. 1.9). However, the transmission capacity of the optical network is not limitless and is bounded by the nonlinear Shannon limit [13]. Existing systems have started to approach this limit, resulting in the impending capacity crunch [18]. Continued capacity growth can be achieved through parallelism and there is significant work on techniques such as multi-core fiber [19] and multiple spatial modes [20] to enable this. However, parallel systems do not solve the energy constraint problem that is bottleneck to network growth. The Information and Communication Technology (ICT) industry's global greenhouse gas emissions is currently $2-2.5\%$ and given current trends, is projected to reach 4% by 2020 [21]. The increasing energy consumption is due to the huge and unsustainable
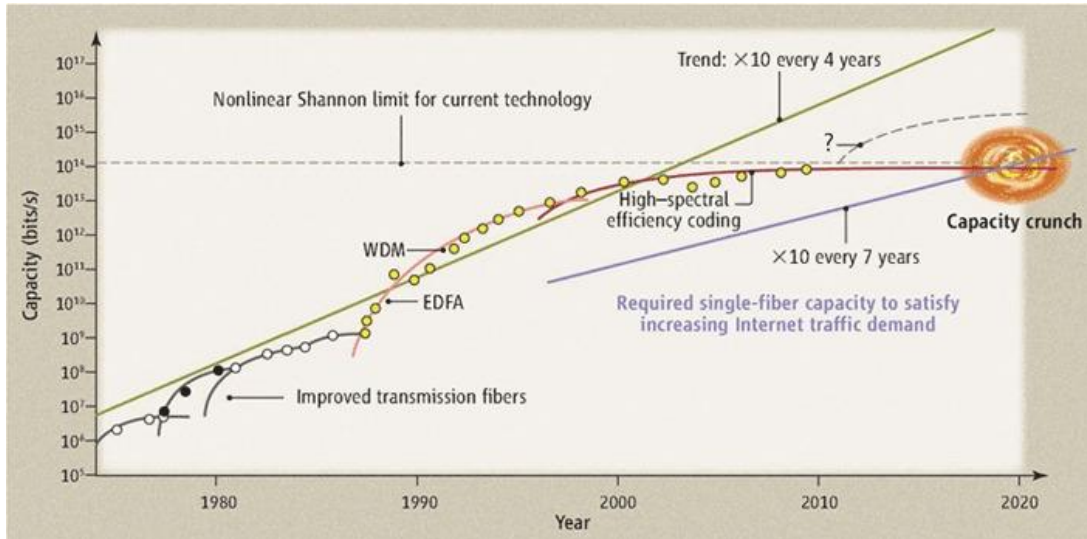
Figure 1.9: Data transmission capacity of fiber transmission systems as a function of year along with an estimate of the single-fiber capacity required to meet the Internet traffic. The nonlinear Shannon limit for the existing fiber technology is rapidly being approached and a capacity crunch looms ahead (adapted from [7])
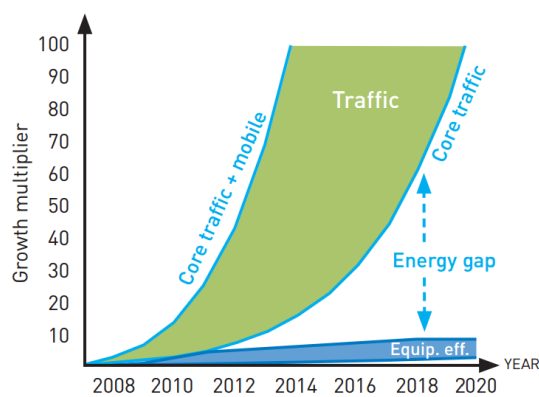
Figure 1.10: Unsustainable energy gap created due to equipment energy efficiency lagging traffic growth (adapted from [4])

8

energy gap that is caused by equipment energy efficiency improving only linearly while traffic grows near-exponentially. Parallelism involves increasing the amount of network equipment and consequently, results in linear increases in cost, energy and footprint with capacity growth. This poses a severe challenge moving forward as central office equipment are already at thermal density limits [22, 23, 24]. For parallel systems to scale, denser, lower power optics are required and new network infrastructure have to designed for efficient energy usage. Thus, optical networking solutions that can reduce the processing of high-bandwidth data flows in electronic switches and routers are highly desirable [4].

1.3 Key Requirements for Agility

1.3.1 Rapid Wavelength Reconfiguration Capabilities

Network agility requires wavelengths in the optical layer be provisioned in real-time in accordance to changing traffic patterns so that it can enable promising technologies such as real time wavelength switched optical bypass, physical layer protection/restoration, energy-efficient transceiver sleep modes etc. Since network traffic is becoming increasingly bursty (section 1.2), wavelengths have to be re-configured on the order of seconds in order to mimic the traffic patterns. Thus, rapid wavelength reconfiguration is key to achieving a dynamic optical network. While there has been significant work on protocols to enable dynamic wavelength reconfiguration and studies have shown light-path set-up times below 3 seconds [25, 26, 27], fast wavelength reconfiguration has yet to be implemented at scale in commercial networks. The world record for fastest wavelength provisioning in a commercial network was recently reported as 19 minutes and 1 second [28]. A key unresolved obstacle to rapid wavelength reconfiguration is the channel power excursions that arise and propagate throughout a network due to changing channel wavelength configurations in an automatic gain controlled (AGC) optically amplified system [29, 30]. The amplifier dynamics that cause these power excursions are discussed in detail in section 2.1. In current generation quasi-static optical transmission systems, power excursions are avoided by using off-line planning tools and long reconfiguration times encompassing many adjustments along an optical path [28, 29]. While there has been significant work on suppression of transient dynamics of amplifiers, complete mitigation of this phenomenon has not yet been achieved [31, 32, 33, 34, 35, 36].

Even recent studies on dynamic optical networks use either pre-reserved wavelengths or assume that the power dynamics problem will be solved [37]. To realize a truly agile optical network, techniques that enable wavelength reconfiguration on the order of seconds or faster while maintaining stable network operation have to be developed.

1.3.2 Real-Time Awareness of Physical Layer Impairments

An optical signal traverses various passive and/or active optical elements in its path and accumulates physical layer impairments (PLI) that affect its intensity level and temporal, spectral and polarization properties. The end-to-end optical signal quality after accumulating all the PLIs in its path must still surpass a certain threshold for error-free data transmission. The quality of a signal is commonly estimated using the quality of transmission (QoT) factor [38, 39]. QoT models are based on either the numerical calculation of OSNR [40] or analytical or experimental evaluation of the Q-factor [41], both of which are accurate indicators of the signal bit-error-rate (BER). QoT models take into account the impact of both linear and non-linear PLIs. Linear PLI are signal power independent and affect each wavelength individually; the most important linear PLIs are insertion loss, optical-signal-to-noise (OSNR) degradation, chromatic dispersion (CD), polarization mode dispersion (PMD), polarization dependent losses (PDL), crosstalk (XT) and filter concatenation (FC) [42]. Non-linear PLI, such as self phase modulation (SPM), cross phase modulation (XPM), four wave mixing (FWM), stimulated brillouin scattering (SBS), and stimulated Raman scattering (SRS), are signal power dependent and cause interference among wavelengths [43].

In current quasi-static network, impairment aware routing and wavelength assignment (RWA) algorithms are used to compute the QoT of candidate lightpaths before establishment to determine their feasibility [44]. Once the feasible lightpaths have been provisioned based on these algorithms, they are left undisturbed. Thus, unpredictable impairments rarely occur in current networks and are caused mainly by fiber cuts and equipment failure. An agile optical network on the other hand, is characterized by persistent unpredictable impairments arising due to the continuously changing wavelength configuration. Power levels along different links in an agile network is constantly fluctuating, resulting in varying PLIs, especially the non-linear types. This problem is further compounded by channel power excursions that occur due to changing loading conditions in optical amplifiers. Channel power excursions grow rapidly in amplifier

cascades, which are very common in metro-area networks, and result in unpredictable impairments and can even lead to network instability [29, 45].

Knowledge about the state of the PL is key to making intelligent resource allocation decisions. However, PL conditions in an agile network can not be reliably extrapolated from QoT models because of all the unpredictable impairments. Instead, the PL has to be continuously monitored using distributed advanced optical performance monitors (OPM) to provide the control plane with real-time information about the PL conditions. Advanced OPM have long been considered an enabling technology for next-generation optical networks [46, 47, 48, 49, 50] and there has been considerable work on cross-layer techniques – that allow bidirectional information exchange between the layers of the network protocol stack – so that information provided by OPMs embedded in the PL can used in conjunction with higher layer service requirements for intelligent routing and traffic engineering decisions [51, 52, 53, 54, 55, 56, 57]. Since PL impairments in an agile network can change drastically from one link to another, monitors distributed ubiquitously throughout the network are required to accurately capture the current state of the PL. Thus, it is imperative to develop energy-efficient and cost-effective monitoring solutions that support a wide range of advanced modulation formats to enable network agility.

1.4   Scope of Thesis

The work in this dissertation is focused on realizing the key requirements for enabling agile optical networks: (i) rapid and stable wavelength reconfiguration capability and (ii) real-time awareness of the state of PL through the use of cost-effective and energy efficient OPMs.

In order to enable rapid wavelength reconfiguration, a new technique that distributes optical signal across multiple wavelengths at time scales much faster than the response times of the optical amplifiers optical signal is developed. Since amplifier averages any power fluctuation occurring faster than its response time, these switching wavelengths are perceived as static channels whose powers are proportional to the wavelength dwell time. By leveraging this property and varying the dwell time of switching wavelengths, rapid wavelength reconfiguration can be achieved while maintaining power

excursions on other channels within acceptable margins. This work is summarized in chapter 2.

The work done to progress the advanced monitoring capabilities are detailed in chapter 3. Delay-line-interferometer (DLI) based optical-signal-to-noise (OSNR) monitor is a promising distributed monitoring solution as it supports advanced modulation formats for single channel systems. The functionality of this device is extended to monitor: (i) single channel systems autonomously by realizing modulation-format and bit-rate awareness and (ii) multiple-carrier orthogonal frequency division multiplexed (OFDM) signals, an emerging modulation format for next-generation networks.

Chapter 2

Rapid Wavelength Reconfiguration Capabilities

2.1 EDFA Dynamics and Channel Power Transients
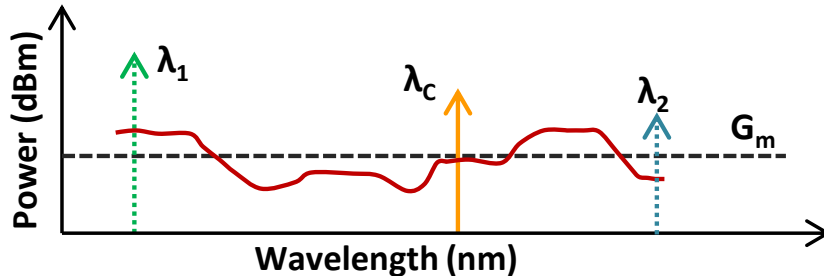
Figure 2.1: Automatic gain control (AGC) amplifier output spectrum for three channels, λ_1, λ_2, and λ_C. Solid curve show the gain spectrum (dB) and the dashed curve shows the mean gain across all channels, G_m. Arrows indicate channel output powers for equal input power on each.

Channel powers in networks have to be maintained within a certain range to meet the OSNR requirements and avoid XT from high-power neighboring channels (lower bound) and to avoid non-linear transmission impairments (upper bound). Channel power excursions can be highly detrimental when they cause deviation from this required power range. These power excursions occur because AGC algorithms maintain constant gain by monitoring the total input and output optical powers, and do not take into account the wavelength dependent gain arising from the gain tilt and ripple of the amplifier and

fiber plant. Consequently, a change in input wavelength configuration into an amplifier, even for constant input power on each channel, can affect the gain of individual channels, as depicted in Fig. 2.1. Consider initially λ_C as the only input channel. If λ_1, which has higher gain than λ_C, is added at the same input power, the total input power doubles but total monitored output power increases by more than 2x. In order to maintain constant gain, the AGC decreases the gain and λ_C undergoes a negative power excursion. The reverse process happens if λ_2 is added instead, and λ_C undergoes a positive power excursion. The size of the excursions depends on a variety of factors such as number of channels, channel distribution, number of links etc. These excursions can further be impacted by spectral hole burning and mean gain dependent gain tilt in erbium doped fiber amplifiers (EDFAs) and SRS in the transmission fiber [58]. Excursion values as high as 7.5 dB for a 20 channel add/drop have been reported [59]. The channel power coupling effect described above grows with a cascade of amplifiers [60] and power divergences of 15 dB were observed in recirculating loop experiments with AGC EDFAs [29]. As a result, the effect of a single reconfiguration event can propagate through the network and cause persistent power excursions and network instability, and even oscillations in the worst case [30, 45, 61]. This issue is particularly acute in mesh metro-area networks, which is characterized by a large number of short amplified ROADM links with many amplifiers. The capability to manage these power excursions, thus enabling rapid wavelength reconfiguration, is key to achieving an agile optical network.

2.2   Wavelength Switching at Different Time Scales

EDFAs have long time constants, on the order of hundreds of microseconds [31]. The amplifier is unable to temporally resolve any repetitive power fluctuations occurring faster than its response time and averages these power fluctuations. For example, when a fast-tunable laser switches continuously between two wavelengths, λ_1 and λ_2, at time scales faster than the amplifier time constant, they are perceived as two static wavelengths by the EDFA. The input power on the switching channels, as perceived by the EDFA, is proportional to wavelength dwell time duty cycle. Fig. 2.2 illustrates the EDFA transient response when a tunable laser switches between two wavelengths at time scales faster and slower than the amplifier time constant. For the faster case, the

Figure 2.2: (a) Laser switching between wavelengths, λ_1 and λ_2, with a period of 250 μs. Since switching rate is slower than the amplifier's time constant, it is able to detect the continuous change in loading conditions, resulting in transients effects on the wavelength output powers. (b) Laser switching between wavelengths, λ_1 and λ_2, with a period of 19 μs. Since switching rate is faster than the amplifier's time constant, it is unable to detect the switching event, resulting in no transient effect on the wavelength output powers.

15

amplifier is unable to detect the changing loading conditions; it perceives two, lower power static channels and consequently, the wavelengths experience no transient effects. For the slower case, the amplifier is able to identify that channel loading conditions have changed after each switching event, and consequently the wavelengths experience transient effects. This time dependent response property of the EDFA is leveraged to achieve rapid wavelength reconfiguration capabilities by using lasers that switch faster than EDFA time constants.

2.3   Hitless Wavelength Reconfiguration in Amplified Optical Networks

This section describes a technique of reprovisioning a wavelength in an optically amplified transparent network by pulsing it at a rate faster than the EDFA response time and varying its duty cycle in steps. This allows the effective loading conditions, as perceived by the EDFA, to be changed in small steps so that power excursions in the network are kept within margins of tolerance. Data loss during the reconfiguration process is significantly reduced by maintaining data transmission wavelengths being reconfigured throughout.

2.3.1   Background

Wavelength reconfiguration in current quasi-static systems involves numerous small and repetitive adjustments to ensure that power fluctuations caused on the other channels in the network are within margins of tolerance. As can be seen from Fig. 2.3, the power excursion caused on an existing channel in an amplified link when adding (and similarly dropping) another wavelength depends both on the position and the power of added the wavelength. Consequently, the best way to maintain power excursions on existing channels within required margins is to make small power changes in the wavelength being added or dropped and adjusting for any fluctuations caused. Currently, when a new wavelength is added, its power is increased in small increments until it reaches the target power. After each power increment on the wavelength being added, the power of all the other wavelengths in the network are examined and adjusted to ensure that their target powers are maintained. This process is repeated when a wavelength is dropped. Wavelengths being added or dropped can not transmit data error-free once its power

falls below a certain threshold due to OSNR limitations. Consequently, wavelength reprovisioning is a lengthy process [28] that can take up to several days and results in significant data loss. Since wavelength reconfiguration is rare event in current networks, this data loss is acceptable. However, in dynamic optical networks that rely on frequent wavelength reconfiguration, the long reconfiguration times and accompanying data loss pose a major obstacle.

Dynamic optical networks have to support rapidly changing traffic patterns by continuously adapting the wavelength assignment for optimum resource utilization. However, it is imperative that these physical layer changes do not affect service quality adversely; no disruption can occur to exiting services and low latency has to be maintained for many short-lived but high bandwidth applications. Furthermore, network dynamicity entails spectrum fragmentation as resources are continuously being assigned for new connections and released from expired connections. Spectral fragments are neither contiguous in the frequency domain nor aligned along the link, making it difficult to utilize them or to avoid them from becoming stranded bandwidths. This can potentially cause high blocking probabilities and limit the maximum traffic volume the network can accommodate. Various spectrum defragmentation algorithms [62, 63] and integer linear programming solutions [64] have been proposed to mitigate this issue. These
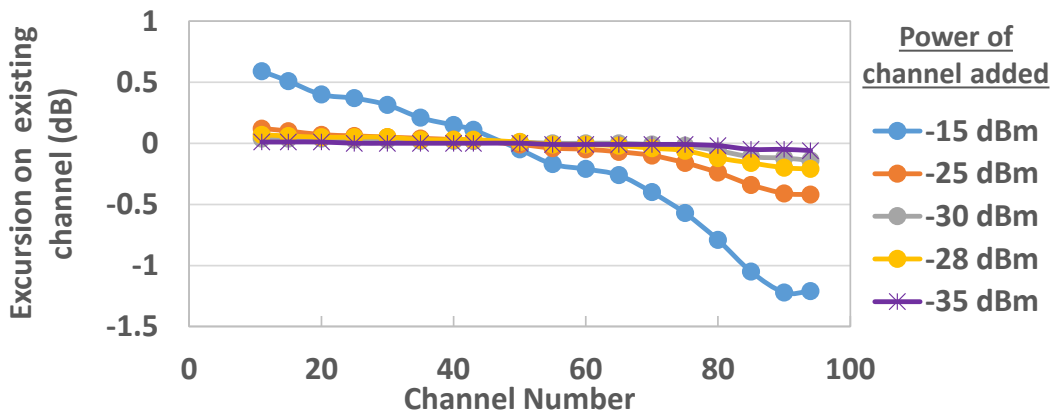
Figure 2.3: Power excursion on an existing channel in an amplified link when another channel at a given wavelength and power is added. The power excursion caused on the existing channel when adding (and similarly dropping) another wavelength depends both on the position and the power of added the wavelength.

techniques typically utilize devices in the physical layer to enable wavelength conversion [65, 66] or continuous tuning of the transmitted wavelengths [67, 68] to change the network wavelength configuration. Thus, it is crucial to develop rapid wavelength reprovisioning techniques that cause minimal data loss.

2.3.2 Proposed Technique

The key to managing power excursions in the network is small step-wise power adjustments on the wavelengths being reconfigured. The proposed technique achieves this by pulsing the wavelength being reprovisioned at a rate faster than the EDFA response time and varying its duty cycle in steps so that its effective power, as perceived by the EDFA, also changes in steps. The actual power of the wavelength is constant and maintained at the target power for data transmission. Thus, data transmission can continue to occur during the time periods when the laser is on, resulting in significantly reduced data loss. For example, when a new wavelength is added using this technique, it is initially pulsed a low duty cycle and the duty cycle is increased in steps until the wavelength is on at all times. The reverse process occurs when a wavelength
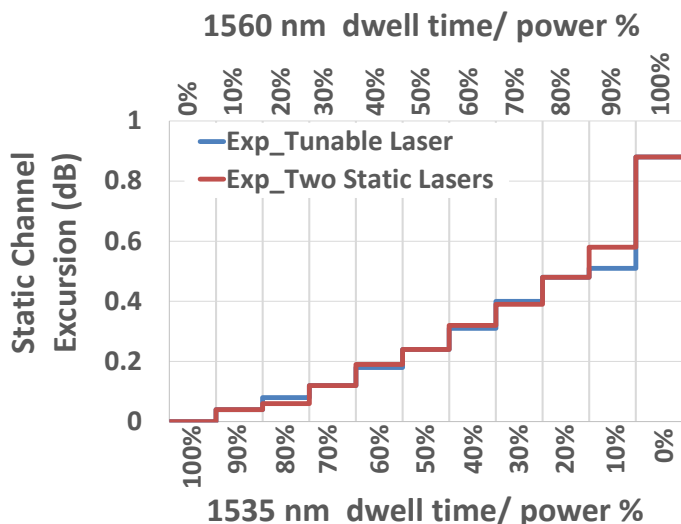
Figure 2.4: Power excursion on an existing channel in an amplified link when another channel at a given wavelength and power is added. The power excursion caused on the existing channel when adding (and similarly dropping) another wavelength depends both on the position and the power of added the wavelength.

is dropped; pulsing is started at a high duty cycle and decreased in steps until the wavelength is completely turned off. The add/drop wavelength is on and transmitting data on average for 50% of the time for the duration of the reconfiguration time. Thus, this technique has the potential to halve the data loss due to individual wavelength add or drop processes. Data loss can be reduced even further when a signal is reprovisioned from one wavelength to another (network defragmentation, for example). In this case, a fast tunable laser is pulsed between the final and initial wavelength with variable duty cycle for simultaneous wavelength add/drop. Data transmission occurs at all times throughout this process, allowing for hitless wavelength reconfiguration. Fig. 2.4 shows the power excursions on a static channel when a wavelength at 1535 nm (λ_1) is moved to 1560 nm (λ_2) using:

1. a fast tunable laser and the proposed technique

2. two static lasers with the same power ratio as the dwell time ratio. The sum of the total power of the two channels is constant and equal to the output power of the tunable laser

For example, if the tunable laser power is -19 dBm and the DTR for λ_1 to λ_2 is 90:10, then the power on λ_1 to λ_2 for the second case is -19.45 dBm and -29 dBm respectively. if the DTR for λ_1 to λ_2 is 50:50, then the power on the two wavelengths is -22 dBm each. Case 2 thus generates the power distribution for the proposed technique that is perceived by the EDFA. As can be seen from Fig. 2.4, the two power excursion profiles are almost identical, establishing conclusively that the EDFA perceives the tunable channels as static channels with power proportional to wavelength dwell time. Note that, two static lasers can be used to achieve the same effect as a fast tunable laser switching between two wavelengths. However, this requires an extra transceiver during the re-provisioning process and may pose synchronisation issues, making the use of a single tunable laser the more practical option.

2.3.3 Experimental Set-up

In order to establish the efficacy of the proposed technique, the use of pulsed signals for wavelength reconfiguration in a metro-scale test-bed was studied. The experimental set up is shown in Fig. 2.5. A field-programmable gate array (FPGA) controlled Sampled
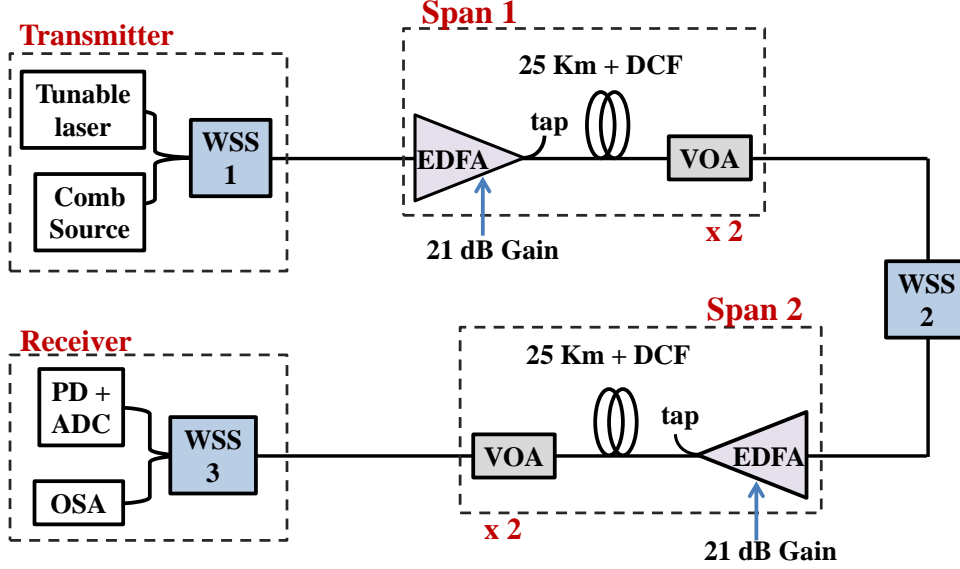
Figure 2.5: Metro-scale test-bed to study the power excursions caused in the network due to rapid wavelength provisioning using proposed and current methods. PD = photodiode, ADC = Analog to Digital Convertor.

Grating-Distributed Bragg Reflector (SG-DBR) fast tunable laser is used to perform rapid wavelength switching between wavelengths being reprovisioned. The laser can operate in both static and fast-switching modes and can access 80 wavelengths across the 50 G C-band ITU grid. Previous work using similar lasers has demonstrated that data on the switching wavelengths can be received error-free within nanoseconds of the switching event. Error free transmission is achieved 30 ns after switching for mth power double differential QPSK signals [69] and 8 ns after switching [70] for direct detection burst mode orthogonal frequency division multiplexing (OFDM) signals. In this work, the period of switching is 18 μs, i.e the laser spends x μs on λ_1 and then switches to λ_1 for the remaining (18-x) μs and this process is repeated. The value of x is varied to achieve different DTRs. Note that, it is possible to pulse the laser with nanosecond switching periods. The limitation in this specific implementation was the speed of the FPGA controller used to trigger the laser switching. The focus of this work is to study the power excursions that the proposed technique would cause on both existing wavelengths and those being re-provisioned. Since the power coupling effect due to the wavelength switching is agnostic to the presence of data and depends solely on the wavelength configuration and power values, a comb source in conjunction with a

wavelength selective switch (WSS 1) is used to add the other static wavelengths into the test-bed. This allows a wide range of wavelength configurations to be tested so that the worst case scenario can be selected for in-depth study. The test-bed is comprised of two amplified spans (spans 1 and 2) that are separated by a WSS (WSS 2) and terminate at a receiver set-up. Each span contains of two AGC-EDFA, fiber and VOA link. A metro network typically has 2 to 5 amplified links between ROADM/ WSS sites and this test-bed with 4 EDFAs is a realistic replication of a real network. Furthermore, the tilt of the amplifiers are adjusted to be high to emulate the effect of a much larger amplified system; as shown previously, a single amplifier with large ripple or tilt is equivalent to the combined ripple and tilt cascade of identical amplifiers, neglecting gain dependent tilt [60]. In this case, the tilt of each span is 5.5 dB. Wavelengths are injected into the text-bed at -19 dBm power each. Each link is configured to have net zero insertion loss. All EDFAs operate in constant gain mode with gain of +21 dB and VOAs are adjusted to provide a total passive loss of -21 dB in each link. WSS 3 is used to select the wavelength for power measurements at the receiver. All power measurements are made using a 250 MHz PIN photo-detector, followed by a 2 MSa/s analog-to-digital (ADC) data acquisition board.

2.3.4 Modelling of EDFA Dynamics

Equations outlined in [71] can be used to model the power coupling phenomenon in AGC amplified system that cause power excursions. Given information about the cumulative gain ripple and tilt in an amplified link, the model can be used to predict the output powers of WDM channels for different input conditions. The fewer the number of amplifiers cascaded together and treated as a single, greater the accuracy of this model. The ability to predict power excursions in a network is highly beneficial as it provides greater intelligence to the network management plane, enhancing network performance. For example, the model can be used to predict the maximum step size of a power adjustment that can be made on a wavelength being reconfigured. Similarly, the model can be used to select from among available wavelengths the ones that will cause minimum disruption. In a real network comprised of a wide variety of amplifiers from different vendors, determining the cumulative gain ripple and tilt function is complicated, making it difficult to create a model. The proposed technique can overcome this difficulty by using a low duty cycle, and hence "low power", probe signal to sample

(a)

(b)

(c)
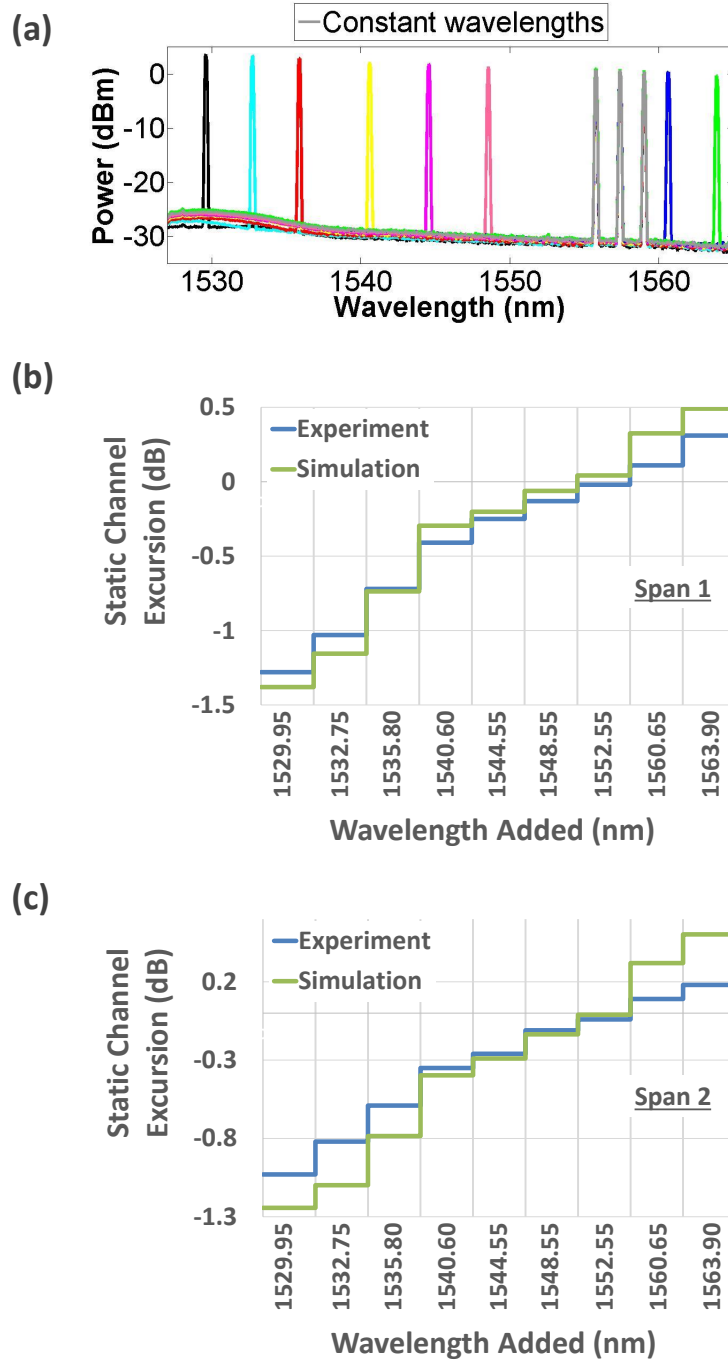
Figure 2.6: (a) Output spectra from span 1 for different input configurations. Power excursion caused by adding any wavelength across the C-band on the three existing channels in (b) Span 1 and (c) Span 2 (refer to Fig. 2.5). Experimental measurements and predictions from models are presented.

the gain spectra and extract the ripple-tilt function [72, 73]. A model was created each for Span 1 and 2 in the test-bed and their accuracy in predicting power excursions for the proposed technique is investigated. Both spans exhibit some degree of SHB at the shorter wavelengths and this is accounted for in the model as well [74, 75].

Fig. 2.6 shows the predictions of the power excursions caused on existing channels in the network when a new wavelength is added. Initially, the system is loaded with three closely spaced wavelengths centered around 1557.5 nm. Due to their spatial proximity, the wavelengths experience very similar power excursions and the average power excursion is recorded. After the power excursion caused by a newly added wavelength is measured, it is removed and replaced with another wavelength. Thus, at any one time, there are at most four wavelengths in the system. All wavelengths have equal input powers. As can be seen from Fig. 2.6 (b) and (c), the models predict the power excursion within ± 0.3 dB. The models can be used to predict the power excursions for a wide range of scenarios, as will be presented in the following sections.

2.3.5 Basic Operation

The conventional method, hereafter designated as the "static" method, of reprovisioning a signal from one wavelength to another involves attenuating the initial wavelength (λ_1) in steps until it is completely turned off (phase 1) and then bringing up the power of the new wavelength (λ_2) in steps (phase 2). The proposed method, hereafter known as "tunable" method, simultaneously decreases the power on λ_1 and increases the power on λ_2, effectively merging phases 1 and 2 and decreasing the number of steps for re-provisioning. Another benefit of the tunable method is that is always causes unidirectional power excursions.

In many cases, depending on the positions of λ_1, λ_2 and the existing wavelength under test, the power excursions caused by both phases 1 and 2 occur in the same direction i.e. both positive or both negative. For these instances, both the static and tunable methods have unidirectional excursion profiles. Such a scenario is presented in Fig. 2.7. A wavelength at 1535 nm (λ_1) and 3 other wavelengths centered around 1557.5 nm are injected into the test-bed. The 1535 nm wavelength is re-provisioned to 1560 nm (Fig. 2.7(a)) using the static and tunable methods and the average power excursions on the constant wavelengths are recorded(Fig. 2.7(b) and (c) respectively). Both methods cause the same amount of excursion. In other cases, power excursions caused by phases

(a)

(b)

(c)
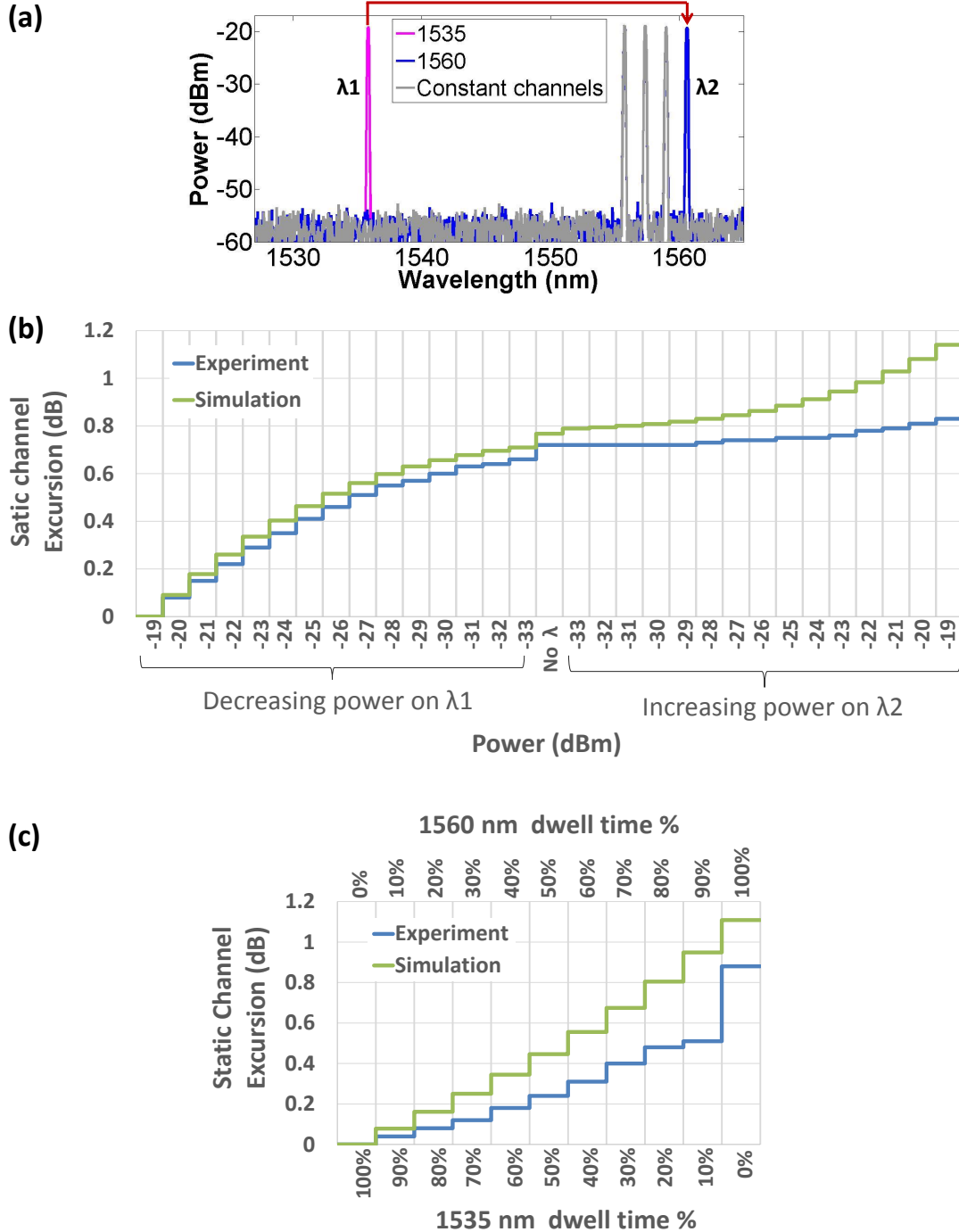
Figure 2.7: (a)Wavelength is re-provisioned from 1535 nm to 1560 nm. (b) Power excursion on the constant wavelengths in the network for static re-provisioning is unidirectional and total excursion is 0.88 dB. (c)Power excursion on the constant wavelengths in the network for tunable re-provisioning is also unidirectional and total excursion is 0.88 dB.

(a)

(b)

(c)
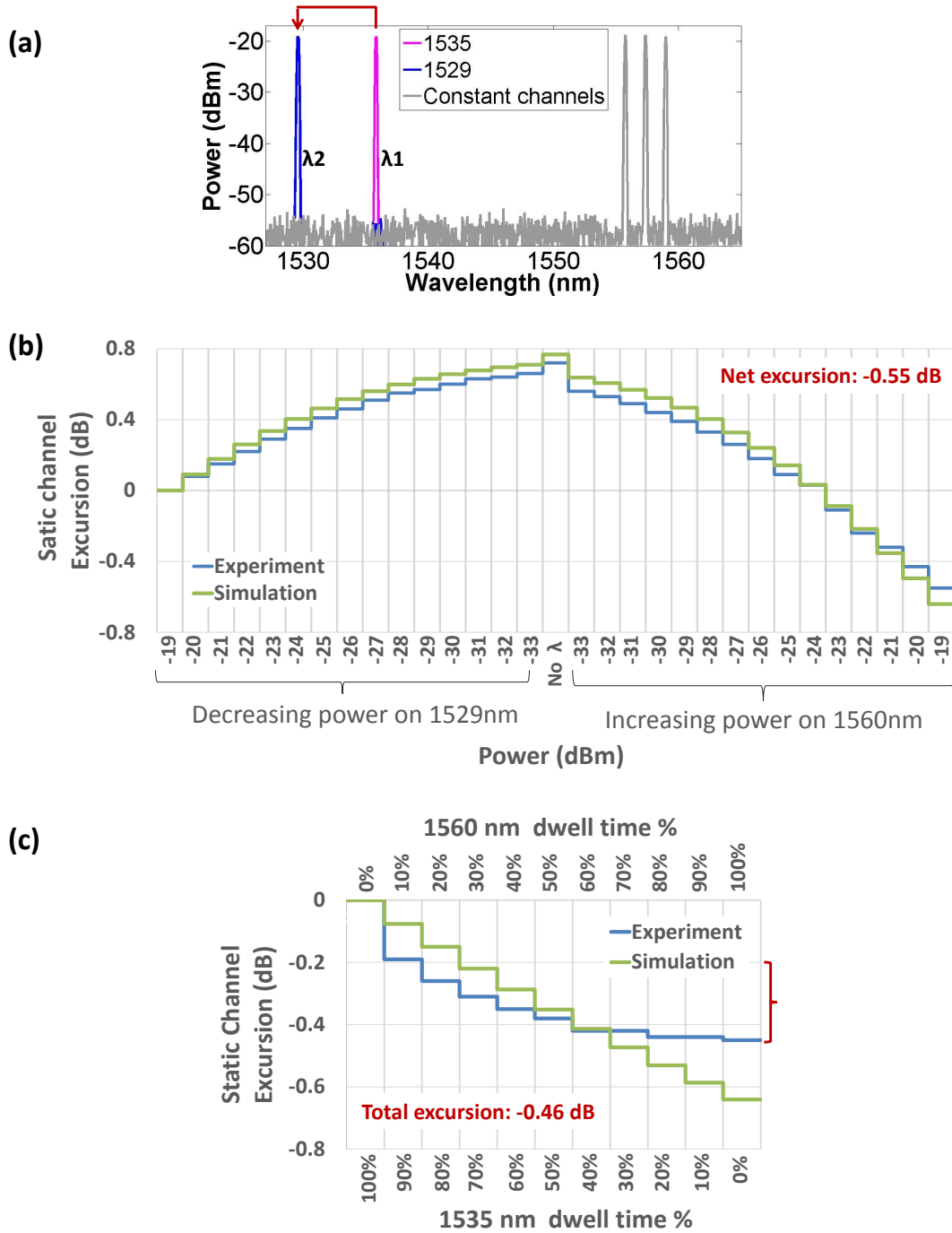
Figure 2.8: (a)Wavelength is re-provisioned from 1535 nm to 1529 nm. (b) For static re-provisioning, positive excursion occurs during phase 1 and negative power excursion occurs during phase 2, resulting in net excursion of -0.55 dB. (c)Only negative excursion occur for the tunable method and the total excursion is -0.46 dB. The discrepancy is due to slight change in wavelength that occurs when the laser is operated in static versus tunable mode.

1 and 2 are in opposite directions and the control system has to adjust for both positive and negative power excursions over the course of a single re-provisioning event. For these instances, when the tunable method is used, the wavelengths experience only the net excursion. In addition to power excursions being unidirectional, the magnitude of excursion is also reduced. Such a scenario is presented in Fig. 2.8. In this case, the wavelength at 1535 nm (λ_1) is re-provisioned to 1529 nm instead (Fig. 2.8(a)). As can be seen from Fig. 2.8(b), positive excursion occurs during phase 1 of the static method, followed by negative excursion during phase 2, resulting in a net excursion of -0.55 dB. Only negative excursion occur for the tunable method (Fig. 2.8(c)) and the total excursion is -0.46 dB. The discrepancy is due to slight change in wavelength that occurs when the laser is operated in static versus tunable mode. All power excursion measurements made in this section are at the end of span 1 of the test-bed (refer to Fig. 2.5). The predictions from the model for span 1 are also included in Fig. 2.7(b),(c) and Fig. 2.8(b),(c) and the discrepancy between measured and calculated values are within ± 0.3 dB.

2.3.6   Performance in Different Network Scenarios

In this section, performance of the proposed technique is compared with to that of the conventional method for wavelength reprovisioning to achieve defragmentation in a range of network scenarios. Defragmentation is chosen as the test case since: (i) AON will have to de-fragment significantly more frequently than current quasi-static network, and (ii) by choosing a corner case defragmentation scenario, where the initial and final wavelengths are widely separated and thus cause the most excursion, the performance of the proposed technique can be stringently evaluated. For the work in this section, the initial loading condition of the network is a fragmented spectrum with a wavelength at 1535 nm and three other wavelengths centered around 1557.5 nm. The wavelength at 1535 nm is re-provisioned to 1560 nm for defragmentation. The three wavelengths centered around 1557.5 nm remain in the network at all times and are referred to as the static channel. For the tunable method, wavelengths being reprovisioned are continuously switching between each other and therefore, are designated as switching channels. The wavelength reprovisioning time and data loss time for static and tunable cases are compared. The wavelength reprovisioning process can be broken down into two main processes:

1. Power adjustment on the wavelengths being reconfigured, followed by power measurements on the wavelengths in the network to determine if any thresholds have been surpassed (designated as steps hereafter).

2. Power adjustment on channels that have deviated from the optimum range to maintain the target power. This can be done by adjusting the WSS attenuation for that channel(designated as WSS adjustments hereafter) or changing the laser output power directly (designated as laser output adjustments hereafter).

The wavelength reprovisioning time thus can be estimated using the following formula:

$$Wavelength\ reprovisioning\ time = (\#\ steps\ *\ Step\ time)$$

$$+$$

$$(\#\ WSSadjustments\ *\ WSS\ adjustment\ time)$$

$$+$$

$$(\#\ laser\ output\ adjustments\ *\ Laser\ output\ adjustment\ time) \quad (2.1)$$

For static reprovisioning, the data loss time is equal to the wavelength reprovisioning time.

$$Static\ data\ loss\ time = Wavelength\ reprovisioning\ time \quad\quad (2.2)$$

For the tunable case, data transmission is continued on the wavelengths being reprovisioned. However, there is some data loss after each switching event [69, 70] and the total data loss is given by:

$$Tunable\ data\ loss\ time \quad = \quad \#\ switching\ events\ *\ Data\ loss\ time\ per\ switch$$

$$= \quad 2\ *\ \frac{wavelength\ reprovisioning\ time}{Switching\ Period}$$

$$*$$

$$Data\ loss\ time\ per\ switch \quad\quad (2.3)$$

Each WSS adjustment takes about hundreds of milliseconds [76] while the step time varies depending on the method of adjusting the power on wavelengths being reprovisioned. If the power of wavelength if adjusted by directly changing the laser

output, step time is considerably shorter and on the order of tens of milliseconds. On the other hand, if power is adjusted by keeping the laser power constant and changing the WSS attenuation on the channel, the step process can take up to hundreds of the milliseconds as well. The latter is the more common step process in current network. Here, estimations are based on shortest achievable step time achievable for a given scenario. The assumptions used in the calculations are:

1. WSS adjustment time is 500 ms.

2. Laser output adjustment time is 50 ms.

3. Short step time is 50 ms and long step time is 500 ms

4. For the tunable reprovisioning case, data loss time after a switching event is 30 ns [69].

5. WSS adjustments occur simultaneously on many wavelengths. For example, if all three static channels were adjusted simultaneously after a step, the WSS adjustment time would be 500 ms plus some overhead time to account for imperfect synchronization. However, the decreased time due to simultaneous WSS adjustment is not used in the calculations here. Rather, the total number of individual WSS adjustments are used for worst-case performance estimations.

2.3.6.1   ROADM to ROADM Amplified Link
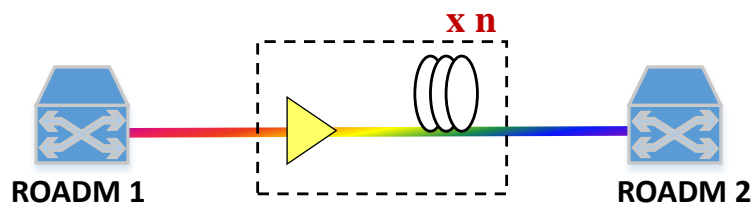
Figure 2.9: ROADM to ROADM amplified link. n = 4 for test-bed used in this experiment (refer to Fig. 2.5)

In this section, the power excursions in a ROADM to ROADM amplified link, as shown in Fig. 2.9, are studied. This network scenario is implemented in the test-bed by setting WSS 2 (refer to Fig. 2.5) to all pass-mode so that it acts purely as a passive

loss element. The VOAs are adjusted to maintain the required insertion losses. Two different test cases are studied:

1. Test case 1: Equal launch powers. ROADM 1 adjusts the input power of all wavelengths into the network to ensure that they are injected at the target launch power. Wavelengths experience wavelength dependent gain in the amplified link and reach ROADM 2 with unequal power. ROADM 2 adjusts the attenuation on each wavelength by a different amount to maintain the target power at the receiver.

2. Test case 2: Unequal launch powers. ROADM 1 adjusts the input power of all wavelengths into the network to pre-compensate for wavelength dependent gain of the amplified link. The launch powers are adjusted to ensure that the target power at the receiver at ROADM 2 is maintained. All power adjustments occur at ROADM 1.

Test case 1: Equal Launch Power

The cumulative power excursion measured on the static channel at ROADM 2 i.e. WSS 3 in the test-bed (refer to Fig. 2.9,2.5)for static wavelength reprovisioning is shown in Fig. 2.10. The figure also includes the cumulative power excursion predicted by the amplifier models (section 2.3.4). The models for span 1 and span 2 are cascaded to generate the results, resulting in a compounding of error from each model. Consequently, the discrepancy between measured and predicted values (maximum of 0.7 dB) in this case is higher than those for single spans. The error can be reduced by refining the models to take into account additional network parameters, such as fiber non-linearities for example. The allowable end-to-end power fluctuation margin for the link is set to be ±0.5 dB. Once the cumulative power excursion on a channel surpasses the ±0.5 dB threshold, the WSS attenuation for that channel is adjusted to bring it back to target power. As can be seen from Fig. 2.10, 3 WSS adjustments on each of the static channels are required to ensure the system operates within the margin. Thus for this scenario, the static reprovisioning process entails 30 steps and 9 WSS adjustments. Since this is a point-to-point link, the power of the laser can be adjusted directly, yielding a short step time of 50 ms. The reconfiguration time and data loss in this case is 6 s.
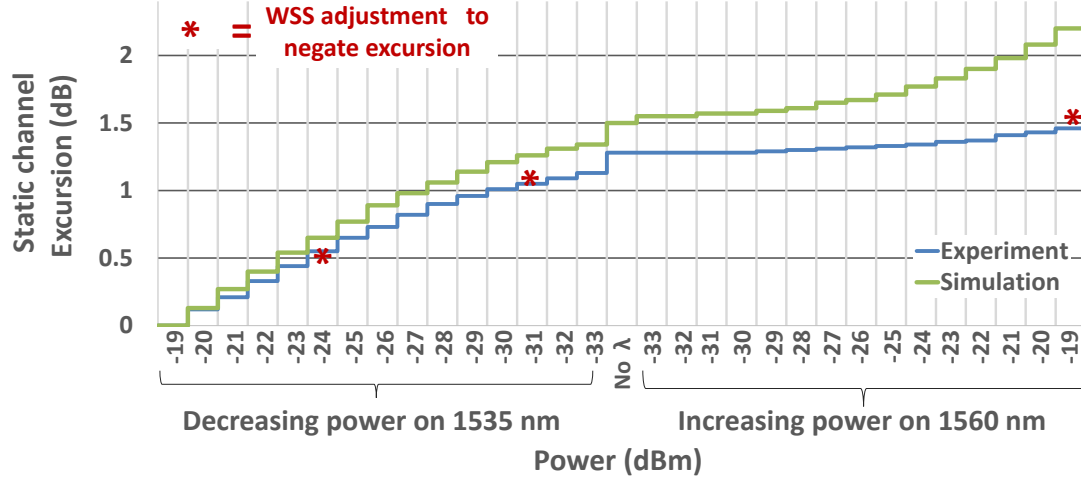
Figure 2.10: Cumulative power excursion measured on the static channel at ROADM 2 i.e. WSS 3 in the test-bed (refer to Fig. 2.9,2.5)for static wavelength reprovisioning.
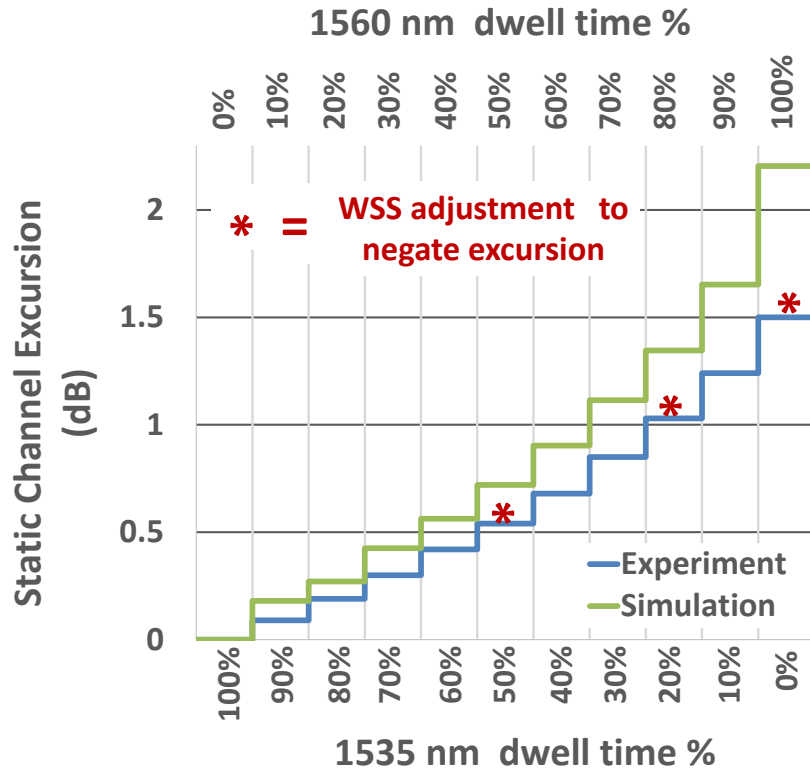
Figure 2.11: Cumulative power excursion measured on the static channel at ROADM 2 i.e. WSS 3 in the test-bed (refer to Fig. 2.9,2.5)for tunable wavelength reprovisioning.

(a)

(b)
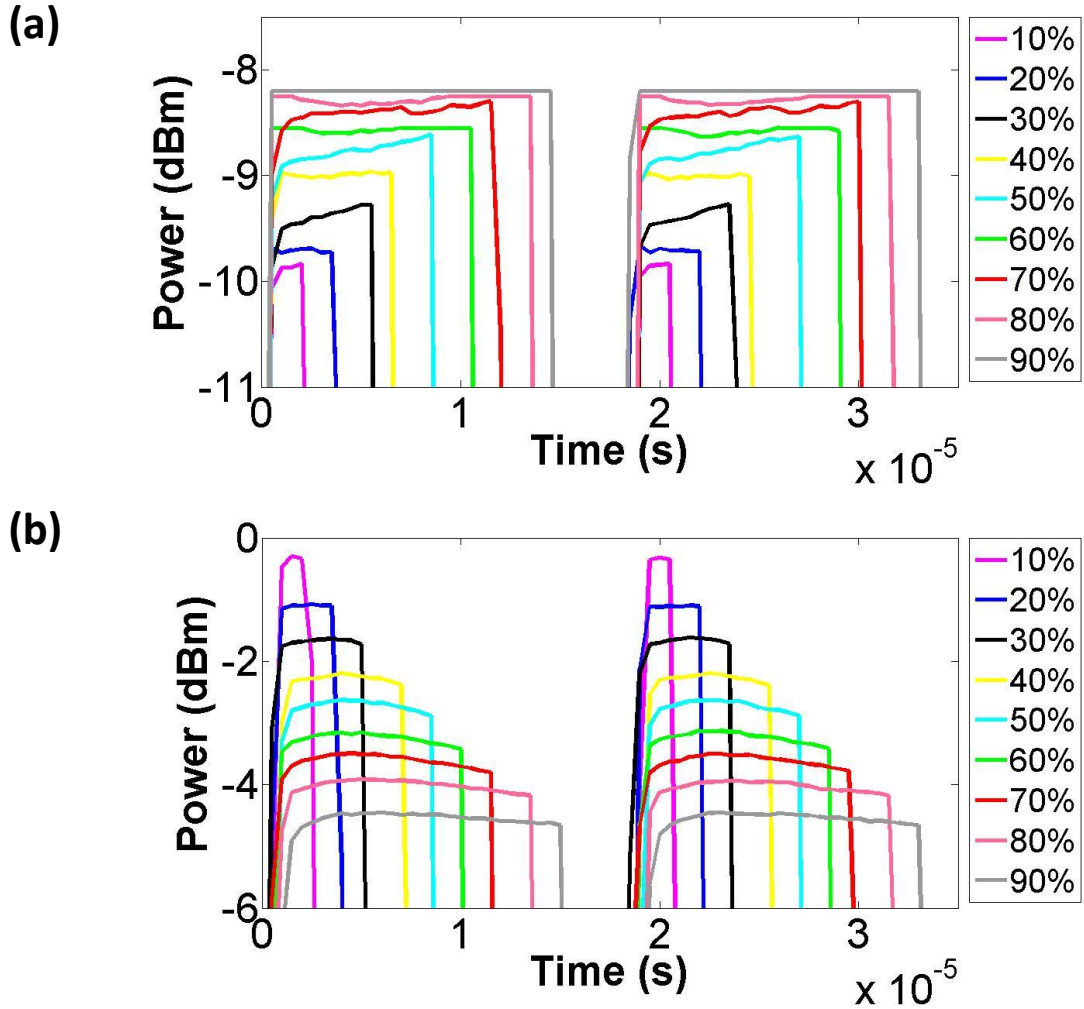
Figure 2.12: Power on the switching wavelengths at the receiver changes as the DTR is varied during the reconfiguration process. (a) 1560 nm (b) 1535 nm

The cumulative power excursion measured on the static channel for tunable wavelength reprovisioning is shown in Fig. 2.11. The total excursion is the same as the static reprovisioning case and 3 WSS adjustments on each of the static channels are required. In the tunable case, data transmission is continued on the switching wavelengths and consequently, the powers on these channels also have to maintained within certain margins. Fig. 2.12 shows how the power on the switching wavelengths at the receiver changes as the DTR is varied during the reconfiguration process. The cumulative power excursions on the switching channels is shown in Fig. 2.13. The 1560 nm chan-
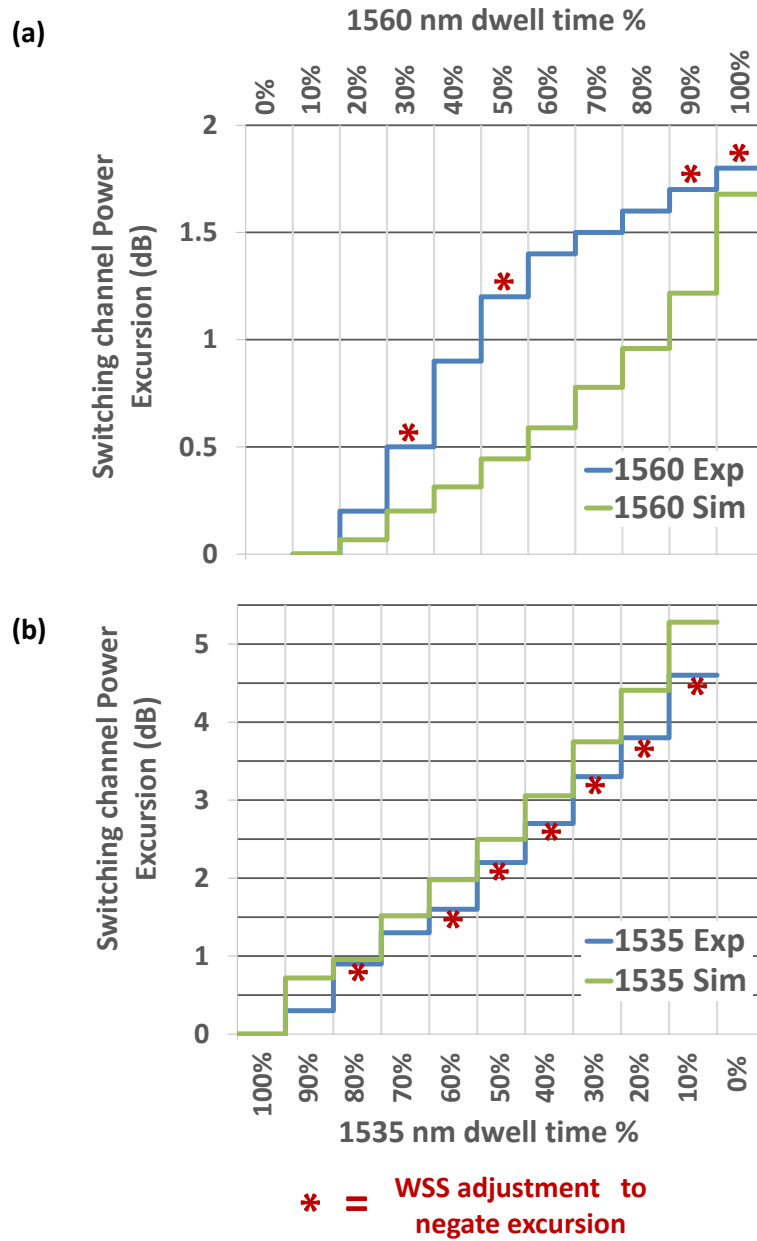
Figure 2.13: Cumulative power excursion measured on the switching channels at ROADM 2 i.e. WSS 3 in the test-bed (refer to Fig. 2.9,2.5)for tunable wavelength reprovisioning.(a) 1560 nm (b) 1535 nm

nel is in the same spectral region as the static channels and consequently, experiences similar cumulative power excursion (Fig. 2.13(a)). 4 WSS adjustments are required to maintain its target power. The 1535 nm channel experiences significantly greater cumulative power excursion (Fig. 2.13(b)) as SHB suppresses its gain at high powers. The power on 1535 nm channel has to be adjusted after almost ever step, requiring 7 WSS adjustments in total. Thus, for this scenario, the tunable reprovisioning process entails 10 steps and 20 WSS adjustments, resulting in a reprovisioning time of 10.5 s and data loss time of 35 ms.

Test case 2: Unequal Launch Power
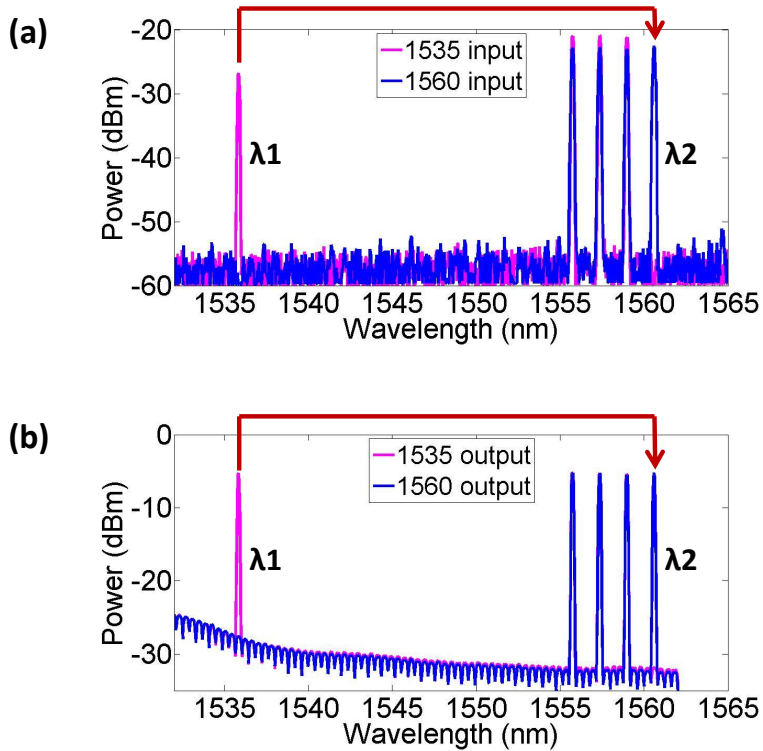
Figure 2.14: (a) Unequal launch power to compensate for wavelength dependent gain in the link. (b) Wavelengths reach the end of the link with equal powers.

The power of the input wavelengths are adjusted such that they all reach ROADM 2 with equal target power (Fig. 2.14), resulting in the 1535 nm channel being launched with approximately 6 dB less power than the static channels. The cumulative power
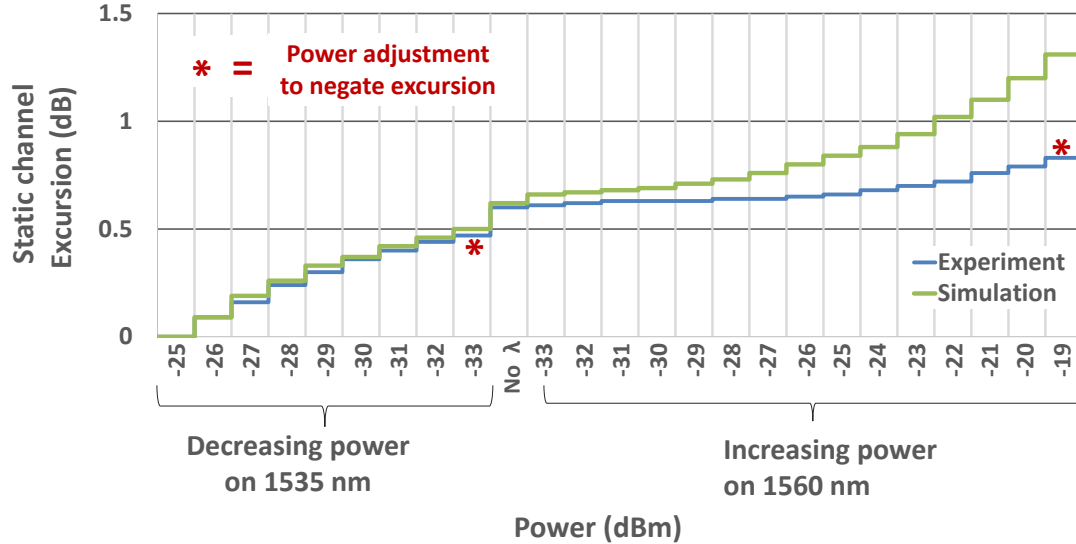
Figure 2.15: Cumulative power excursion measured on the static channel at ROADM 2 i.e. WSS 3 in the test-bed (refer to Fig. 2.9,2.5)for static wavelength reprovisioning. Wavelengths are launched with unequal powers to pre-compensate for the wavelength dependent gain in the link.
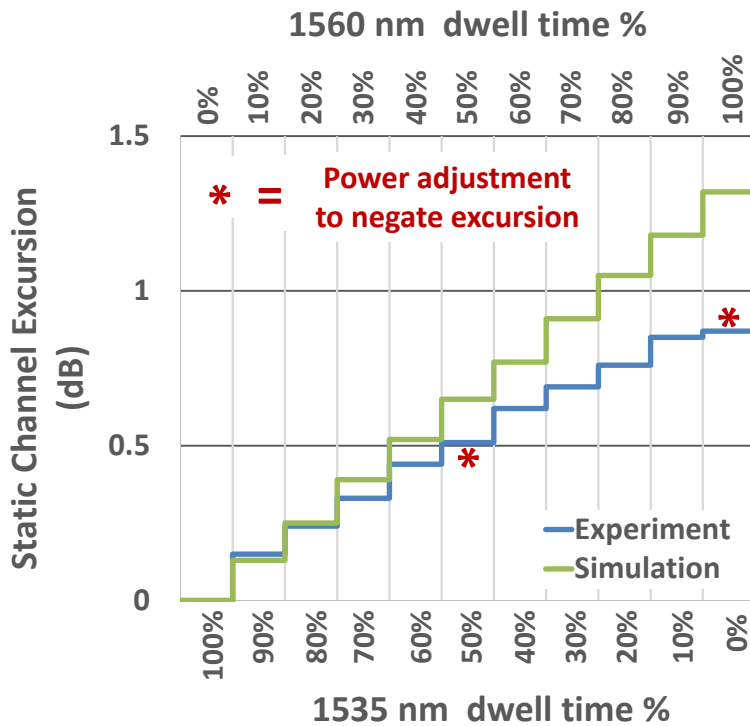
Figure 2.16: Cumulative power excursion measured on the static channel at ROADM 2 i.e. WSS 3 in the test-bed (refer to Fig. 2.9,2.5)for tunable wavelength reprovisioning. Wavelengths are launched with unequal powers to pre-compensate for the wavelength dependent gain in the link.
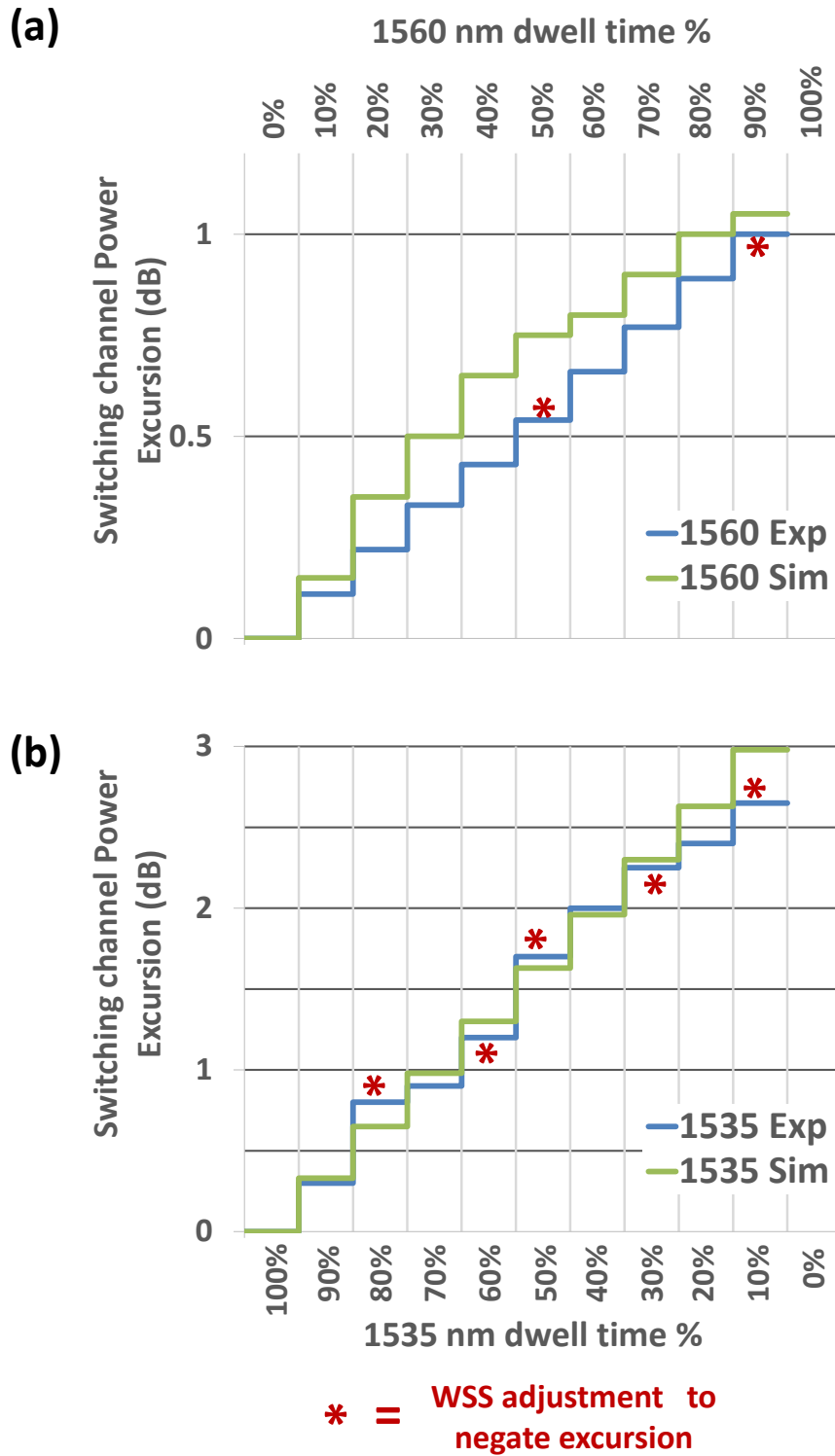
Figure 2.17: Cumulative power excursion measured on the switching channels at ROADM 2 i.e. WSS 3 in the test-bed (refer to Fig. 2.9,2.5)for tunable wavelength reprovisioning.(a) 1560 nm (b) 1535 nm. Wavelengths are launched with unequal powers to pre-compensate for the wavelength dependent gain in the link.

excursion measured on the static channel at ROADM 2 for static wavelength reprovisioning is shown in Fig. 2.15. Since 1535 nm starts out at a lower launch power, the total number of steps decreases to 24. The total power excursion on the static channel is also lower than that in test case 1, requiring 2 power adjustments on each of the three static channels. Since these channel power adjustments are made at the source, before the amplified link, they are achieved by adjusting the laser output power. Thus for this scenario, the static reprovisioning process entails 24 short steps and 6 laser output adjustments, resulting in reconfiguration and data loss time of 1.5 s.

The cumulative power excursion measured on the static channel for tunable wavelength reprovisioning is shown in Fig. 2.16 and it too requires 2 power adjustments on each of the three static channels. The cumulative power excursions on the switching channels is shown in Fig. 2.17. The cumulative excursions on both 1560 nm and 1535 nm are lower that than the equal launch power case and require 2 and 5 WSS adjustments respectively. Since a single laser is switching between the two wavelengths, the output power of the laser is kept constant and the individual wavelength attenuation on the WSS is adjusted. Thus, for this scenario, the tunable reprovisioning process entails 10 short steps, 6 laser output adjustments and 7 WSS adjustments, resulting in a reprovisioning time of 4.3 s and data loss time of 14.3 ms.

2.3.6.2 Multiple ROADM Amplified Link
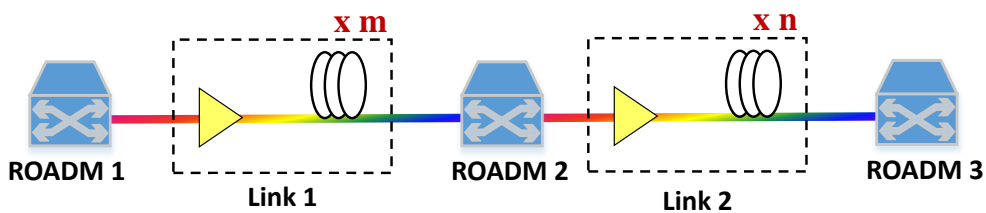
Figure 2.18: Multiple ROADM amplified link. Links 1 and 2 are spans 1 and 2 in the test-bed used in this experiment (refer to Fig. 2.5).

In this section, the power excursions in a ROADM to ROADM amplified link, as shown in Fig. 2.18, are studied. This network scenario is implemented in the test-bed by using spans 1 and 2 as links 1 and 2 respectively and WSS 2 functions as ROADM 2. This is the most common network scenario in mesh metro-networks which constitutes of short amplified links with a large number of WSS for path diversity. Since power

(a) <u>Attenuate λ1 in link 2; λ2 blocked in link 2</u>
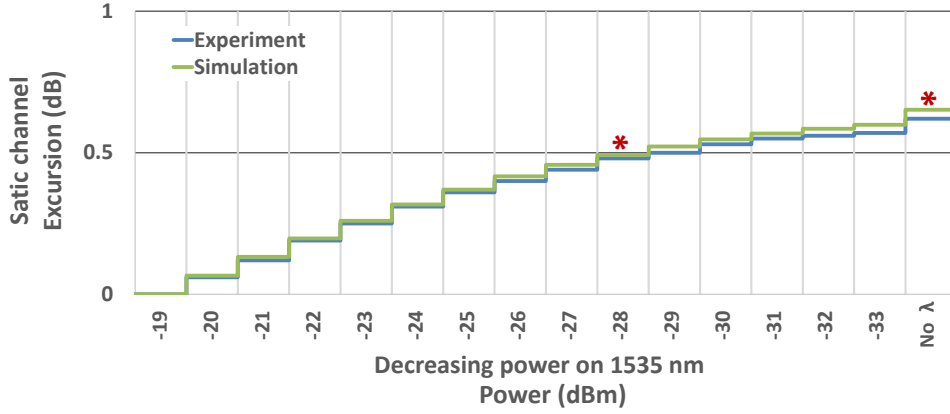
(b) <u>Attenuate λ1 in link 1; Increase λ2 in link 1</u>
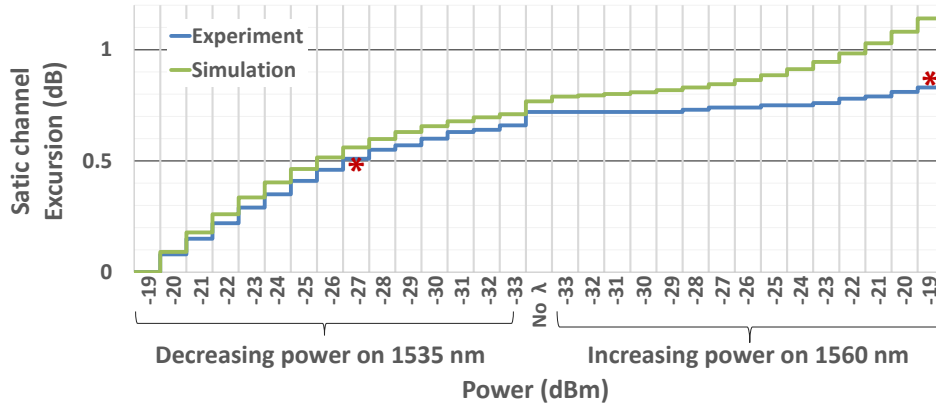
(c) <u>Increase λ2 in link 2</u>
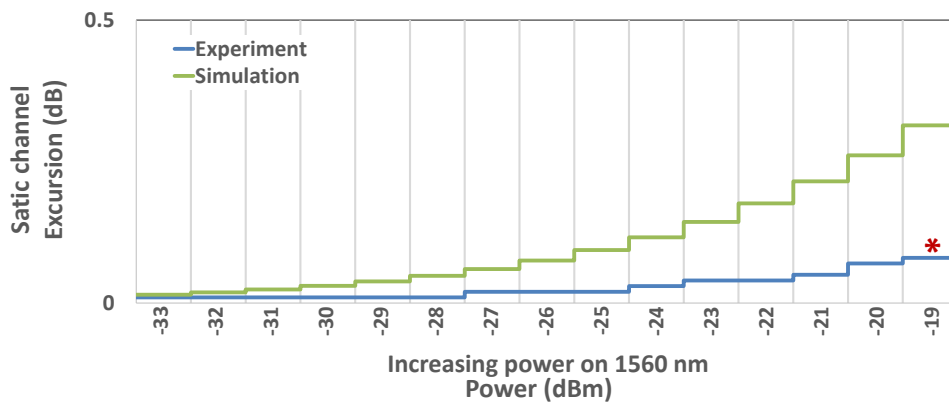
✱ = **WSS adjustment to null excursion**

Figure 2.19: Cumulative power excursion on static channels during static wavelength reconfiguration in a multi-ROADM link. (a) Cumulative power excursion on static channels in span 2 when 1535 nm is attenuated in span 2 only. (b)Cumulative power excursion on static channels in span 1 when 1535 nm is reconfigured to 1560 nm in span 1 only. (c) Cumulative power excursion on static channels in span 2 when the power on 1560 nm is increased in span 2.

excursion grow rapidly in amplifier cascades [60], power adjustments are made at every ROADM site along the end-to-end path for optimum network performance. During a conventional reconfiguration event in such a network scenario, power adjustments on the wavelengths being reconfigured are made on a link by link basis, starting from the last link in the path and working backwards. By isolating the power adjustment process to one link at a time, transient are prevented from compounding. For example, when reconfiguring 1535 nm(λ_1) to 1560 nm(λ_2) in the test-bed, the power on λ_1 in span/link 2 is attenuated in steps by WSS 2 until it is completely turned off. Fig. 2.19(a) illustrates the cumulative power excursion on the static channels in span 2 during this process. Loading conditions and hence wavelength powers in span 1 are unaffected while λ_1 is attenuated in span 2. Once λ_1 has been removed from span 2, its power in span/link 1 is decreased in steps until the it is completely removed from the network. The power on λ_2 is then increased in steps until the target power is reached; λ_2 is blocked at WSS 2 in the meantime to ensure that channel loading conditions in span 2 remain unchanged. Fig. 2.19(b) illustrates the cumulative power excursion on the static channels in span 1 during this process. In span 1, the power adjustment on wavelengths being reprovisioned can be made by directly decreasing the laser output power. Once all the power adjustments in span 1 have been completed, the power on λ_2 in span 2 is increased in steps by decreasing its attenuation at WSS 2(Fig. 2.19(c)). Thus, the static reconfiguration process entails 30 long steps, 30 short steps, and 15 WSS power adjustments, resulting in a reconfiguration and data loss time of 24 s for the static reconfiguration method.

The tunable wavelength reconfiguration process doesn't allow for individual links to be isolated for power adjustments. In this case, a tiered thresholding system, with the link closest to the transmitter having the tightest margins, is used instead to maintain power excursions within the margins of tolerance. For example, the maximum allowable power excursions at the receiver is ±0.5 and so, the power excursion margin at ROADM 2 is set to ±0.25. By clamping down the power excursions early in the amplified path, they are prevented from growing uncontrollably. The cumulative power excursion on the static channels at the end of span 1 is shown in Fig. 2.20. The total excursion is 0.8 dB and 3 WSS adjustments on each of the static channels are made. As can be seen from Fig. 2.21, illustrating the cumulative power excursions on the switching channels, the 1560 nm channel requires 4 WSS adjustments and the 1535

nm channel requires 7 WSS adjustments to maintain the power fluctuation within the requisite ±0.25 range. Adjusting for the power fluctuations at ROADM 2 decreases the cumulative power excursions of the channels at ROADM 3 significantly, as can be seen from Fig. 2.22,2.23, 2.24. The cumulative excursion of static channels at the end of span 2 is 1.5 dB when no adjustments are made at WSS 2; with adjustments, the maximum power excursion drops to 0.8 dB and requires 2 WSS adjustments at WSS 3. Similarly, adjustment at WSS 2 decreases the maximum power excursion on 1560 nm from 1.8 dB to 1 dB (Fig. 2.23) and 1535 nm from 4.6 dB to 1.4 dB(Fig. 2.24). 1560 nm and 1535 nm channels both require 2 WSS adjustments at WSS 3 to maintain the power at WSS 3 within the margins. Thus, the tunable reconfiguration process for the multiple-ROADM network scenario entails 10 short steps and 30 WSS power adjustments resulting in a reconfiguration time of 15.5 s and data loss time of 52 ms. For longer paths with greater number of links, the step size has to be made smaller (e.g. changing DTR by 5% instead of by 10% in each step) to ensure that the end-to-end
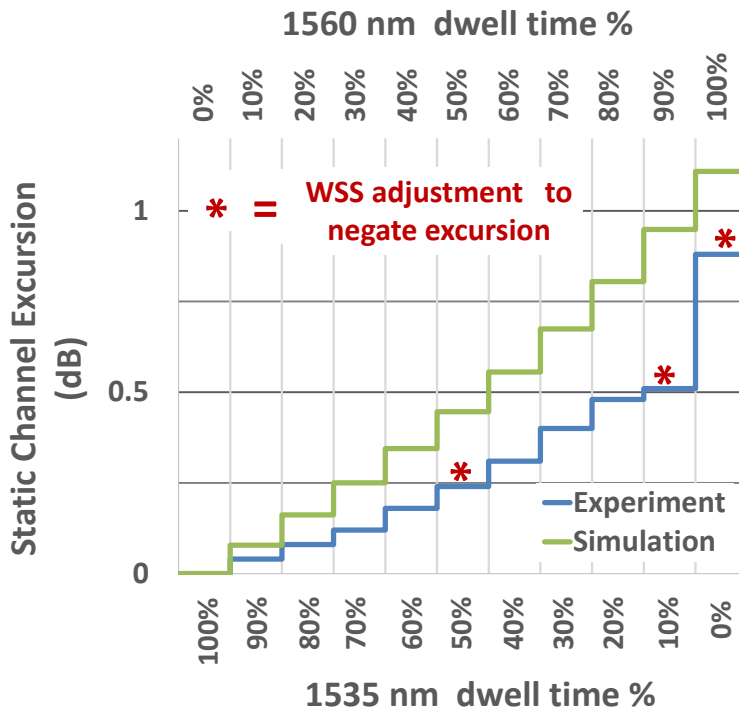
Figure 2.20: Cumulative power excursion of static channels after span 1 at ROADM 2 i.e. WSS 2 in the test-bed (refer to Fig. 2.18,2.5)for tunable wavelength reprovisioning.
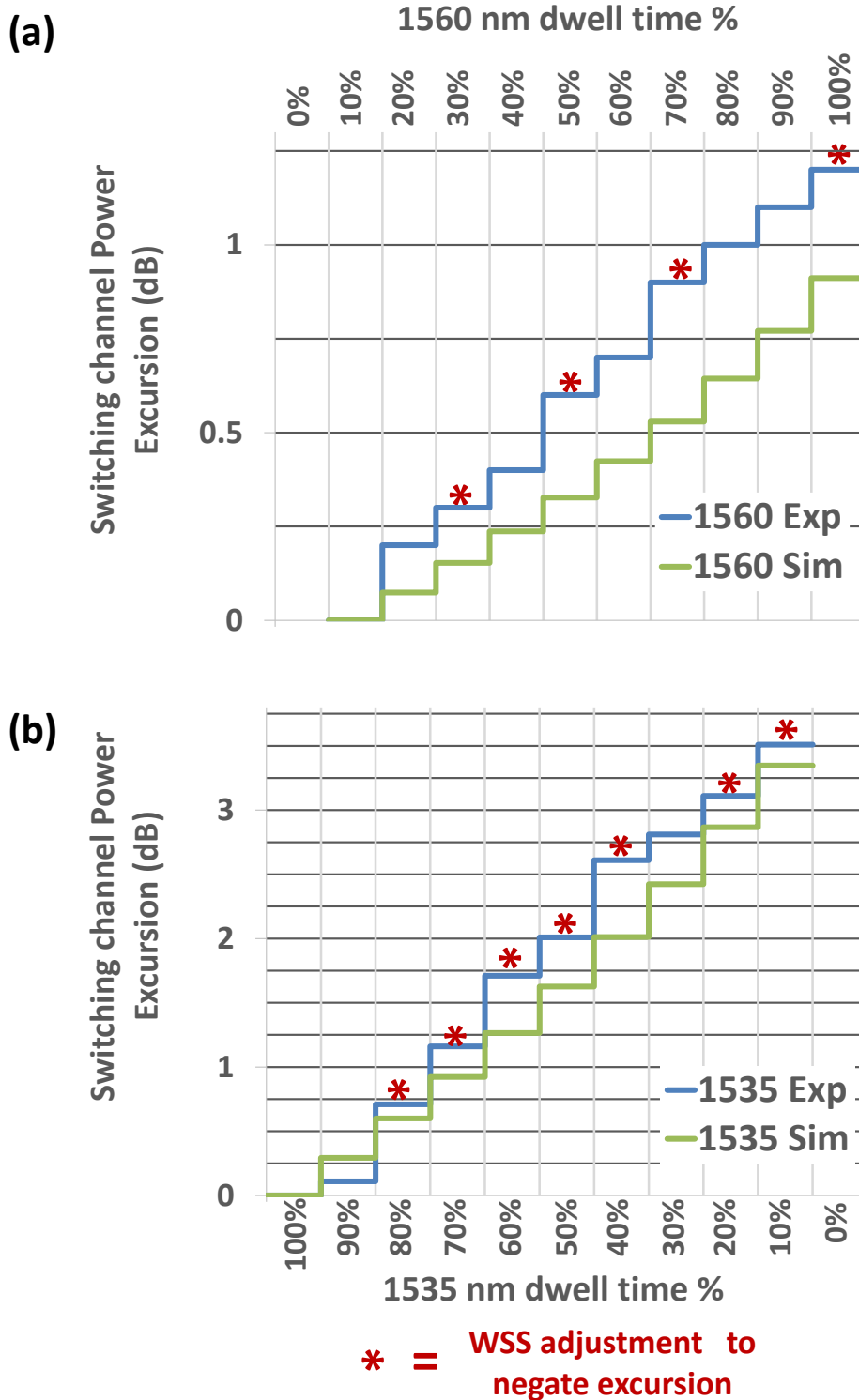
Figure 2.21: Cumulative power excursion of switching channels after span 1 at ROADM 2
i.e. WSS 2 in the test-bed (refer to Fig. 2.18,2.5)for tunable wavelength reprovisioning.(a)
1560 nm (b) 1535 nm.

power excursion after each step remains within margins. While this will increases the data reconfiguration and data loss time, the performance will still be better than the static case where the number of long steps increases linearly with the number of links.
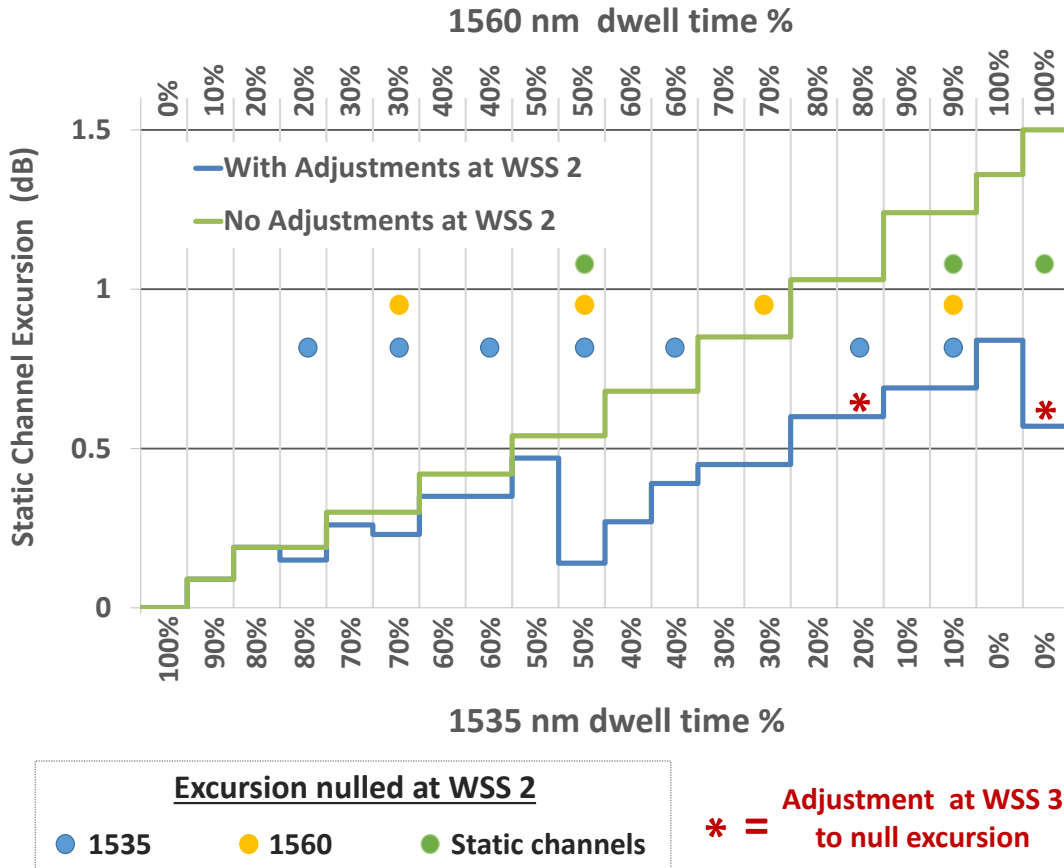
Figure 2.22: Cumulative power excursion of static channels after span 2 at ROADM 3 i.e. WSS 3 in the test-bed (refer to Fig. 2.18,2.5)for tunable wavelength reprovisioning. Excursions with and without adjustments at WSS 2 are compared.
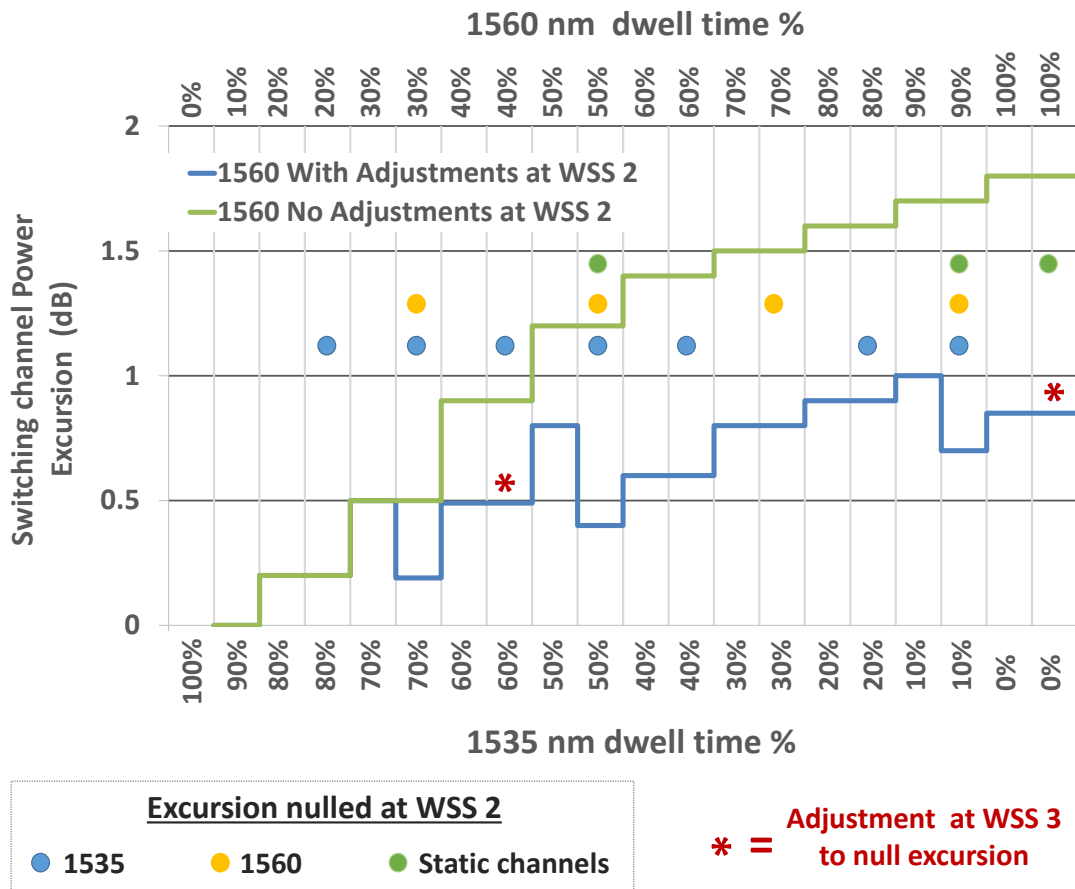
Figure 2.23: Cumulative power excursion on 1560 nm switching channel after span 2 at ROADM 3 i.e. WSS 3 in the test-bed (refer to Fig. 2.18,2.5)for tunable wavelength reprovisioning. Excursions with and without adjustments at WSS 2 are compared.
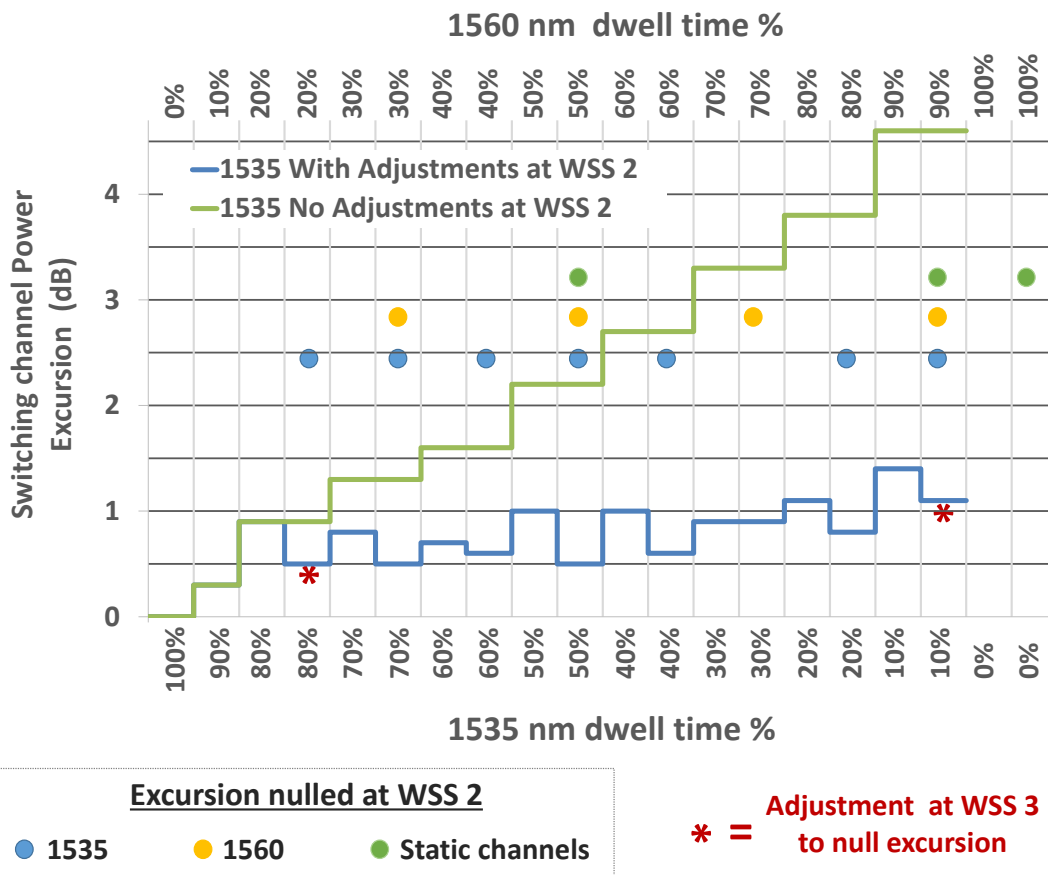
Figure 2.24: Cumulative power excursion on 1535 nm switching channel after span 2
at ROADM 3 i.e. WSS 3 in the test-bed (refer to Fig. 2.18,2.5)for tunable wavelength
reprovisioning. Excursions with and without adjustments at WSS 2 are compared.

2.4 Excursion-Free Dynamic Wavelength Switching in Amplified Optical Networks

This section details a technique of distributing an optical signal across multiple wavelengths chosen to reduce or cancel the power dynamics so that excursion-free switching can be achieved in an optically amplified transparent network. The use of variable wavelength dwell times for excursion-free switching using arbitrary wavelength pairs is presented. Spectral efficiency lost in utilizing multiple wavelengths is recovered through time-division-multiplexing (TDM) two signals distributed over the same wavelengths.

2.4.1 Proposed Technique

2.4.1.1 Principle of Operation

The proposed technique distributes the optical power of a single signal over multiple wavelengths such that the individual gain excursions cancel one another, so that the power dynamics of wavelength reconfiguration is reduced or eliminated. Fast tunable lasers that can switch between wavelengths on nanosecond time scales are used to distribute the optical power. EDFAs have gain response time constants on the order of hundreds of micro-seconds or even milliseconds and therefore do not respond to any power fluctuations occurring at a faster time scale. For example, if the tunable laser switches over N wavelengths with equal dwell times summing to less than a microsecond, the EDFA perceives it as N static channels, each at $\frac{1}{N}$ the total laser power. By using balanced wavelengths, that cause equal and opposite power excursions, the power fluctuations that arise when switching these signals can be negated. Due to network constraints it may not always be possible to choose a balanced pair/set of wavelengths that cause equal and opposite excursions. However by varying the dwell time ratio (DTR) between a pair of unbalanced switching wavelengths, their relative contributions to the resultant excursions can be skewed so that excursion free operation is achieved. For example, two unbalanced wavelengths, λ_1 and λ_2, added at equal power, cause excursions of $+x$ dBm and $-y$ dBm respectively, where $|x| > |y|$. Since the amount of excursion caused by a wavelength depends on its power, zero net excursion can be achieved by decreasing the power on λ_1 and increasing the power on λ_2. For the fast switching scenario, the effective power on a wavelength, as perceived by the EDFA, is

proportional to the dwell time on that wavelength and excursion free switching using λ_1 and λ_2 can be achieved by increasing the dwell time on λ_2.

2.4.1.2 Time Division Multiplexing for Spectral Efficiency
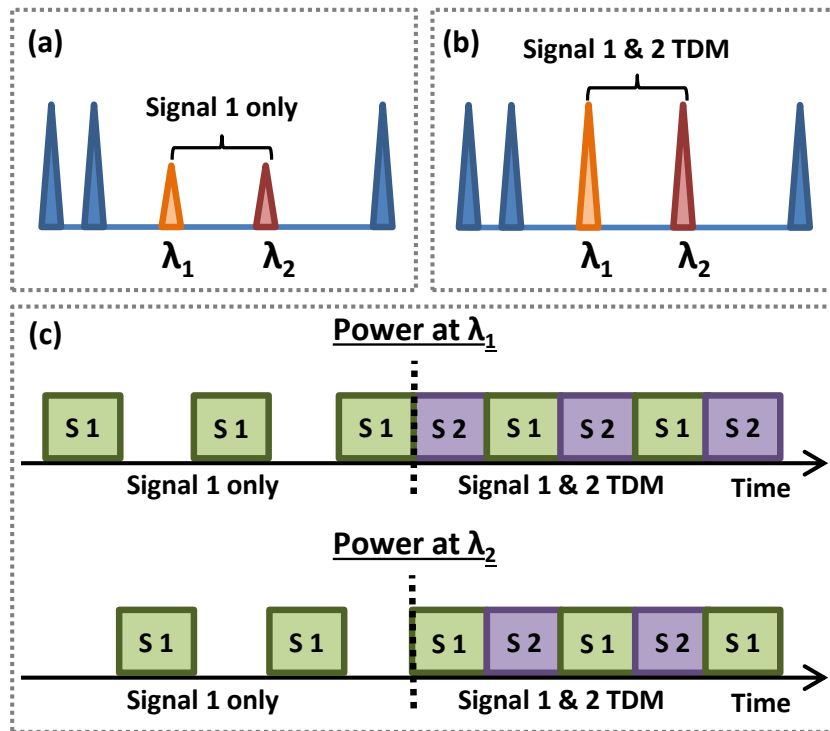
Figure 2.25: (a) Single signal, S1 distributed over two wavelengths (λ_1 and λ_2) as perceived by the EDFA; (b) Additional signal S2 also distributed over the same wavelengths; (c) Power at the two wavelengths at nano-second time scale, illustrating how TDM is achieved

Since the signal is switching over multiple wavelengths, it occupies only a single wavelength at any given instant in time. Thus there are times when a wavelength is not being utilized but is still reserved for the signal, resulting in spectral inefficiency. While this not a problem in lightly loaded networks, it is not scalable for networks that have higher traffic demands. For example, if signals are distributed over 2 wavelength positions, then the total spectral efficiency of the system would be reduced by $\frac{1}{2}$. In order to overcome this issue, time division multiplexing can be used. For example, initially

signal 1 is distributed over λ_1 and λ_2 but occupies either the λ_1 or the λ_2 time slot at any given instant in time. When a new demand for capacity is initiated, and signal 2 is provisioned, it can be distributed over λ_1 and λ_2 as well by ensuring that it occupies the λ_1 slot when signal 1 is at λ_2 and vice versa. The effective power on each wavelength, as perceived by the EDFA, doubles in this case. This concept is illustrated in Fig. 2.25.

2.4.1.3   Network Considerations

New wavelength assignment and network control techniques have to be developed in order to deploy this paradigm in the network. The response of an AGC amplified system can be modeled using the dynamic power control equations outlined in [71]. The model predicts the output powers of WDM channels from an amplified system for different input conditions so that wavelength sets can be chosen intelligently for zero-excursion. The model requires information about the accumulated gain ripple in the amplified link and this can be measured using probe wavelength signals [72, 73]. Fast-tunable lasers can also be used as short duration probes for gain spectrum measurements. In systems that use a wide variety of makes and models of amplifiers, the variation in gain ripple will limit how well the power excursions are reduced. The extent of benefit will depend on how many wavelengths the signals are distributed over and how well they sample the range of gain spectra. Synchronization techniques for the TDM operation have to be explored. Signals from the same source location may use a common low frequency clock for synchronization. Additional TDM synchronization will be required when sources from different locations are multiplexed. Since a signal is distributed over multiple wavelengths, the amount of dispersion will be different for the different wavelengths across the band. Electronic dispersion compensation needs to rapidly compensate for the different amount of dispersion and this can be achieved by using pre-set values given that the switching is between known wavelength sets. For metro-area networks, where dynamicity will be most beneficial, differences in dispersion is not going to be considerable as distances traversed are relatively short. Data on the switching wavelengths can be received error-free within nanoseconds of the switching event. Previously, it was demonstrated that for mth power double differential QPSK signals, data transmission is error free 30 ns after switching [69]. For direct detection burst mode orthogonal frequency division multiplexing (OFDM) signals, error-free transmission is achieved after 8ns [70]. Note that additional delays may be introduced due to group delay differences

between channels at different wavelengths. For dispersion shifted fibers and dispersion compensated systems, this effect is likely to be negligible. For uncompensated standard single mode fiber (SSMF) delays on the order of 1 ns/km are possible leading to 100 ns scale delays in large metro networks. This introduces some amount of overhead in the system. For example, 200 ns dwell time on each wavelength, which is the configuration for this experiment, the overhead (neglecting fiber group delay variations) is 15% for DD-QPSK and 4% for DD-OFDM signals. The overhead can be decreased by increasing the dwell time on each wavelength. For dwell times of 10 s (which is still significantly lower than the EDFA response time), the overhead is less than 1%. The capacity loss due to this amount of overhead is acceptable since this technique allows wavelength re-provisioning on the order of seconds and faster, limited by the switching speeds and not by the optical power tuning. Wavelength re-provisioning using current techniques can take up to days and results in significantly greater capacity loss. The world record for the fastest wavelength provisioning was recently reported as 19 minutes and 1 second [28].

2.4.2 Experiment
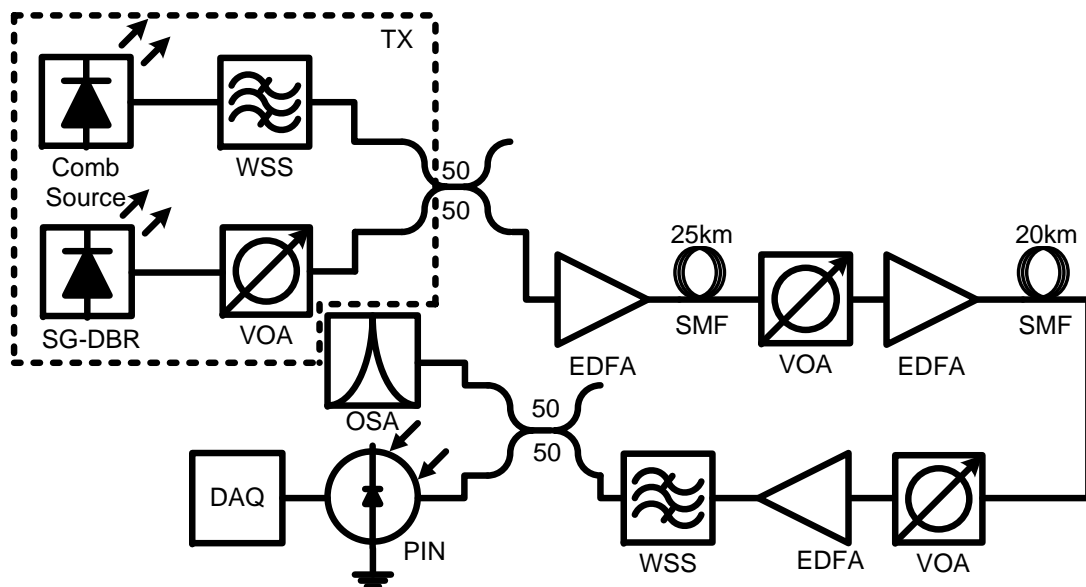
Figure 2.26: Experimental set-up to study the power excursions caused by wavelength switching in a three EDFA metro-scale network
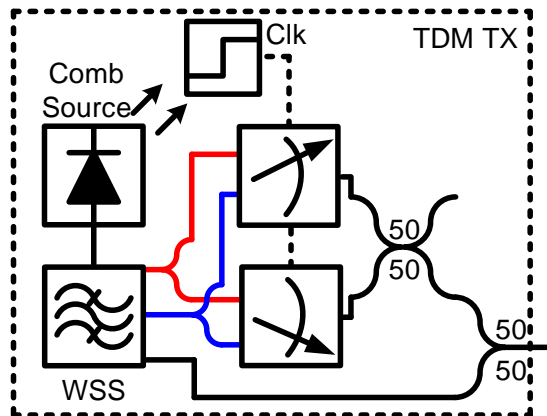
Figure 2.27: Experimental implementation of fast-switching TDM transmitter using a comb source and electro-optic switches, WSS=wavelength selective switch

The experimental set up is shown in Fig. 2.26. A software controlled SG-DBR fast tunable laser is used to perform wavelength switching. The laser can operate in both static and fast-switching modes and can access 83 wavelengths (numbered 11-94) across the 50 G C-band ITU grid. In fast-switching mode, each wavelength can be assigned a dwell time of between 200 ns and 10 μs. Since the power coupling effect due to the wavelength switching is agnostic to the presence of data and depends solely on the wavelength configuration and power values, a comb source in conjunction with a wavelength selective switch (WSS) is used to introduce additional wavelengths across the band. This provides the flexibility to study a wide range of channel configurations and the results for a worst-case scenario are presented in the following section. The input power of all wavelengths is maintained at -23 dBm per wavelength into the first EDFA. All EDFAs operate in constant gain mode at $+18$ dB. Two spans of standard single mode fiber (SSMF) (25 km and 20 km) are used, and VOAs after each span adjust the optical power to an average of -23 dBm per wavelength. A WSS is used to drop one of the static wavelengths which are detected with a 250 MHz PIN detector, followed by a 2 MSa/s data acquisition (ADC) board to measure power dynamics. In order to study time division multiplexing operation, the transmitter block of the setup diagram in Fig. 2.26 is replaced with the transmitter block shown in Fig. 2.27. As only one SG-DBR was available, the TDM operation was synthesized by time multiplexing a pair of CW signals from the comb source using electro optic switches. In this case the switching wavelengths are always on as the fast electro-optic switches are used to switch,

alternately, between the two wavelengths. The two pairs of signals are synchronized with a common clock and combined in a 50/50 optical combiner. Note that this is also an alternative implementation to using a fast tunable laser source: using multiple single wavelength signals and selectively activating or modulating them with a fast switch or modulator. The switch dwell time in this experiment for the TDM case was varied from μs to seconds, with no additional excursions on other wavelengths.

2.4.3 Results and Discussion

2.4.3.1 Balanced Wavelength Switching: Basic Operation

(a)

(b)
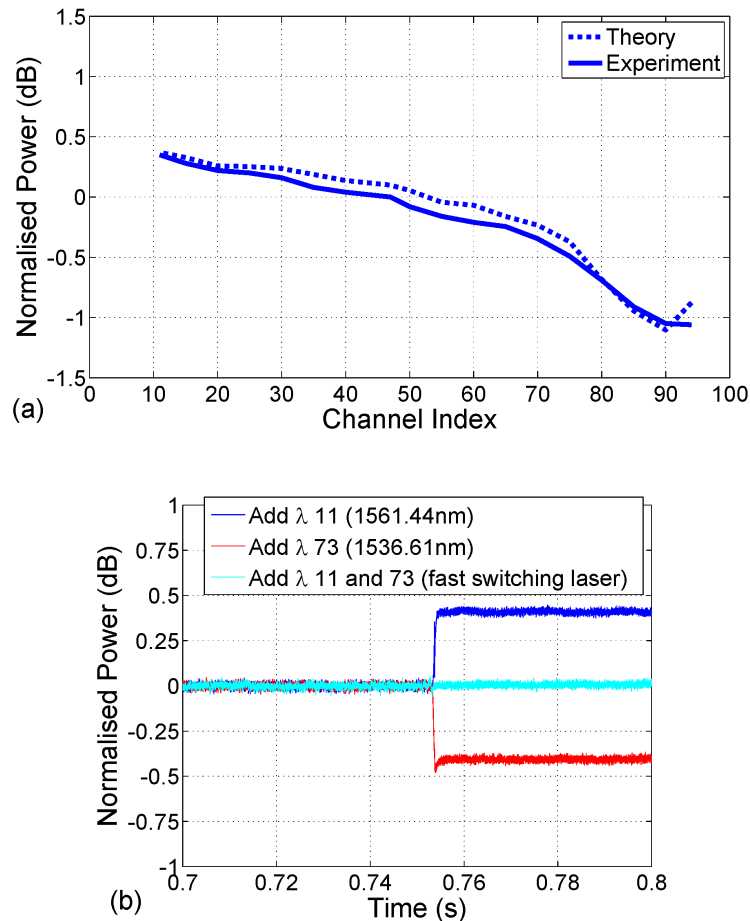
Figure 2.28: (a) Excursions on wavelength 1547.72 nm due to addition a wavelengths across the C-band and (b) Excursions on wavelength 1547.72 nm in the time domain due to addition of individual wavelengths and a balanced pair

Fig. 2.28(a) shows the experimental and modelled power excursion amplitudes, caused by transmission through one EDFA, on wavelength 1547.72 nm (no. 45) when an additional wavelength is added at a wavelength corresponding to the Channel Index on the horizontal axis. The figure shows that the observed wavelength experiences both positive and negative excursions as channels are added at different wavelengths across the spectrum. These excursions are not symmetric as the tilt and ripple functions of the EDFA are not symmetric and the tilt varies with the gain. The figure shows that the addition of wavelength number 11(1561.44 nm) causes an opposite excursion to that caused by wavelength number 73(1536.61 nm): ± 0.4 dB (referred to here as a balanced pair). These excursions are shown in the time domain in Fig. 2.28(b). This figure also shows that no excursion is caused when the laser switches quickly (dwell time = 200 ns) between these two balanced wavelengths. Since the dwell time of the two fast switching channels is below the gain response time of the EDFA (microseconds), they have the same effect as two static channels that cause opposite excursions. Thus, by distributing the channel power over two or more wavelengths that are balanced in this way, the system no longer exhibits channel power excursions when the new signal is added or removed. Thus, persistent power excursions, which are a key limitation preventing dynamic wavelength operation, are removed.

2.4.3.2 Balanced Wavelength Switching: Network Scenario

It is important to show how excursion-free fast wavelength switching can work in a metro network scenario as excursions grow larger with each additional amplifier along the path [60]. To study this we examine wavelength switching of such wavelength distributed signals in a WDM system (the setup in Fig. 2.26) with multiple wavelengths. Figure 6 shows the output spectra of the WDM signals used to test the technique. The accumulated wavelength dependent gain ripple through the system is 7.5 dB. Here the tilt is adjusted to be high to emulate the effect of a much larger amplified system. A single amplifier with large ripple or tilt has been shown to be equivalent to a cascade of identical amplifiers with a combined ripple and tilt of the same form, neglecting gain dependent tilt [60]. Excursions on four wavelengths provided by the comb source (pink) are measured as the SG-DBR is repeatedly moved (on a millisecond time scale) from one balanced pair (switching on a nanosecond time scale) of wavelengths (light blue, 1538.98 nm and 1539.77 nm), to an unbalanced pair (black, 1529.95 nm

and 1530.33 nm), i.e. the SGDBR initially switches on a ns time scale between two balanced wavelengths (light blue), and is quickly reconfigured to switch between two unbalanced wavelengths (black). This reconfiguration, between the balanced pair and the unbalanced pair, is continuously repeated on millisecond time scales. The same measurements are made as the laser repeatedly tunes from one balanced pair (light blue) to another balanced pair (orange, 1535.45 nm and 1554.95 nm). The resultant excursions on the four static wavelengths in the system (pink channels in Fig. 2.29) are shown in Fig. 2.30 which exhibits excursions of around 2 dB on each channel, as the laser repeatedly tunes between a balanced and unbalanced pair. In contrast, excursion-free operation is obtained on all wavelengths when the laser repeatedly tunes between two balanced pairs of wavelengths. We observe similar behavior in simulation. Note that the tuning back and forth between different wavelength pairs, shown in these figures, is on the scale of 100s of microseconds, which is the typical response time of AGC EDFAs. These results show how choosing the ns switching wavelength locations intelligently can provide excursion-free addition, and re-routing, of packet/burst/circuit switched data channels in a network.
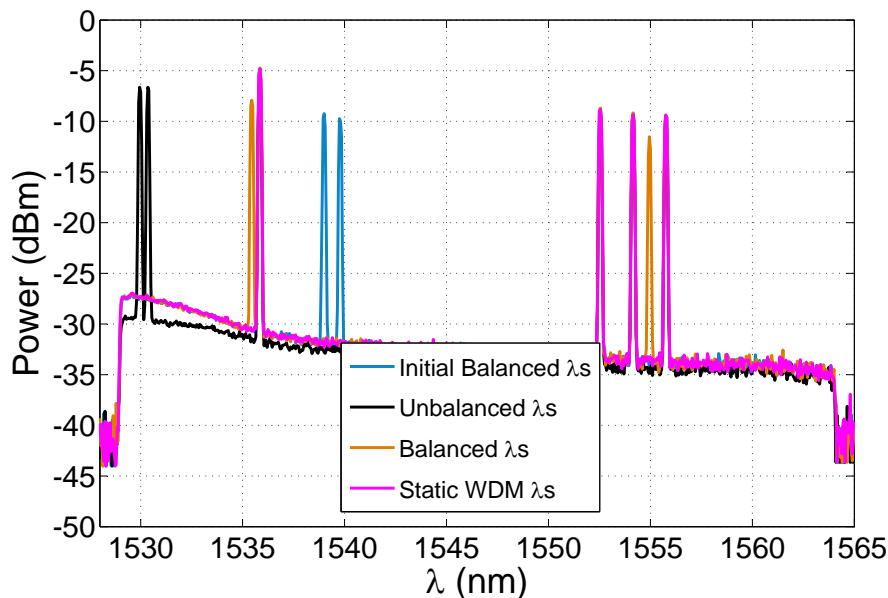
Figure 2.29: Output spectra of static WDM wavelengths and groups of balanced and unbalanced switching wavelengths.
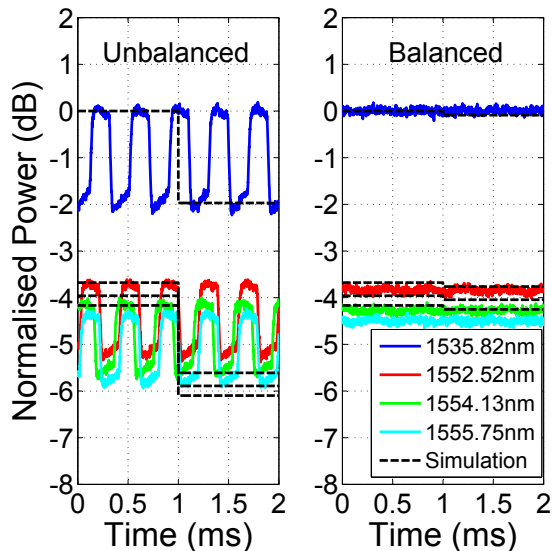
Figure 2.30: Excursions on all static wavelengths, including predictions from the simulation model.

2.4.3.3 Variable Dwell Time Ratio

The results in previous section show the mitigation of power excursions using balanced wavelengths with equal dwell times. As dwell times are well below the EDFA response time, the addition of this pair of switching wavelengths is the equivalent, to the amplifier, of adding two static wavelengths at 3 dB below their actual input power. i.e. the equal allocation of sub EDFA response dwell times, translates (from the point of view of the EDFA) to distributing the instantaneous optical power equally over two wavelengths. This effect can be observed in Fig. 2.29 because the sweep time of the optical spectrum analyzer used is also significantly longer than the dwell time. In the figure, switching wavelength pairs are both shown to have a power of 3 dB below neighboring static wavelengths, even though all launch powers are maintained instantaneously at -23 dBm. As the AGC EDFA algorithm works by monitoring the total input optical power, power excursions arising from the addition of new wavelengths depend on the input power of those wavelengths (as they appear to the EDFA) and by extension, the ratio of the switching wavelength dwell times. Fig. 2.31 shows unbalanced switching wavelengths with variable DTRs used for excursion free operation. The same static wavelengths (pink) and initial balanced switching wavelengths (blue), as outlined in

section 2.4.3.2, are used. This time however, the laser is reconfigured to switch between the unbalanced pair 1561.42 nm and 1530.33 nm (solid black, Fig. 2.31 a). A second unbalanced pair, 1549.75 nm and 1530.33 nm (dashed black, Fig. 2.31 b), is also demonstrated. Fig. 2.32 a shows excursions on all static channels when the laser is reconfigured from the balanced pair (blue) to the unbalanced pair (solid black in Fig. 2.31 a), for DTRs of 1:1 and 4:1. When equal dwell times are employed there is a residual excursion of about 1 dB on all wavelengths. However, with a DTR of 4:1, excursion free operation is achieved as the effective contributions to excursion, from either wavelength, are equalized. Fig. 2.32 b shows the same results for the second wavelength pair used (dashed black in Fig. 2.31 b). In this case, a wavelength closer to the mean gain of the channel, 1549.75 nm, is used in conjunction with 1530.33 nm to balance the excursions. As the new wavelength causes smaller excursion than the previous one, an increased DTR of 6:1 is required to achieve excursion free operation.
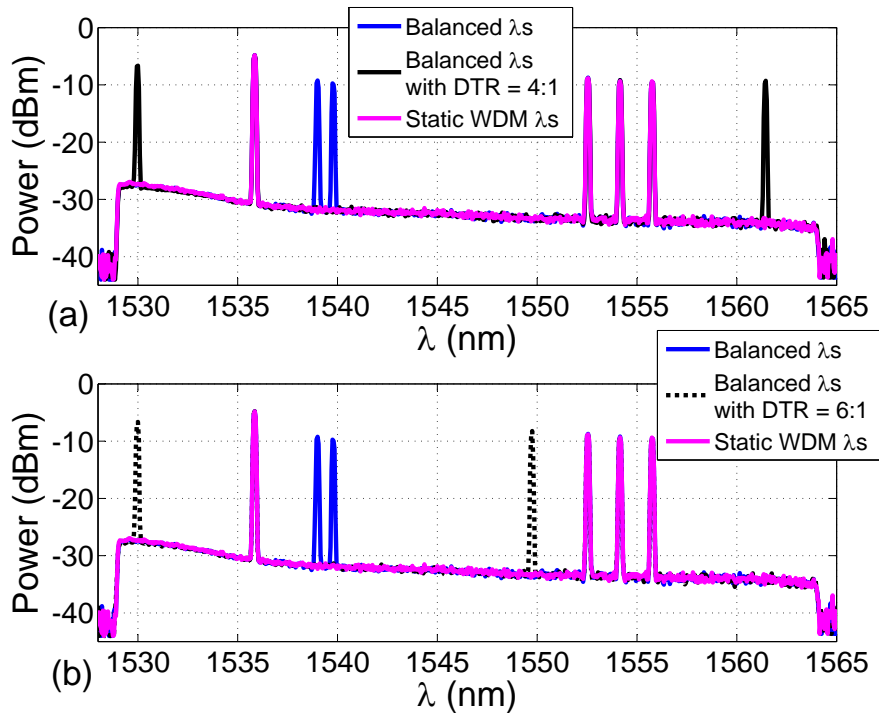
Figure 2.31: Spectra of the network configuration with a balanced wavelength pair (blue) and balanced wavelength pairs with different dwell time ratios (black).
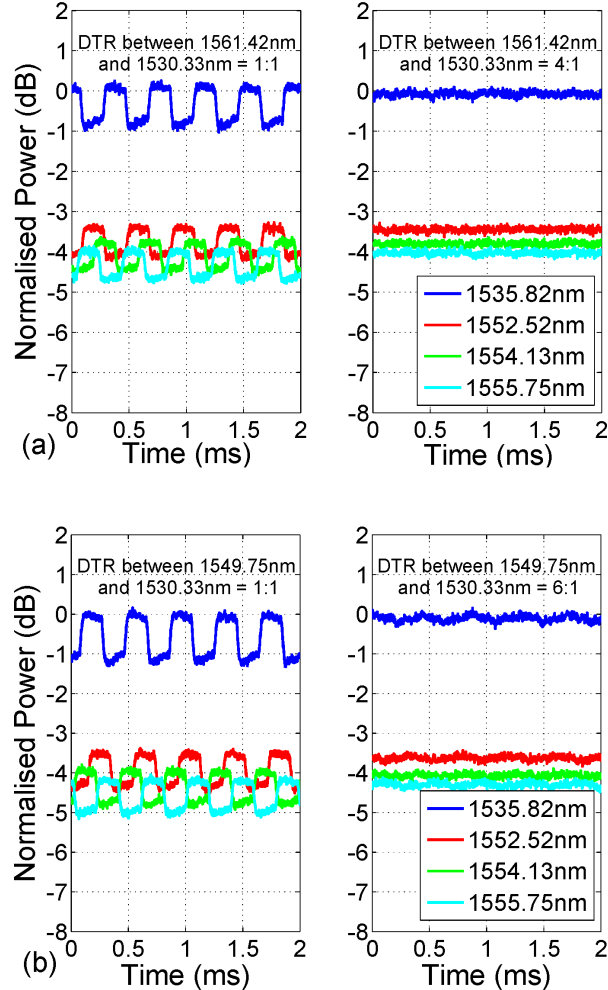
Figure 2.32: Excursions on all static wavelengths for (a) wavelength switching with DTRs
of 1:1 and 4:1 (solid black, Fig. 2.31 a), (b) wavelength switching with DTRs of 1:1 and
6:1 (dashed black, Fig. 2.31 b)

2.4.3.4 Time Division Multiplexing

The effect of TDM switching signals on channel power is also studied. Fig. 2.33
shows the excursions on the wavelengths in the system (pink in Fig. 2.29) when the
two time multiplexed CW signals are changed, between the two balanced wavelength
pairs (light blue and orange in Fig. 2.29) as outlined in section 2.4.3.2. Excursions
of <0.1 dB are achieved on all measured wavelengths. In the TDM configuration, for
dwell times ranging from seconds down to 125 μs, negligible excursions are observed
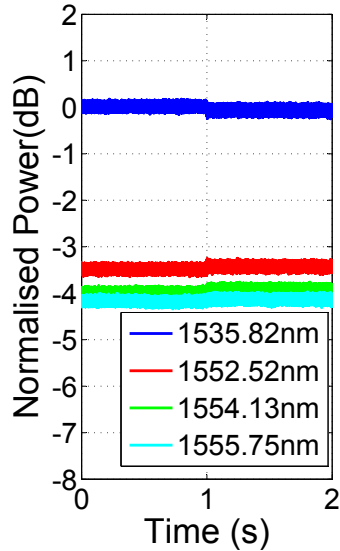
Figure 2.33: Power excursion from balanced TDM wavelength switching

as the multiplexed wavelengths smoothly alternate within the time slots and are well synchronized.

2.5 Conclusion

This chapter presents two different techniques of enabling rapid wavelength reconfiguration in amplified optical networks by leveraging the temporal properties of amplifiers to manage the amount of channel power transients.

The first technique, which can be easily integrated into current networking systems, results in either longer or shorter reconfiguration times compared to conventional method, depending on the specific network scenario. However, regardless of the total reconfiguration time, the proposed technique always yields a significantly lower data loss during the reconfiguration process. Results from implementing this technique in a metro-scale test-bed establish that the data loss using the proposed technique is 1000X less than the conventional method, making it a viable option for frequent, rapid wavelength re-configuration.

The second method, where optical channel is distributed over multiple wavelengths chosen to null any power excursions, opens up an entirely new form of wavelength division multiplexing paradigm. As results of deploying this technique in a metro-

55

scale test-bed demonstrate, it can be used for excursion-free switching over a range of wavelengths, without loss of spectral efficiency, enabling rapid growth and re-routing of wavelengths in a network.

Chapter 3

Real-Time Awareness of Physical Layer Impairments

3.1 Cross-Layer Approach
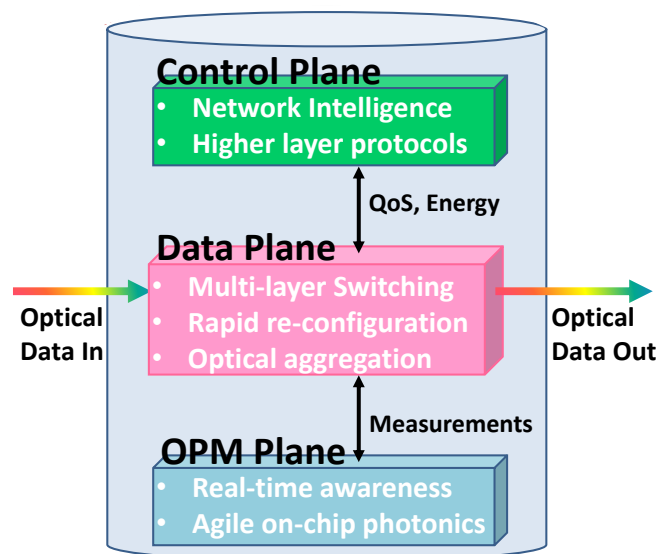
Figure 3.1: Cross-layer node that allows bi-directional communication between the different layers of the network protocol stack.

Cross-layer networking has been proposed as an enabler of intelligence and agility in the optical layer [2, 55, 77, 78, 79, 80]. Fig. 3.1 depicts the architecture of a cross-layer enabled node that allows bi-directional signalling between the different layer of

the network protocol stack. Such a networking paradigm is crucial for achieving real-time awareness in an agile optical network as it allows the measurements made by the advanced optical performance monitors embedded in the physical layer to be communicated to the control plane. Real-time introspection into the physical layer can thus be used in conjunction with awareness of higher layer network constraints (e.g., application, quality of service requirements, and energy consumption) for informed routing, regeneration, modulation, and power control decisions, enhancing the network performance. Several advanced optical performance monitors have been successfully integrated in the cross-layer node; here, we focus on extending the functionality of one of the OPMs [54, 81].

3.2 Delay-Line-Interferometer(DLI) based Optical-Signal-to-Noise-Ratio (OSNR) Monitor

OSNR monitoring using a delay-line interferometer (Fig. 3.2) has been extensively studied since it was first proposed in 2001 [82]. It is a promising distributed OSNR monitoring solution of single channel systems as it supports multiple advanced modulation formats [8, 83] and can be easily integrated in the silicon photonics platform [84]. This technique relies on the fact that the signal is coherent and undergoes constructive and destructive interference in the DLI whereas noise is incoherent and experiences simple power splitting. The OSNR of a signal is thus proportional to the ratio of the average powers at the constructive (P_{Const}) and destructive (P_{Dest}) output ports of the DLI. Signal and noise behavior at a $\frac{1}{4}$-bit DLI is illustrated in Fig. 3.3 to explain this concept. In order to calculate the OSNR of a signal from the ratio, the signal distribution ratio (α) and the noise distribution ratio (β) is determined. α is the ratio of constructive power to destructive power in presence of signal only (> 30 dB OSNR) while β is the same ratio is presence of noise only. The values of α and β are determined by the filter bandwidth, free spectral range of the DLI and modulation format of signal. Due to the superposition property of the monitor components, the following equations can be used to calculate the measured OSNR:

$$P_{Const} = \frac{\alpha}{\alpha + 1} P_{Signal} + \frac{\beta}{\beta + 1} P_{Noise} \tag{3.1}$$

$$P_{Dest} = \frac{1}{\alpha + 1} P_{Signal} + \frac{1}{\beta + 1} P_{Noise} \tag{3.2}$$

$$ONSR = \frac{P_{Signal}}{P_{Noise}} = \frac{(\alpha + 1) * (P_{Const} - \beta * P_{Dest})}{(\beta + 1) * (\alpha * P_{Dest} - P_{Const})} \tag{3.3}$$
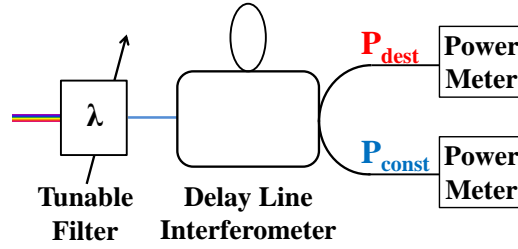
Figure 3.2: Block diagram of a DLI-based OSNR monitor for WDM channels
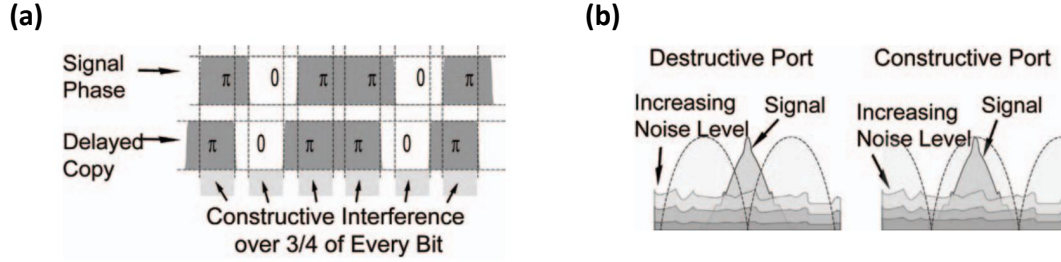
Figure 3.3: (a) Concept of $\frac{1}{4}$-bit delay interferometer. Constructive interference of a signal bit onto itself for $\frac{3}{4}$ of the bit period while noise splits between the constructive and destructive arm. (b) Concept of $\frac{1}{4}$-bit delay in the spectral domain. Most of the signal is notched out in the destructive port. The power ratio between the two arms is directly related to the OSNR. (adapted from [8])

3.3 Pilot Tones for Autonomous OSNR Monitoring and Cross-Layer Control

In this work, modulation-format and bit-rate awareness is realized in DLI-based OSNR monitor (section 3.2) using pilot tones. The use of PT assisted DLI OSNR monitor for autonomous signal quality decisions in a mixed-signal environment is demonstrated.
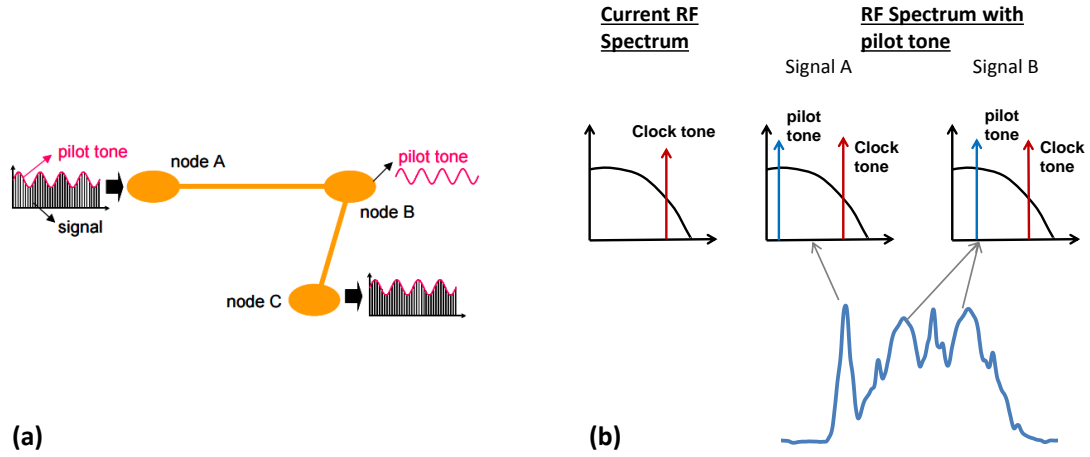
Figure 3.4: (a) Unique low frequency pilot tone is added to each signal at the transmitter to act as a signature for that signal. (adapted from [9]) (b) RF spectrum can be used to detect the pilot tone.

3.3.1 Pilot Tones for Signal Identification

One of the limitations of the DLI-based OSNR monitor described in section 3.2 is that its measurements are dependent on the data rate and modulation format of the signal under test. For this device to function effectively in future optical networks, which will potentially be operating in a mixed line rate and modulation formats framework [85], it is imperative to distinguish the properties of the monitored signal. In this work, low frequency pilot tones – weak modulation components added to WDM signals – are used to identify the signal properties at the monitoring site, enabling the use of a DLI-based OSNR monitor for cross-layer impairment-aware routing in a mixed signal environment. This concept is illustrated in Fig. 3.4. Pilot tones have a relatively small effect on the signal quality and can be easily detected at the monitoring site with simple low power digital signal processing without hampering integration efforts. In addition, pilot tones can be used as an indicator of channel presence, enabling the monitor to detect channel loss rapidly. The proposed pilot-tone assisted OSNR monitor enables a network node to operate as an autonomous monitoring and control unit, a functionality that becomes highly advantageous as next generation network architectures evolve towards a Unified Control Plane (UCP) paradigm. Centralized control platform provides flexible network management capabilities and is promising for dynamic service-aware optical networks. Software defined networking (SDN), using the OpenFlow protocol based UCP, has al-

ready been demonstrated to enable dynamic cross-layer path creation, restoration and transponder control and application aware dynamic path configuration in multi-layer multi-granularity optical networks [86, 87]. However the centralized controller runs the risk of being overwhelmed by the level of signaling that would be required to control the physical layer. Providing autonomous and distributed monitoring and control capabilities within the physical layer has the potential to reduce the complexity of the control plane and improve network performance. If the UCP were to become isolated from a network node or if it were disseminating erroneous information regarding the signal type, a network node would continue to operate independently using information from the monitoring device, thus ensuring data protection.

3.3.2 Pilot Tone Assisted Delay-Line-Interferometer

The structure of the proposed pilot-tone assisted DLI-based OSNR monitor is shown in Fig. 3.5. It has been modified from the DLI-monitor illustrated in Fig. 3.2 to include a simple DSP unit that processes the output from the photodiode at the constructive port to extract the pilot tone frequency. This is reported along with the powers to the control plane which can then determine the actual OSNR of the signal. The mapping of the actual OSNR and the measured ratio varies with the data rate and modulation format (Fig. 3.6). In our proposed solution, a unique low frequency pilot tone is added to each type of signal at the transmitter to act as an identification code. In the past, pilot tones have been shown to be an effective means of labeling signals and for providing signal presence and power information. In this work, we investigate their use in conjunction with advanced OPM to facilitate measurements in a mixed
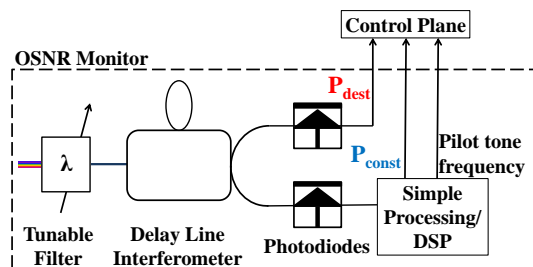
Figure 3.5: Pilot tone assisted DLI-based OSNR monitor which uses pilot tones to identify signal properties for correct interpretation of OSNR from $\frac{P_{const}}{P_{dest}}$ ratio

Experimental Results **VPI Simulation Results**
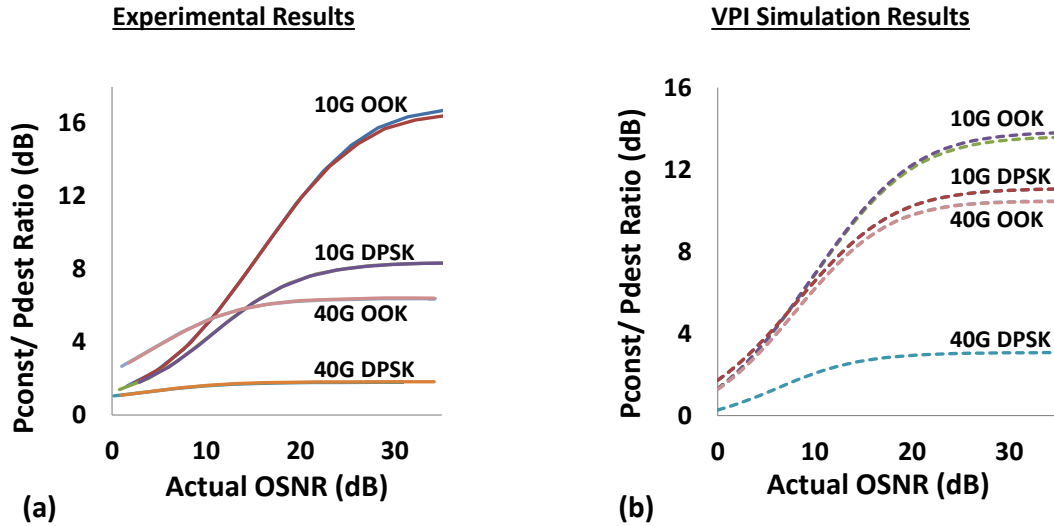
Figure 3.6: Measured(a) and simulated(b) ratio for different signals. Each set consists of no pilot tone and the worst discrepancy pilot tone, establishing that pilot tones have negligible effect on DLI readings. Simulation results were generated by VPITransmissionMaker

signal environment in conjunction with a cross-layer centralized controller. For the purposes of characterizing and demonstrating the key performance requirements, we use a single frequency intensity modulated tone, however, these results are relevant for a variety of tone modulation techniques [9]. To ensure that pilot tones do not have a significant impact on the DLI measurements, the effect of the following on the OSNR curves of different data signals (10G OOK, 40G OOK, 10G DPSK and 40G DPSK) was investigated:

1. Different frequency pilot tones (5MHz, 10MHz, 15MHz, and 1GHz) at constant modulation index (0.2)

2. Constant frequency pilot tones (10MHz) at different modulation indices (0.1, 0.2, and 0.3)

The worst case discrepancies from both experiment and simulations (Fig. 3.6) establish that pilot tones have no significant effect on monitor readings and can be used for signal property identification. The DLI used in the experiment is a commercially available 40GHz optical DPSK demodulator from Optoplex.

3.3.3 Experimental Validation in Cross-Layer Enabled Network Node
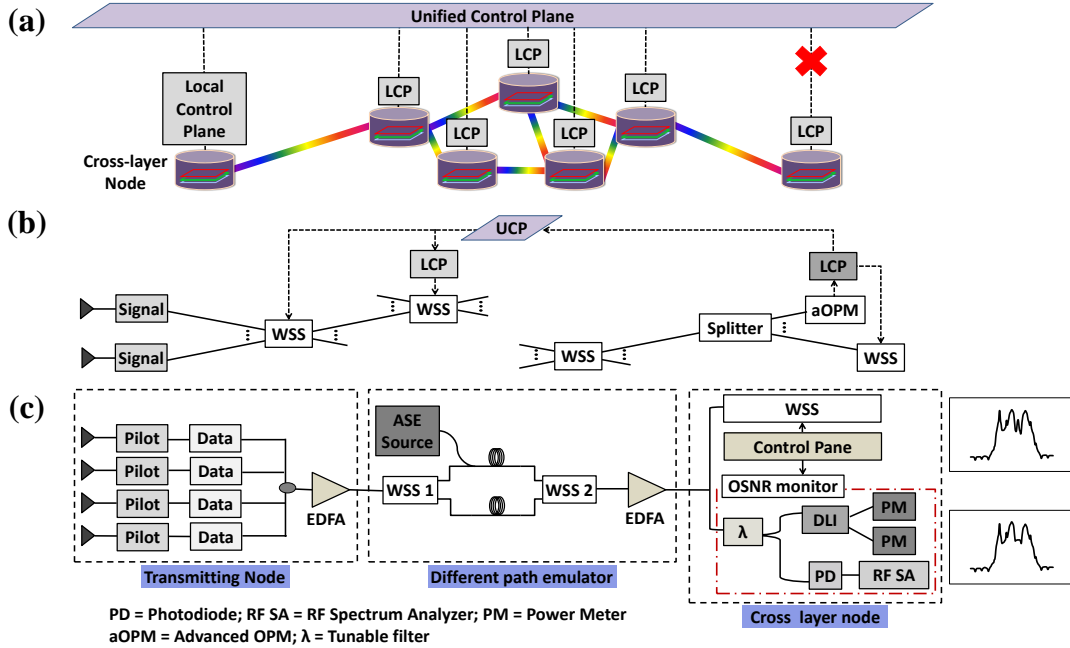
Figure 3.7: (a) Cross-layer enabled network with local control plane for autonomous monitoring and control. (b) Component level view of the network illustrating the control loop initiated in response to a low OSNR signal detected at a node. The signal is dropped locally and the LCP communicates with the UCP to implement intelligent rerouting. (c) Experimental test-bed to validate the performance of the monitor in a mixed signal environment. The cross-layer node emulates an isolated node and is demonstrated to have autonomous monitoring and management capabilities. Optical spectra of different test cases at the cross-layer node are shown.

The performance of the proposed monitor in a cross-layer enabled node is experimentally validated using the testbed depicted in Fig. 3.7 . The transmitting node injects four different types of signals (10G OOK, 10G DPSK, 40G OOK and 40G DPSK), each with a unique intensity modulated pilot tone, into the test-bed to create a mixed signal environment. To emulate traversal over different distances and paths, wavelength selective switch (WSS 1) switches each signal either onto the impaired or the good link to vary the OSNR and amount of cross-talk on each signal. At the cross-layer enabled node, a portion of the power is tapped off for monitoring. The tapped signal is divided equally between a photodiode connected to a radio-frequency (RF) spectrum analyzer

and a DLI whose output ports are connected to power-meters. A software control plane communicates with these measurement devices and extracts the values for Pconst, Pdest and the pilot tone frequency with the highest signal-to-noise-ratio (SNR) to calculate the OSNR of the signal. If the calculated OSNR is below a pre-defined threshold, that particular signal is dropped. The proposed monitor operates accurately even in a dense-wavelength-division-multiplexed (DWDM) system where cross-talk causes pilot tone leakage between neighboring channels. To ensure the robustness of the proposed monitor, we studied the behavior of pilot tones for the worst cross-talk signal configuration in our test-bed (10G DPSK signal surrounded by two 40G DPSK signal on the 50G ITU grid) under different test conditions. In particular, we demonstrate the results of: (i) varying the OSNR of the center channel (signal under test) and (ii) varying the
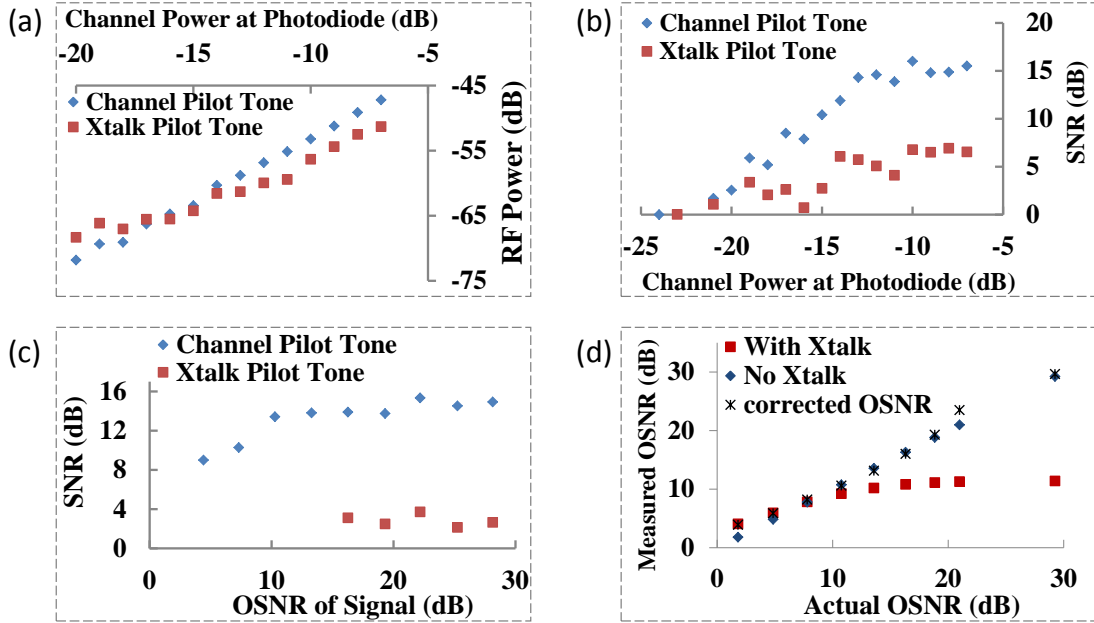
Figure 3.8: (a) In the presence of high cross-talk, even at low OSNRs, there is a strong enough channel pilot tone and no cross-talk pilot tone.(b) Using SNR at a given frequency, the channel pilot tone can be distinguished from the cross-talk frequency up to -18 dBm input power at detector. (c) Using the RF power at a given frequency, the channel pilot tone can be distinguished from the cross-talk frequency up to -13 dBm input power at detector. (d) Presence of high cross-talk causes errors in the OSNR measured by DLI-based OSNR monitor. The strength of the cross-talk pilot tone can be used as an indicator of the level of cross-talk to determine a correction factor.

signal power of high OSNR center channel while maintaining high power and OSNR at neighboring channels. Results show that the pilot tone frequency of the signal under test is always the dominant frequency, ensuring correct operation of the monitor even with significant amounts of cross-talk (Fig. 3.8 a,b,c). The cross-talk frequency can instead be used as a signal to the control plane to correct for the error in the OSNR measurement of the DLI that arises due to cross-talk (Fig. 3.8 d).

3.3.4 Impact of Cross-Talk on Pilot Tone and OSNR Monitor Measurements

The impact of varying the amount cross-talk on the DLI power ratio, signal PT and XT PT measurements is investigated for the worst cross-talk signal configuration in the test-bed. The power of the channel under test (designated CuT hereafter) is kept constant while the power of the two neighboring channels (designated NC hereafter) are varied to achieve different amounts of XT. XT values are measured at WSS 1 and defined as the the following:

$$Cross - Talk = \frac{power\ of\ CuT\ in\ the\ filter\ passband\ of\ CuT}{power\ on\ NC\ in\ the\ filter\ passband\ of\ CuT} \qquad (3.4)$$

For each cross-talk value, the OSNR of the CuT is varied while maintaining high OSNR on the NC; the corresponding DLI power ratio and SNRs of the pilot tones of CuT and NC at the OSNR monitor are recorded. The power at the monitor kept constant. As can be seen from Fig. 3.9, increasing channel cross-talk results in decreasing the dynamic range of the DLI power ratio. For cross-talk values less than -21 dB, the DLI power ratio for a signal with XT is very similar to the that with no XT. As cross-talk increases beyond -21 dB, the measured DLI power ratio deviates significantly from that of a signal with no XT. Fig. 3.10 illustrates the impact of varying signal cross-talk on the SNRs of the CuT pilot tone and XT pilot tone. XT PT is detected only when signal cross-talk exceeds -10 dB and its SNR increases with increasing XT. The power of the CuT PT, on the other hand, is fairly steady at low cross-talk values and start decreasing with increasing cross-talk when XT exceeds -10 dB. This phenomenon arises because total power into the monitor is kept constant, resulting in decreasing power

on CuT and increasing power on NCs as cross-talk increases. While it is unlikely that at such high XT values, the data on the CuT to be recovered error-free, the XT PT measurements at the DLI-OSNR monitor can serve as a powerful diagnostic tool for network management. XT PT provides information on the specfic signals inducing the XT and the magnitude of the XT. This information can be used by the network control plane for loaclising where in the network the cross-talk arises.
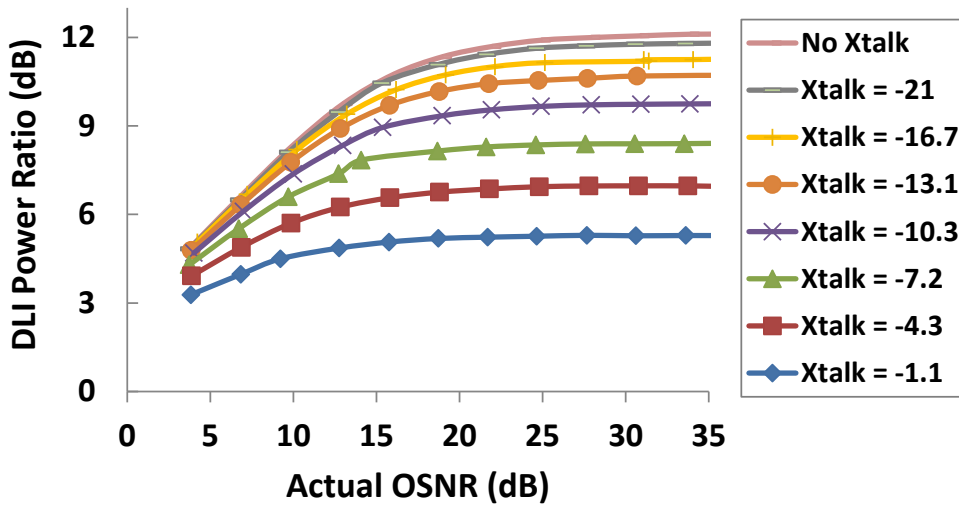
Figure 3.9: Impact of signal cross-talk on the DLI power ratio.
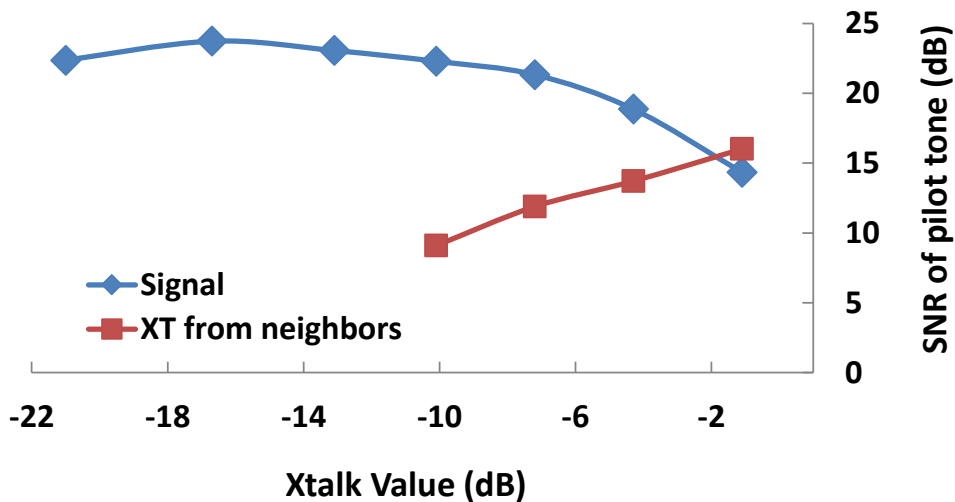
Figure 3.10: Impact of signal cross-talk on the SNRs of the PT of channel under test and corss-talk PT induced by neighboring channels.

3.4 In-Band OSNR Monitoring of Orthogonal Frequency Division Multiplexed (OFDM) Signals

In this work, the use of the DLI-based monitoring technique (described in section 3.2) for measuring OSNR of electrical OFDM signals is investigated. Since OFDM is emerging as a potential modulation format for next-generation networks, it is critical to develop reliable monitoring solutions for such signals. The response of the DLI monitor to OFDM signals with different bandwidths and modulation formats, including adaptive modulation formats, is studied. The use of this monitor for cross-layer impairment-aware modulation format adaptation and wavelength re-routing of WDM OFDM channels is demonstrated in a metro-scale test-bed.

3.4.1 OFDM Signals for Agile Networks

Orthogonal Frequency Division Multiplexing (OFDM) is a MultiCarrier Modulation (MCM) technique where data is distributed over multiple orthogonal, low data rate sub-carriers. Since the sub-carriers are orthogonal, they can overlap without any detrimental interference effects. By leveraging this property, OFDM can transmit a greater number of sub-carriers in a given bandwidth compared to WDM systems, where wavelengths have to kept separate for minimum cross-talk. Thus, OFDM enables more efficient use of limited spectral resources, as illustrated in Fig. 3.11. Another advantage of OFDM signals is its lower susceptibility to inter-symbol interference (ISI). Since OFDM is comprised of multiple lower data rate sub-carriers, the per-subcarrier symbol duration is significantly longer than that of a single-carrier system at the same total data rate, resulting in reduced ISI. OFDM is emerging is a potential modulation format for agile optical networks as it can accommodate varying traffic demands
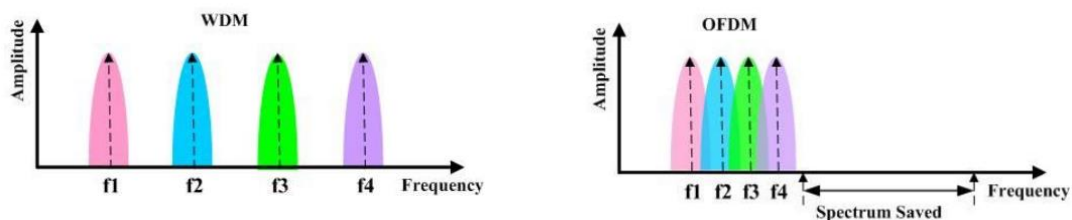
Figure 3.11: Spectrum of WDM signals and OFDM signal (adapted from [10])

with fine-granularity by adaptively changing the subcarrier number, symbol rate, or modulation format.

As detailed in chapter 1, network traffic is increasing at a near exponential rates and is comprised of predominantly unpredictable, short-lived but high bandwidth edge traffic flows. As network traffic becomes more uncertain and heterogeneous, traditional wavelength-routed WDM networks, with coarse and rigid granularity, result in inefficient capacity utilization, a problem that will become more acute with the deployment of higher capacity WDM networks (40Gb/s and 100Gb/s per channel systems) [88, 89]. A promising direction to address these challenges in a cost-effective, scalable and energy efficient manner is a flexible network with fine granularity that can adaptively provide the required capacity to sub- or super-wavelength demands. While approaches such as optical burst switching (OBS) and optical packet switching (OPS) would be ideal solutions, their enabling technologies are still too immature for them to be feasible near-term solutions [90]. Elastic optical networking, employing Orthogonal Frequency-Division Multiplexing (OFDM), is being considered as a potential enabling technology [91, 92]. Elastic networking techniques such as bandwidth-variable (BV) transponders, bandwidth-variable optical cross-connects, dynamic resource allocation through SDN protocols have been demonstrated in OFDM architectures [89, 93, 94, 95, 96].

3.4.2 DLI for OSNR Monitoring of OFDM signals

As outlined in section 3.1, real-time advanced optical performance monitoring (aOPM) is advantageous for managing signal quality and reliability, especially in an agile network. OSNR required for error-free transmission of an OFDM signal depends on the modulation format, subcarrier count and spacing to the neighboring channels [97]. Routing and traffic allocation algorithms have to take these factors into account when provisioning or rerouting a channel and will benefit greatly from real-time knowledge the state of the physical layer. Previous work has demonstrated improved network performance with the use of an OpenFlow based control plane for dynamic allocation of OFDM signal resources in response to changing transmission link conditions [96].

The DLI-based technique (section 3.2) is a particularly attractive monitoring solution for OFDM signals because it would provide three distinct advantages over other proposed in-network OSNR monitors:

- more cost-effective as it relies on low power and low speed electronics for optical power measurements [98, 99]

- unlike spectral analysis, it can accurately measure the in-band OSNR for high spectral density WDM including narrowly spaced OFDM channels [100]

- it supports polarization-muxed, advanced modulation format data streams [83]

However, while this technique has been widely studied for phase and amplitude modulated signals, this is the first investigation of its response to OFDM signals. In the case of OFDM, continuous wavelength (CW) light is amplitude modulated with the complex electrical OFDM modulation signal. The resulting optical amplitude will exhibit large fluctuations over the sub-carrier symbol period, given by the sum of the complex amplitudes of each of the sub-carrier symbols. The highest frequency components will be $\frac{2}{T_S}$, where T_S is the OFDM symbol period. Thus, for DLI delays much less than T_S, the signal should behave like CW light. For DLI delays approaching and longer than the symbol period, the extinction of the signal will be limited by the differences in amplitude between the interfering fields and these variations will be averaged in the monitor detectors. This effect will limit the dynamic range of the monitoring signal. Because the OFDM signals are amplitude modulated onto the optical carrier, different modulation formats should show similar behavior depending on the baud rate and on the magnitude of the amplitude fluctuations. We performed experiments to study these effects for OSNR monitoring on OFDM signals with different modulation formats and baud rates.

3.4.2.1 Experimental Set-Up

The experimental set-up for studying the DLI based OSNR monitor used for OFDM signals is shown in Fig. 3.12. MATLAB is used to generate the OFDM signal offline and since intensity modulation and direct detection (IMDD) OFDM scheme is used, the IFFT size is twice the total number of OFDM subcarriers to maintain Hermitian symmetry. 512 point IFFT scheme for 256 subcarrier OFDM is used in this experiment. No cyclic prefix is used as the OFDM signals are transmitted over relatively short, dispersion compensated transmission links in a metro-scale test-bed and consequently,

the effect of dispersion is mild. The OFDM signal is pre-compensated for the zeroth-order hold frequency response of the arbitrary waveform generator (AWG) digital-to-analog converter (DAC). Electrical OFDM signal from the AWG is used to drive a Mach-Zehnder modulator (MZM) biased at quadrature to generate a WDM double side-band (DSB) optical OFDM signal. OSNR is degraded by coupling in variable amounts of noise from a high-power ASE source into the signal. Half of the impaired signal is sent to an optical spectrum analyser (OSA) for reference OSNR measurements at 0.1 nm bandwidth and the other half is sent to the DLI-based OSNR monitor, where the signal under test is filtered using a tunable optical filter. The DLIs used in this experiment are commercially available Optoplex 40G fixed and tunable wavelegth optical DPSK demodulators with a delay of 25 ps. Power meters, with 0.01 dB resolution and 200 ms averaging time, are used to measure the optical power at the constructive and destructive ports.
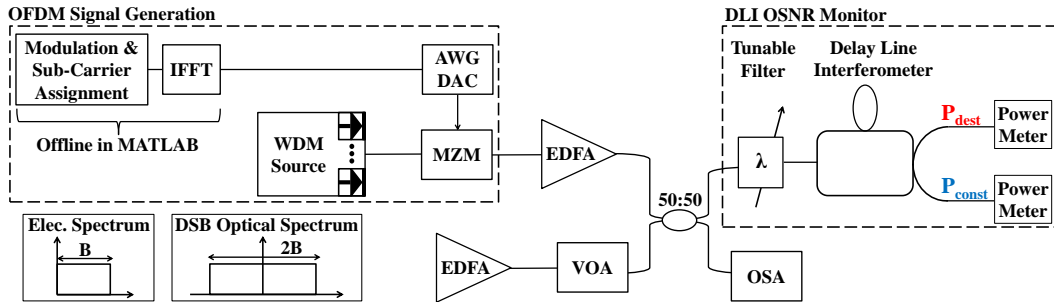
Figure 3.12: Experimental set-up for coupling a double side band OFDM signal with variable amounts of noise to investigate the reliability of the DLI-based OSNR monitor in measuring the OSNR

3.4.2.2 Measurement of In-Band OSNR of Wavelength-Division-Multiplexed (WDM) OFDM Channels

One of the biggest advantages of an OFDM transmission system is that, by enabling flexible networking with much finer granularity than traditional WDM, it can achieve high spectral efficiency. However, as the spacing between neighboring wavelengths decreases, it becomes increasingly difficult to identify the noise levels associated with a given wavelength channel. The ability to use even a high resolution OSA for in-service,
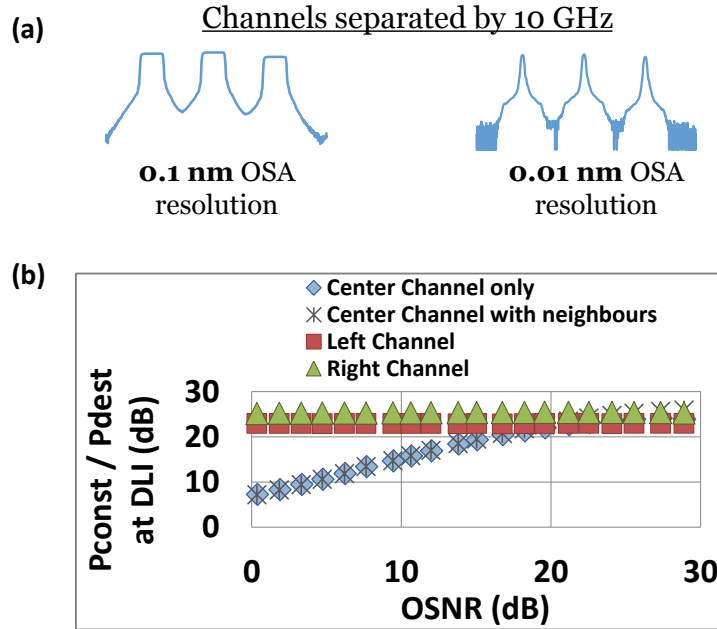
Figure 3.13: (a) Three OFDM channels separated by 10 GHz at different OSA resolutions. Even at 0.01 OSA resolution, it is difficult to isolate the noise associated with a given channel. (b) Measurements of the DLI power ratio of the center channel made in the presence and absence of neighboring channels are identical for OSNRs up to 22 dB, indicating that this technique can be used to reliably measure OSNR of narrowly spaced wavelength channels.

in-band OSNR measurements becomes very limited. Since the DLI technique uses the actual in-band noise for measurements, OSNR readings of any given signal are not affected by the spacing between it and its neighboring signals. As long as a wavelength channel can be distinctly filtered from its neighbours, its in-band noise will undergo passive power splitting at the DLI-monitor and its OSNR will be measured accurately. To demonstrate that OSNR measurement of a signal is not affected by presence of neighboring signals, three OFDM signals at 1550.836 nm, 1551.12 nm and 1551.395 nm are used to create a 35 GHz spaced WDM signal. Each signal is modulated with 12 Gbaud QPSK data and since double side-band ODFM is used, the total spectral bandwidth of each signal is 24 GHz. Initially all three wavelength channels have high OSNRs; the OSNRs of the left and right channels are kept constant while that of the center the channel is varied. Every time OSNR of the center channel is changed, each of the three channels is individually filtered and the ratio of the constructive

and destructive powers at the DLI is measured, as shown in Fig. 3.13. The two
neighboring channels are then turned off and the procedure is repeated. DLI power ratio
measurements of the center channel made in the presence and absence of neighboring
channels are identical for OSNRs up to 22dB.

3.4.2.3 DLI Response to OFDM signals with Different Parameters

In order to study the parameter space of DLI response to OFDM signals, the following
scenarios were investigated:

1. different bandwidth signals with the same modulation format (Fig. 3.14 a,b,c,d)

2. different modulation format signals for a given baud rate (Fig. 3.15 a,b,c,d)

3. different wavelengths across the C-band for the same signal (Fig. 3.16 a,b)

The experimental results for 1 and 2 are further validated using commercial simu-
lation software, VPItransmission Maker V9.1. Simulation results indicate that the DLI
monitor is agnostic to the bandwidth of the signal under test (Fig. 3.14 a) and the
response is identical to that of CW light at low OSNRs. For experimental results as
well, the response is very similar to that of CW light at low OSNRs. However, for band-
widths greater than a certain critical bandwidth the response diverges from that of CW
light. At low baud rates, the frequency of amplitude fluctuations is much longer than
the delay between the two arms of the DLI and therefore the signal does not change
over the delay and as expected, the response is similar to CW light. For symbol periods
approaching the DLI delay, the delayed copy will differ in amplitude with increasing
frequency and the DLI ratio will reach a limit. For a DLI delay of 25 ps, we find that
the dynamic range of the monitoring is limited for baud rates above 6 Gbaud, which
corresponds to maximum amplitude fluctuations of roughly 12 GHz or 83 ps. Thus the
DLI delay is sampling at a third of the period of the fastest variations. The DLI ratio
of constructive to destructive interference is still roughly 22 dB in experiment and 30
dB in simulation. Note that the baud rate corresponds to a single side band of the
double sideband OFDM signal. Using the specific values of α and β for each signal, the
measured OSNR of the signal is calculated from the power ratios (Fig. 3.14 c). Since
a fixed-wavelength DLI was used for the characterization, a constant correction factor
is added to Eq. 3.3 to account for the lack of fine tuning. The error i.e. the difference

between the actual OSNR and that measured by the DLI (Fig. 3.14 d) is maintained between ± 0.5 dB for OSNRs up to 28 dB.
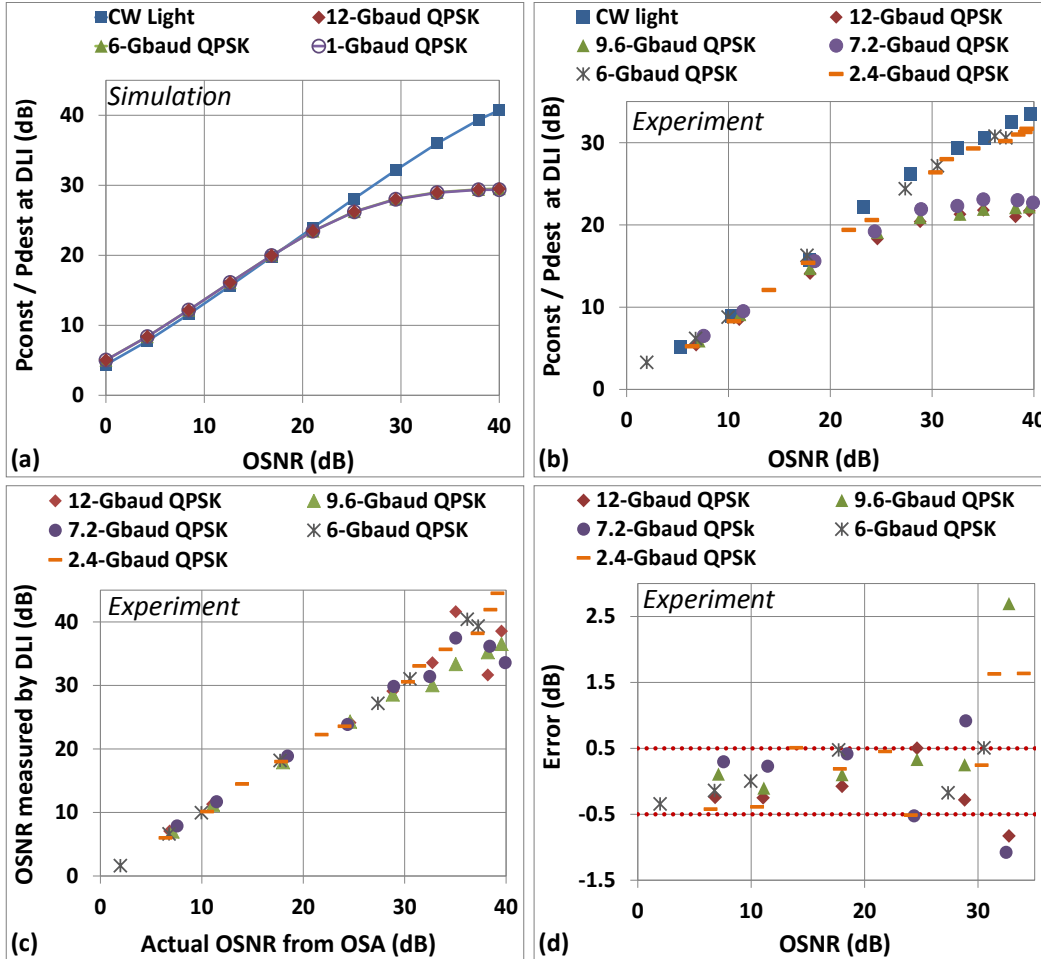
Figure 3.14: (a) Simulated DLI response to different bandwidth QPSK OFDM signals; (b) Experimental DLI response to different bandwidth QPSK OFDM signal; (c) Ratio of powers measured at DLI output ports converted into OSNR measurements using Eq (3) [experiment]; (d) Error in OSNR measured by DLI versus the actual OSNR [experiment]. The wavelength used is at 1550.12 nm.

Figures 3.15 a and 3.15 b show the simulated and experimental response of the DLI-based OSNR monitor to different modulation format OFDM signals. The impact of the amplitude fluctuations remains small in all cases and very similar behavior is observed for each format. In simulations, the DLI response to 12 Gbaud QPSK, 16

QAM and 64 QAM OFDM signals was studied. Experimentally, two different test-cases were studied: (i) all the SC in the signal were assigned the same modulation format and (ii) adjacent SCs in the signal were grouped into blocks and each block was assigned a different modulation format. The modulation formats used for test-case 1 were QPSK, 8 QAM, 16 QAM, and 64 QAM. For test-case 2, the bandwidth was divided into three equal blocks and modulation formats 64 QAM, 16 QAM and QPSK were assigned. Test
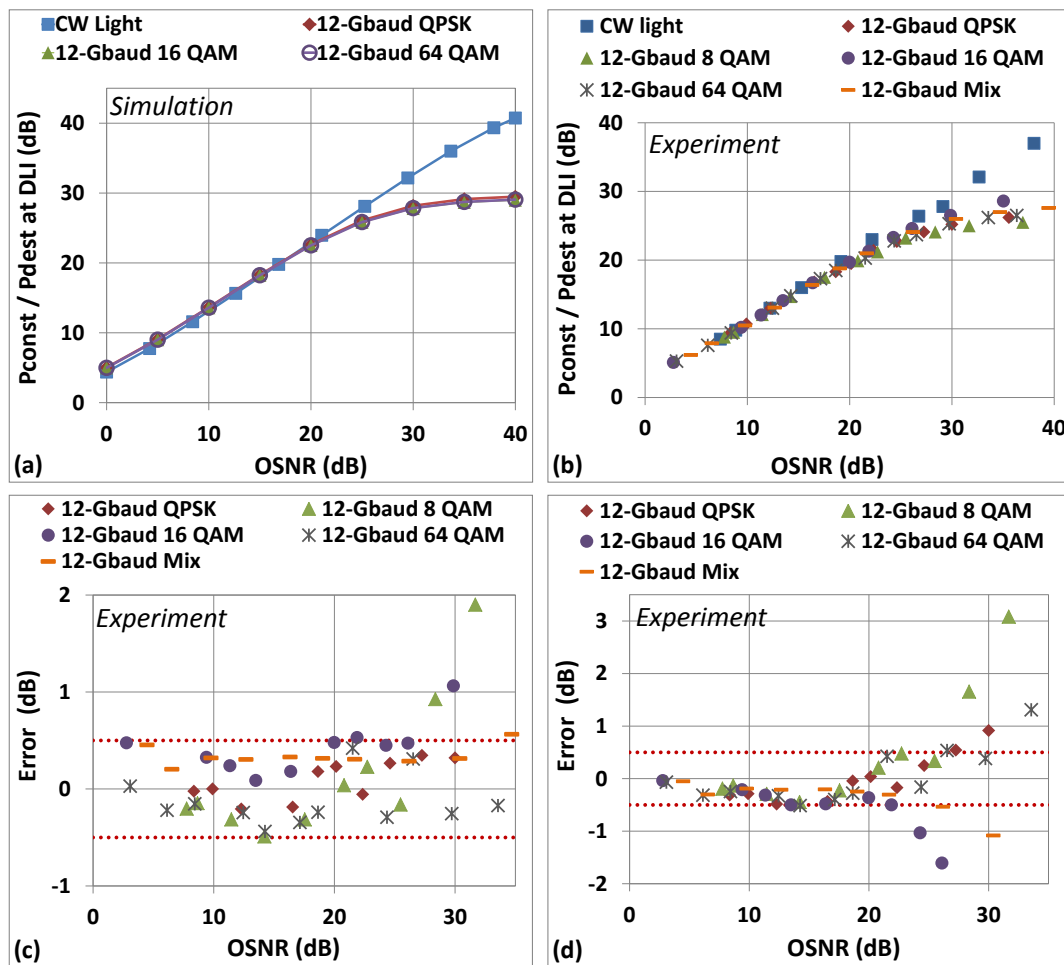
Figure 3.15: (a) DLI response to different modulation OFDM signal at the same bandwidth; (b) DLI response to different modulation OFDM signal at the same bandwidth; (c) Error when the specific values of α and β and correction factor for each signal are used to determine the measured OSNR [experiment]; (d) Error when constant values of α and β and correction factor are used to determine the measured OSNR calculations [experiment]. The wavelength used is at 1550.12 nm.
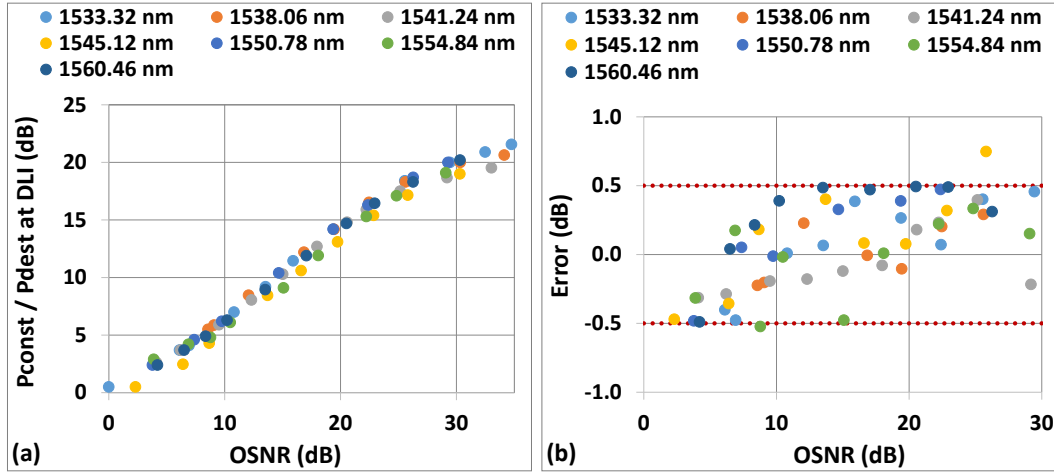
Figure 3.16: (a) DLI response to 12 Gbaud QPSK signal at different wavelengths across the C band; (b) Error in OSNR measured by DLI versus actual OSNR for the different wavelengths

case 2 is particularly important as it shows that monitoring accuracy is not affected by OFDM signals comprised of SCs with different modulations, which is very common in OFDM communication systems. One of the key advantages of OFDM systems is the flexibility in the allocation and modulation format assignment of the SC to be used for data transmission. Since an OFDM signal is comprised of many parallel SC, the modulation format of each SC can be individually assigned. Adaptive modulation (or adaptive bit-loading), where the modulation format of each SC is based on the received signal-to-noise ratio (SNR) of that SC, is a commonly used technique in OFDM systems to improve signal resiliency to transmission channel conditions.

The DLI response for the different modulation format OFDM signals is very similar (Fig. 3.15 a and 3.15 b) resulting in similar α and β values for the different modulation format signals. This indicates that, unlike single channel systems, the modulation format of OFDM signals doesnt significantly affect the DLI ratio. Since DLI-based OSNR monitor is not data rate or modulation format agnostic for single channel systems, pilot tones have been used to identify the signal characteristic at the monitoring site [101]. However, since the monitor doesnt exhibit data rate or modulation format dependency for OFDM signals, this functionality is not required for OFDM systems, potentially simplifying the control plane functions. Fig. 3.15 c shows the error when the specific

values of α and β and correction factor for each signal are used to determine the measured OSNR. The error is maintained between ±0.5 dB for OSNRs up to 28 dB. Fig. 3.15 d illustrates the error when constant values of α and β and correction factor are used to determine the measured OSNR calculations. In this case, the error is maintained between ±0.5 dB for OSNRs up to 22 dB and this performance is comparable to that of the DLI in monitoring single channel systems [83].

In order to study the DLI-based OSNR monitor wavelength dependence, the DLI response to 12 Gbaud QPSK signal at different wavelengths across the C-band was measured (Fig. 3.16 a). The error in measured OSNR for each wavelength is maintained between ±0.5 dB for OSNRs up to 25 dB (Fig. 3.16 b).

3.4.3 OSNR Monitoring in a Cross-layer Enabled Metro-Scale Test-Bed
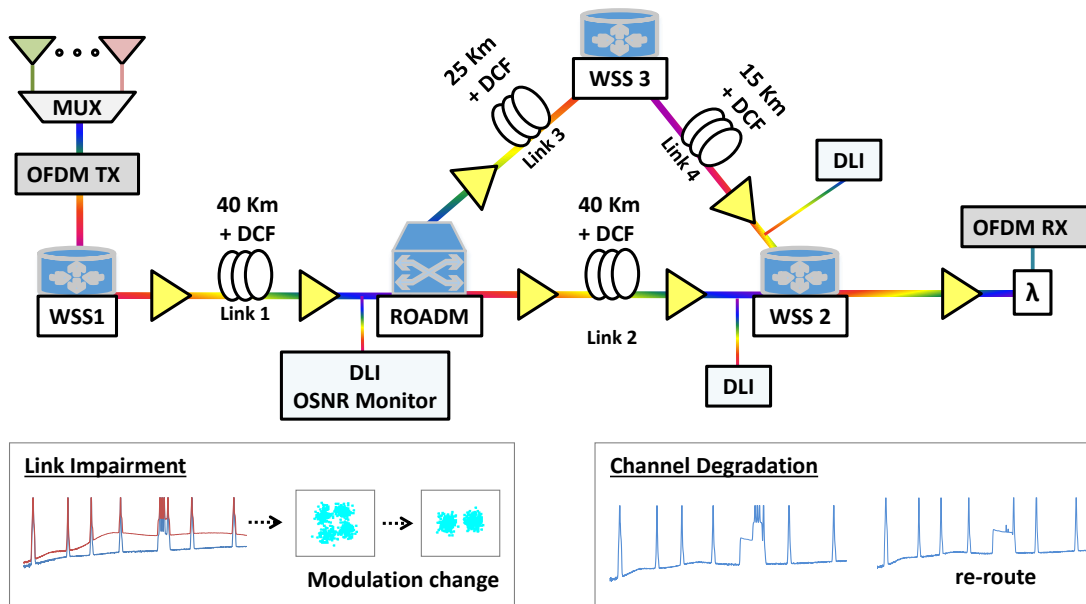
Figure 3.17: Metro-scale testbed to validate the performance benefits of deploying the DLI-based OSNR monitor for impairment-aware resource allocation and rerouting. Ability to detect link impairment as well as single channel degradation is demonstrated.

The DLI-based OSNR monitor is inserted into a metro-scale test-bed, depicted in Fig. 3.17, to investigate its efficacy in actuating impairment-aware resource allocation and
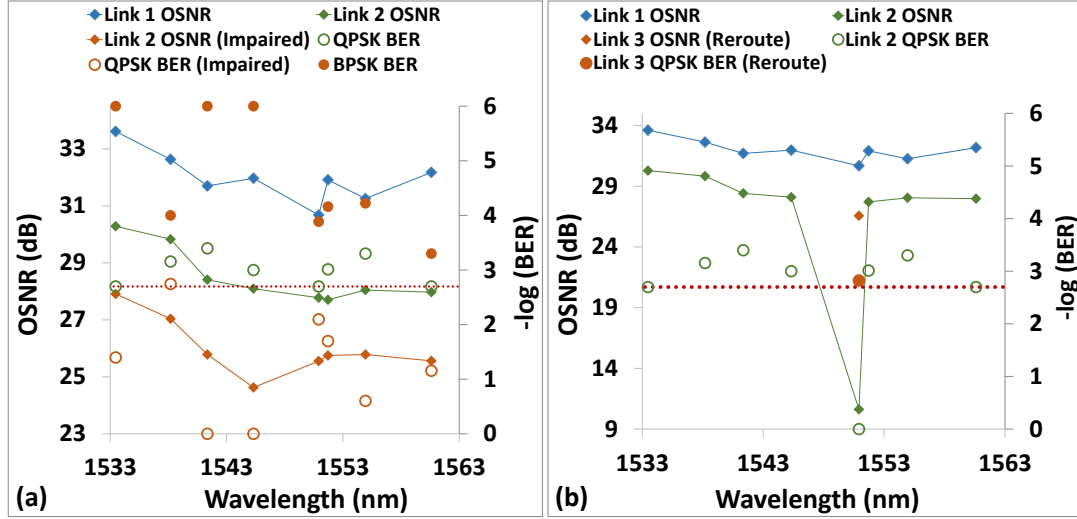
Figure 3.18: (a) Initially, data is transmitted in QPSK format and received error-free.
Link 2 is impaired and the OSNR degradation across all channels traversing link 2 is
detected by the DLI monitor. The control plane recognizes this as a link degradation
and switches modulation format to BPSK so that error-free transmission is continued; (b)
Impairment on a single channel is detected at link 2 and only this channel is rerouted via
link 3 to ensure error-free transmission

rerouting decisions. Ten wavelengths across the C-band were multiplexed together and
sent to the OFDM transmitter. Since a flex grid ROADM that allows a minimum
of 33 GHz channel spacing is used in the test-bed, three of the wavelength channels
are spaced by 33 Ghz to emulate an elastic network. Each wavelength is modulated
with 9 Gbaud QPSK data and injected into the test-bed where it traverses a 40 Km
dispersion compensated amplified link to a reconfigurable optical add-drop multiplexer
(ROADM). The ROADM can switch the incoming traffic on two different paths (link 2
and 3) both of which terminate at the OFDM receiver via WSS 2. Initially the ROADM
is configured with all ten wavelengths transmitting on link 1 and 2 for minimum hop
transmission and they are transmitted error-free to the receiver (Fig. 3.17). The OSNR
of each of the wavelengths along the different links is measured using the DLI-based
OSNR monitor (Fig. 3.18) and the ability to detect both link impairment and individual
channel degradation and adapt accordingly is demonstrated on the test-bed.

To study real-time OSNR monitoring to detect and respond to changing transmis-
sion channel conditions, ASE noise is coupled into link 2 to emulate degraded link

quality. This OSNR deterioration across all channels is detected by the monitor and through comparing OSNRs at links 1 and 2, link degradation at link 2 is identified. Since OSNRs of the channels at link 2 is below 28 dB, data cannot be transmitted error-free in QPSK format. In order to address this issue, the signals can either be re-routed via a less impaired path or the signal modulation format can be switched to a more robust format. Since the OSNR of all the channels is still above 23 dB the threshold above which data can be received error-free in BPSK format for this test-bed - the OFDM transmitter is switched to a more robust modulation format, BPSK in this case. As can be seen from Fig. 3.18 a, the bit-error-rate (BER) falls below the FEC threshold of 2×10^{-3} due to the link impairment but by changing to a more robust modulation format in response to in-network monitoring, error-free transmission is achieved again. To study impairments on individual channels, for example due to high loss on a few channels due to a faulty switch, filtered ASE noise is coupled into link 2 for selective channel OSNR degradation. In this case, significant amounts of noise are added to the channels near 1551 nm. By comparing OSNR across the channels at link 1 and link 2, the channels are being degraded at link 2 are identified and re-routing of these channels to path 3 is initiated (Fig. 3.18 b) for error-free transmission. Since the DLI is on a 100 GHz grid, only 1 of the 3 channels is monitored and its OSNR shown in Fig. 3.18 a,b.

3.5   Conclusion

Agile optical networks are plagued by unpredictable impairments and greatly benefit from distributed optical performance monitoring for real-time awareness of the state of the physical layer. The work in this chapter enhances the capabilities of a DLI-based OSNR monitor so that it can function in future agile optical networks that will be operating in a mixed line rate and modulation formats framework, comprised of both single and multi-channel signals.

The operation of a modulation-format and bit-rate dependent DLI-based OSNR monitor in a mixed signal environment is enabled by using unique pilot tone frequencies to identify signal properties. This monitor is incorporated in a cross-layer node to demonstrate autonomous monitoring and control, a key step towards realizing intelligent impairment aware networks.

Multi-channel OFDM is a good candidate for future optical networks as it provides the bandwidth flexibility and high spectral efficiency required to cope with heterogeneous traffic demand. The DLI-based OSNR monitor is established as a promising in-line monitoring solution for OFDM signals as it can monitor WDM OFDM channels over a range of data rates and modulation formats, including adaptive modulation format.

Chapter 4

Conclusion

4.1 Summary of Contribution

This dissertation addresses the two main challenges to achieving an agile optical network: (i) rapid wavelength reconfiguration and (ii) real-time awareness of physical layer impairments. Two different techniques are developed that overcome the power excursions and data loss plaguing current networks during wavelength reconfiguration. Notably, one technique achieves excursion-free switching while the other decreases the data loss incurred during the reconfiguration process by a factor of 1000. Agile optical networks suffer from unpredictable impairments and require distributed optical performance monitoring for real-time measurements of the state of the physical layer so that intelligent network management decisions can be made. By enabling a DLI-based OSNR monitor to function in a mixed line rate and modulation formats framework comprised of both single and multi-channel signals, it is rendered a promising monitoring solution for agile optical networks.

4.2 Recommendation for Future Work

The fundamental work on enabling rapid wavelength capabilities developed in this dissertation can be further extended in the following ways:

- A comb source was used in the metro-scale experimental test-bed to create a range of network scenarios so that the corner cases could be identified and investigated. The results evaluated the power excursions in the network as they are the best

indicators of both channel transmission quality and network stability. The logical next-step would be to repeat the experiments with data transmission on the channels.

- Preliminary model for amplifier dynamics was presented. This model can be refined further to include additional transmission effects such as non-linear impairments, wavelength dependent loss, raman tilt in fiber and amplifier gain saturation for more accurate prediction of network behavior.

- The model for amplifier dynamics requires information about the accumulated gain and ripple in the amplified link. The ability of the fast tunable laser to extract this information by scanning across the transmission band as a short duration probe can be investigated.

- One of the proposed techniques is a new networking paradigm where a single signal is distributed over multiple wavelengths and TDM is used to maintain spectral efficiency. For this case, new wavelength assignment and network control techniques have to be developed for choosing the optimal wavelength sets and TDM paths. Additionally, synchronization techniques for the TDM operation have to be explored.

The DLI-based OSNR monitor used in this work is a laboratory prototype comprised of bulk components. For network-wide deployment, the device has to be integrated in silicon-photonics. The performance of an integrated device for autonomous monitoring of single channel systems and OFDM signals has to be investigated.

References

[1] LEVEL3. **Level3 network map,**. http://maps.level3.com. Accessed: 2014-09-18. iv, 1

[2] CIAN. **NSF Engineering Research Center for Integrated Access Networks (CIAN),**. http://www.cian-erc.org/. Accessed: 2015-06-02. iv, 2, 3, 57

[3] CISCO. **Cisco Virtual Network Index**. http://www.cisco.com/c/en/us/solutions/collateral/service-provider/visual-network ing-index-vni/VNI_Hyperconnectivity_W P.html. Accessed: 2015-05-26. iv, 3, 4, 7

[4] DANIEL KILPER, KEREN BERGMAN, VINCENT W.S. CHAN, INDER MONGA, GEORGE PORTER, AND KRISTIN RAUSCHENBACH. **Optical Networks Come of Age**. *Optics and Photonics News*, Sept 2014. iv, v, 3, 4, 5, 8, 9

[5] CISCO. **Cisco White Paper: Cisco Global Cloud Index: Forecast and Methodology 2013-2018**. http://www.cisco.com/c/en/us/solutions/co llateral/service-provider/global-cloud -index-gci/Cloud_Index_White_Paper.html. Accessed: 2015-05-26. iv, 4, 5, 6

[6] ALCATEL LUCENT. **Metro Network Traffic Growth: An Architecture Impact Study**. http://www.tmcnet.com/tmc/whitepapers/d ocuments/whitepapers/2013/9378-bell-lab s-metro-network-traffic-growth-an-archi tecture.pdf. Accessed: 2015-06-03. iv, 6

[7] ORI GERSTEL. **The Age of Multi-Layer Networking**. In *Asia Communications and Photonics Conference 2013*, page ATh2A.2. Optical Society of America, 2013. v, 3, 8

[8] Y.K. LIZE, JENG-YUAN YANG, L. CHRISTEN, XIAOXIA WU, S. NUCCIO, TENG WU, A.E. WILLNER, R. KASHYAP, AND F. SEGUIN. **Simultaneous and Independent Monitoring of OSNR, Chromatic and Polarization Mode Dispersion for NRZ-OOK, DPSK and Duobinary**. In *Optical Fiber Communication and the National Fiber Optic Engineers Conference, 2007. OFC/NFOEC 2007. Conference on*, pages 1–3, March 2007. ix, 58, 59

[9] H. JI, K. PARK, J. LEE, H. CHUNG, E. SON, K. HAN, S. JUN, AND Y. CHUNG. **Optical performance monitoring techniques based on pilot tones for WDM network applications**. *J. Opt. Netw.*, **3**(7):510–533, Jul 2004. ix, 60, 62

[10] GUOYING ZHANG, M. DE LEENHEER, A. MOREA, AND B. MUKHERJEE. **A Survey on OFDM-Based Elastic Core Optical Networking**. *Communications Surveys Tutorials, IEEE*, **15**(1):65–87, First 2013. x, 67

[11] LEONARD KLEINROCK. **On Communications and Networks**. *IEEE Transactions on Computers,*, **C-25**(12):1326–1335, December 1976. 1

[12] BBC TECHNOLOGY. **Internet used by 3.2 billion people in 2015**. http://www.bb c.com/news/technology-32884867. Accessed: 2015-06-02. 1

[13] CLAUDE ELWOOD SHANNON. **A mathematical theory of communication**. *ACM SIGMOBILE Mobile Computing and Communications Review*, **5**(1):3–55, 2001. 1, 7

[14] ALCATEL LUCENT. **Agile Optical Networking: More Than Moving Light**. http://www.tmcnet.com/tmc/whitepapers/d ocuments/whitepapers/2013/8052-alcatel-l ucent-agile-optical-networking-more-tha n-moving.pdf. Accessed: 2015-06-03. 3

[15] SERGE MELLE. **Building Agile Optical Networks**. In *Optical Fiber Communication Conference/National Fiber Optic Engineers Conference*, page NME2. Optical Society of America, 2008. 3

[16] XIAOLAN J. ZHANG, MARTIN BIRK, ANGELA CHIU, ROBERT DOVERSPIKE, MARK D. FEUER, PETER MAGILL, EMMANUIL MAVROGIORGIS, JORGE PASTOR, SHERYL L. WOODWARD, AND

JENNIFER YATES. **Bridge-and-Roll Demonstration in GRIPhoN (Globally Reconfigurable Intelligent Photonic Network)**. In *National Fiber Optic Engineers Conference*, page NThA1. Optical Society of America, 2010. 3

[17] AJAY MAHIMKAR, ANGELA CHIU, ROBERT DOVERSPIKE, MARK D. FEUER, PETER MAGILL, EMMANUIL MAVROGIORGIS, JORGE PASTOR, SHERYL L. WOODWARD, AND JENNIFER YATES. **Bandwidth on Demand for Inter-data Center Communication**. In *Proceedings of the 10th ACM Workshop on Hot Topics in Networks*, HotNets-X, pages 24:1–24:6, New York, NY, USA, 2011. ACM. 6

[18] ANDREW CHRALYVY. **Plenary paper: The coming capacity crunch**. In *Optical Communication, 2009. ECOC '09. 35th European Conference on*, pages 1–1, Sept 2009. 7

[19] BENYUAN ZHU, T.F. TAUNAY, M.F. YAN, M. FISHTEYN, G. OULUNDSEN, AND D. VAIDYA. **70-Gb/s Multicore Multimode Fiber Transmissions for Optical Data Links**. *Photonics Technology Letters, IEEE*, **22**(22):1647–1649, Nov 2010. 7

[20] D. CUNNINGHAM. **Multimode Fiber Data Communication**. In *Optical Fiber communication/National Fiber Optic Engineers Conference, 2008. OFC/NFOEC 2008. Conference on*, pages 1–31, Feb 2008. 7

[21] GREENTOUCH. **ICT Industry Combats Climate Change**. http://www.greentouch.org/?page=how-the-ict-industries-can-help-the-world-combat-climate-change. Accessed: 2015-06-03. 7

[22] D.C. KILPER, G. ATKINSON, S.K. KOROTKY, S. GOYAL, P. VETTER, D. SUVAKOVIC, AND O. BLUME. **Power Trends in Communication Networks**. *Selected Topics in Quantum Electronics, IEEE Journal of*, **17**(2):275–284, March 2011. 9

[23] R.S. TUCKER AND K. HINTON. **Energy Consumption and Energy Density in Optical and Electronic Signal Processing**. *Photonics Journal, IEEE*, **3**(5):821–833, Oct 2011. 9

[24] D. KILPER, K. GUAN, K. HINTON, AND R. AYRE. **Energy Challenges in Current and Future Optical Transmission Networks**. *Proceedings of the IEEE*, **100**(5):1168–1187, May 2012. 9

[25] RONALD SKOOG, GEORGE CLAPP, JOEL GANNETT, ARNOLD NEIDHARDT, ANN VON LEHMAN, AND BRIAN WILSON. **Architectures, protocols and design for highly dynamic optical networks**. *Optical Switching and Networking*, **9**(3):240 – 251, 2012. {ONDM} 2010. 9

[26] XIAOLAN JOY ZHANG, STEVEN S LUMETTA, ANGELA L CHIU, AND ROBERT DOVERSPIKE. **Heuristic resource optimization for dynamic wavelength services on optically reconfigurable networks**. In *Computer Communications and Networks (ICCCN), 2010 Proceedings of 19th International Conference on*, pages 1–8. IEEE, 2010. 9

[27] S. SPADARO, J. PERELLO, F. AGRAZ, S. AZODOLMOLKY, M. ANGELOU, Y. QIN, R. NEJABATI, D. SIMEONIDOU, P. KOKKINOS, E. VARVARIGOS, Y. YE, AND I. TOMKOS. **Experimental demonstration of an enhanced impairment-aware path computation element**. In *Optical Fiber Communication Conference and Exposition (OFC/NFOEC), 2011 and the National Fiber Optic Engineers Conference*, pages 1–3, March 2011. 9

[28] INFINERA. **Infinera and DANTE Set Guinness World Record on GANT Network**. http://www.infinera.com/j7/servlet/NewsItem?newsItemID=371. Accessed: 2015-05-26. 9, 17, 47

[29] FRANK SMYTH, DANIEL C KILPER, SETHUMADHAVAN CHANDRASEKHAR, AND LIAM P BARRY. **Applied constant gain amplification in circulating loop experiments**. *Journal of Lightwave Technology*, **27**(21):4686–4696, 2009. 9, 11, 14

[30] DANIEL KILPER, CHANDRA CHANDRASEKHAR, AND CHRIS A. WHITE. **Transient Gain Dynamics of Cascaded Erbium Doped Fiber Amplifiers with Re-Configured Channel Loading**. In *Optical Fiber Communica-*

tion Conference and Exposition and The National Fiber Optic Engineers Conference, page OTuK6. Optical Society of America, 2006. 9, 14

[31] CR Giles, JR Simpson, and E Desurvire. **Transient gain and cross talk in erbium-doped fiber amplifiers**. *Optics Letters*, **14**(16):880–882, 1989. 9, 14

[32] Alberto Bononi, Leslie Rusch, et al. **Doped-fiber amplifier dynamics: A system perspective**. *Lightwave Technology, Journal of*, **16**(5):945–956, 1998. 9

[33] M. Zirngibl. **Gain control in erbium-doped fibre amplifiers by an all-optical feedback loop**. *Electronics Letters*, **27**(7):560–561, March 1991. 9

[34] Stephan Pachnicke, Martin Obholz, Edgar Voges, Peter M. Krummrich, and Erich Gottwald. **Electronic EDFA Gain Control for the Suppression of Transient Gain Dynamics in Long-Haul Transmission Systems**. In *Optical Fiber Communication Conference and Exposition and The National Fiber Optic Engineers Conference*, page JWA15. Optical Society of America, 2007. 9

[35] Cechan Tian and Susumu Kinoshita. **Analysis and Control of Transient Dynamics of EDFA Pumped by 1480-and 980-nm Lasers**. *J. Lightwave Technol.*, **21**(8):1728, Aug 2003. 9

[36] Kiyo Ishii, Junya Kurumida, and Shu Namiki. **Wavelength Assignment Dependency of AGC EDFA Gain Offset under Dynamic Optical Circuit Switching**. In *Optical Fiber Communication Conference*, page W3E.4. Optical Society of America, 2014. 9

[37] A.L. Chiu, G. Choudhury, G. Clapp, R. Doverspike, M. Feuer, J.W. Gannett, J. Jackel, G. Kim, J. Klincewicz, T. Kwon, Guangzhi Li, P. Magill, Jane M. Simmons, R.A. Skoog, J. Strand, A. Lehmen, B.J. Wilson, S.L. Woodward, and Dahai Xu. **Architectures and Protocols for Capacity Efficient, Highly Dynamic and Highly Resilient Core Networks [Invited]**. *Optical Communications and Networking, IEEE/OSA Journal of*, **4**(1):1–14, January 2012. 10

[38] P. Kulkarni, A. Tzanakaki, C.M. Machuka, and I. Tomkos. **Benefits of Q-factor based routing in WDM metro networks**. In *Optical Communication, 2005. ECOC 2005. 31st European Conference on*, **4**, pages 981–982 vol.4, Sept 2005. 10

[39] Jonathan C Li, Kerry Hinton, Sarah D Dods, and Peter M Farrell. **Enabling ASON routing via novel signal quality metrics**. In *Optical Fiber Communication Conference*, page OWR6. Optical Society of America, 2007. 10

[40] R. Martinez, R. Casellas, R. Munoz, and T. Tsuritani. **Experimental Translucent-Oriented Routing for Dynamic Lightpath Provisioning in GMPLS-Enabled Wavelength Switched Optical Networks**. *Lightwave Technology, Journal of*, **28**(8):1241–1255, April 2010. 10

[41] B. Lavigne, F. Leplingard, L. Lorcy, E. Balmefrezol, J. C. Antona, T. Zami, and D. Bayart. **Method for the Determination of a Quality-of-Transmission Estimator along the Lightpaths of Partially Transparent Networks**. In *Optical Communication (ECOC), 2007 33rd European Conference and Ehxibition of*, pages 1–2, Sept 2007. 10

[42] Byrav Ramamurthy, Debasish Datta, Helena Feng, Jonathan P. Heritage, and Biswanath Mukherjee. **Impact of Transmission Impairments on the Teletraffic Performance of Wavelength-Routed Optical Networks**. *J. Lightwave Technol.*, **17**(10):1713, Oct 1999. 10

[43] Govind Agarwal. *Nonlinear Fiber Optics*. Academic Press, 3 edition, 2001. 10

[44] Siamak Azodolmolky, Miroslaw Klinkowski, Eva Marin, Davide Careglio, Josep Sol Pareta, and Ioannis Tomkos. **A survey on physical layer impairments aware routing and wavelength assignment algorithms in optical networks**. *Computer Networks*, **53**(7):926 – 944, 2009. 10

[45] Yan Pan, Dan Kilper, and Gary Atkinson. **Persistent channel power deviations in constant gain amplified long-chain ROADM networks**. In *National Fiber Optic Engineers Conference*, page JWA010. Optical Society of America, 2011. 11, 14

[46] D.C. Kilper, R. Bach, D.J. Blumenthal, D. Einstein, T. Landolsi, L. Ostar, M. Preiss, and A.E. Willner. **Optical performance monitoring**. *Lightwave Technology, Journal of*, **22**(1):294–304, Jan 2004. 11

[47] Calvin CK Chan. *Optical performance monitoring: advanced techniques for next-generation photonic networks*. Academic Press, 2010. 11

[48] Zhongqi Pan, Changyuan Yu, and Alan E. Willner. **Optical performance monitoring for the next generation optical communication networks**. *Optical Fiber Technology*, **16**(1):20 – 45, 2010. 11

[49] A.E.Willner. **he optical network of the future: Can optical performance monitoring enable automated, intelligent and robust systems?** *Optics and Photonics News*, March 2006. 11

[50] **Telecom Italy is a Partner of OR-CHESTRA (Optical Performance Monitoring enabling dynamic networks using a Holistic cross-layer, Selfconfigurable Truly flexible approach)**. `http://www.telecomitalia.com/tit/en/innovazione/rete/European-Project-ORCHESTRA.html`, 2014. 11

[51] *Cross-Layer Design in Optical Networks*. Springer US, 1 edition, 2013. 11

[52] Ignacio de Miguel, Ramón J Durán, Tamara Jiménez, Natalia Fernández, Juan Carlos Aguado, Ruben M Lorenzo, Antonio Caballero, Idelfonso Tafur Monroy, Yabin Ye, Andrzej Tymecki, et al. **Cognitive dynamic optical networks [Invited]**. *Journal of Optical Communications and Networking*, **5**(10):A107–A118, 2013. 11

[53] I. Tomkos, S. Azodolmolky, D. Klonidis, M. Aggelou, and K. Margariti. **Dynamic impairment aware networking for transparent mesh optical networks: Activities of EU project DICONET**. In *Transparent Optical Networks, 2008. ICTON 2008. 10th Anniversary International Conference on*, **1**, pages 6–12, June 2008. 11

[54] Caroline P Lai, Michael S Wang, Ajay S Garg, Keren Bergman, Jeng-Yuan Yang, Mohammad R Chitgarha, and Alan E Willner. **Demonstration of QoS-aware packet protection via cross-layer OSNR signaling**. In *Optical Fiber Communication Conference*, page OTuM2. Optical Society of America, 2010. 11, 58

[55] Raman Kazhamiakin, Marco Pistore, and Asli Zengin. **Cross-layer adaptation and monitoring of service-based applications**. In *Service-Oriented Computing. ICSOC/ServiceWave 2009 Workshops*, pages 325–334. Springer, 2010. 11, 57

[56] Cédric Ware, Caroline P Lai, Daniel Brunina, Wenjia Zhang, Ajay S Garg, Balagangadhar G Bathula, and Keren Bergman. **Cross-layer reconfigurable optical network: Fast failure recovery in testbed for routing algorithms**. In *Transparent Optical Networks (ICTON), 2011 13th International Conference on*, pages 1–4. IEEE, 2011. 11

[57] Michael S Wang, Anjing Wang, Balagangadhar G Bathula, Caroline P Lai, Ilia Baldine, Cathy Chen, Debjyoti Majumder, Deniz Gurkan, George N Rouskas, Rudra Dutta, et al. **Demonstration of QoS-aware video streaming over a metro-scale optical network using a cross-layer architectural design**. In *National Fiber Optic Engineers Conference*, page NThC4. Optical Society of America, 2011. 11

[58] Cornelius Fürst, Roman Hartung, Jorg-Peter Elbers, and Christoph Glingener. **Impact of spectral hole burning and raman effect in transparent optical networks**. In *Proc. ECOC*, 2003. 14

[59] Andrew Lieu, Cechan Tian, and Takao Naito. **Transmission and interactions of WDM burst signals in cascaded EDFAs**.

In *Optical Fiber Communication Conference*, page OTuD5. Optical Society of America, 2006. 14

[60] D.C. Kilper, C.A. White, and S. Chandrasekhar. **Control of Channel Power Instabilities in Constant-Gain Amplified Transparent Networks Using Scalable Mesh Scheduling**. *Lightwave Technology, Journal of*, **26**(1):108–113, Jan 2008. 14, 21, 38, 50

[61] Yan Pan, Dan Kilper, Annalisa Morea, Joseph Junio, and Vincent Chan. **Channel power excursions in GMPLS end-to-end optical restoration with single-step wavelength tuning**. In *National Fiber Optic Engineers Conference*, pages JTh2A–42. Optical Society of America, 2012. 14

[62] Ke Wen, Yawei Yin, D.J. Geisler, Shuo Chang, and S.J.B. Yoo. **Dynamic on-demand lightpath provisioning using spectral defragmentation in flexible bandwidth networks**. In *Optical Communication (ECOC), 2011 37th European Conference and Exhibition on*, pages 1–3, Sept 2011. 17

[63] Xiaosong Yu, Jie Zhang, Yongli Zhao, Tiantian Peng, Yun Bai, Dajiang Wang, and Xuefeng Lin. **Spectrum Compactness based Defragmentation in Flexible Bandwidth Optical Networks**. In *Optical Fiber Communication Conference*, page JTh2A.35. Optical Society of America, 2012. 17

[64] Alberto Castro, Luis Velasco, Marc Ruiz, Miroslaw Klinkowski, Juan Pedro FernáNdez-Palacios, and Davide Careglio. **Dynamic Routing and Spectrum (Re)Allocation in Future Flexgrid Optical Networks**. *Comput. Netw.*, **56**(12):2869–2883, August 2012. 17

[65] Ankitkumar N. Patel, Philip N. Ji, Jason P. Jue, and Ting Wang. **Routing,Wavelength Assignment, and Spectrum Allocation in Wavelength-Convertible Flexible Optical WDM (WC-FWDM) Networks**. In *Optical Fiber Communication Conference*, page JTh2A.36. Optical Society of America, 2012. 18

[66] Scott R. Nuccio, Zahra Bakhtiari, Omer F. Yilmaz, and Alan Willner. **λ-Conversion of 160-Gbit/s PDM 16-QAM Using a Single Periodically-Poled Lithium Niobate Waveguide**. In *Optical Fiber Communication Conference/National Fiber Optic Engineers Conference 2011*, page OWG5. Optical Society of America, 2011. 18

[67] F. Cugini, F. Paolucci, G. Meloni, G. Berrettini, M. Secondini, F. Fresi, N. Sambo, L. Poti, and P. Castoldi. **Push-Pull Defragmentation Without Traffic Disruption in Flexible Grid Optical Networks**. *Lightwave Technology, Journal of*, **31**(1):125–133, Jan 2013. 18

[68] Kyosuke Sone, Xi Wang, Shoichiro Oda, Goji Nakagawa, Yasuhiko Aoki, Inwoong Kim, Paparao Palacharla, Takeshi Hoshida, Motoyoshi Sekiya, and Jens C. Rasmussen. **First Demonstration of Hitless Spectrum Defragmentation using Real-time Coherent Receivers in Flexible Grid Optical Networks**. In *European Conference and Exhibition on Optical Communication*, page Th.3.D.1. Optical Society of America, 2012. 18

[69] Anthony J Walsh, James Mountjoy, Anthony Fagan, Colm Browning, Andrew D Ellis, and Liam P Barry. **Reduced OSNR penalty for frequency drift tolerant coherent packet switched systems using doubly differential decoding**. In *Optical Fiber Communication Conference*, pages Th4D–8. Optical Society of America, 2014. 20, 27, 28, 46

[70] Colm Browning, Kai Shi, Andrew D Ellis, and Liam P Barry. **Optical burst-switched SSB-OFDM using a fast switching SG-DBR laser**. *Journal of Optical Communications and Networking*, **5**(9):994–1000, 2013. 20, 27, 46

[71] Joseph Junio, Daniel C Kilper, and Vincent WS Chan. **Channel power excursions from single-step channel provisioning**. *Journal of Optical Communications and Networking*, **4**(9):A1–A7, 2012. 21, 46

[72] Yvan Pointurier, Mark Coates, and Michael Rabbat. **Cross-layer monitoring in transparent optical networks**. *Journal of Optical Communications and Networking*, **3**(3):189–198, 2011. 23, 46

[73] N Sambo, F Cugini, I Cerutti, L Valcarenghi, P Castoldi, J Poirrier, E Le Rouzic, and C Pinart. **Probe-based schemes to guarantee lightpath quality of transmission QoT in transparent optical networks**. In *Proc. of European Conference on Optical Communication, ECOC 2008*, 2008. 23, 46

[74] John Zyskind and Atul Srivastava, editors. *Optically Amplified WDM Networks: Principles and Practices*. Academic Press, 1 edition, 2011. 23

[75] Maxim Bolshtyansky. **Spectral hole burning in erbium-doped fiber amplifiers**. *Journal of lightwave technology*, **21**(4):1032, 2003. 23

[76] P. Wall, P. Colbourne, C. Reimer, and S. McLaughlin. **WSS Switching Engine Technologies**. In *Optical Fiber communication/National Fiber Optic Engineers Conference, 2008. OFC/NFOEC 2008. Conference on*, pages 1–5, Feb 2008. 27

[77] Ilia Baldine. **Unique optical networking facilities and cross-layer networking**. In *Summer Topical Meeting, 2009. LEOSST'09. IEEE/LEOS*, pages 145–146. IEEE, 2009. 57

[78] Christina Politi, Vasilis Anagnostopoulos, and Alexandros Stavdas. **Cross-layer routing in clustered optical networks**. *Photonic Network Communications*, **25**(1):1–9, 2013. 57

[79] Christina Tanya Politi, Chris Matrakidis, Alexandros Stavdas, Vasilis Anagnostopoulos, and Matthias Gunkel. **Cross layer routing in transparent optical networks**. In *Optical Fiber Communication Conference*, page JThA64. Optical Society of America, 2007. 57

[80] Caroline P Lai and Keren Bergman. **Cross-layer communications for high-bandwidth optical networks**. In *Transparent Optical Networks (ICTON), 2010 12th International Conference on*, pages 1–4. IEEE, 2010. 57

[81] Caroline P Lai, Ali Fard, Brandon Buckley, Bahram Jalali, and Keren Bergman. **Cross-layer signal monitoring in an optical packet-switching test-bed via real-time burst sampling**. In *Proc. 23rd Annual Meeting IEEE Photon. Soc*, 2010. 58

[82] Zhenning Tao, Zhangyuan Chen, Libin Fu, Deming Wu, and Anshi Xu. **Monitoring of OSNR by using a MachZehnder interferometer**. *Microwave and Optical Technology Letters*, **30**(1):63–65, 2001. 58

[83] M.R. Chitgarha, S. Khaleghi, W. Daab, M. Ziyadi, A. Mohajerin-Ariaei, D. Rogawski, M. Tur, J.D. Touch, V. Vusirikala, W. Zhao, and A.E. Willner. **Demonstration of WDM OSNR performance monitoring and operating guidelines for pol-muxed 200-Gbit/s 16-QAM and 100-Gbit/s QPSK data channels**. In *Optical Fiber Communication Conference and Exposition and the National Fiber Optic Engineers Conference (OFC/NFOEC), 2013*, pages 1–3, March 2013. 58, 69, 76

[84] Lianxi Jia, Junfeng Song, Tsung-Yang Liow, Qing Fang, Mingbin Yu, G. Q. Lo, and Dim-Lee Kwong. **Integrated in-band optical signal-to-noise ratio monitor implemented on SOI platform**. *Opt. Express*, **20**(8):8512–8517, Apr 2012. 58

[85] Avishek Nag and Massimo Tornatore. **Optical Network Design with Mixed Line Rates**. *Opt. Switch. Netw.*, **6**(4):227–234, December 2009. 60

[86] Weiyang Mo, Jun He, M.M. Karbassian, J. Wissinger, and N. Peyghambarian. **Situation-aware multipath routing and wavelength reassignment in a unified packet-circuit OpenFlow network**. In *Optical Fiber Communication Conference and Exposition and the National Fiber Optic Engineers Conference (OFC/NFOEC), 2013*, pages 1–3, March 2013. 61

[87] Lei Liu, Dongxu Zhang, T. Tsuritani, R. Vilalta, R. Casellas, Linfeng Hong,

I. Morita, Hongxiang Guo, Jian Wu, R. Martinez, and R. Munoz. **Field Trial of an OpenFlow-Based Unified Control Plane for Multilayer Multigranularity Optical Switching Networks**. *Lightwave Technology, Journal of*, **31**(4):506–514, Feb 2013. 61

[88] Joseph Berthold, Adel A. M. Saleh, Loudon Blair, and Jane M. Simmons. **Optical Networking: Past, Present, and Future**. *J. Lightwave Technol.*, **26**(9):1104–1118, May 2008. 68

[89] O. Gerstel, M. Jinno, A. Lord, and S.J.B. Yoo. **Elastic optical networking: a new dawn for the optical layer?** *Communications Magazine, IEEE*, **50**(2):s12–s20, February 2012. 68

[90] S. J. B. Yoo. **Optical Packet and Burst Switching Technologies for the Future Photonic Internet**. *Lightwave Technology, Journal of*, **24**(12):4468–4492, Dec 2006. 68

[91] E. Palkopoulou, M. Angelou, D. Klonidis, K. Christodoulopoulos, A. Klekamp, F. Buchali, E. Varvarigos, and I. Tomkos. **Quantifying Spectrum, Cost, and Energy Efficiency in Fixed-Grid and Flex-Grid Networks [Invited]**. *J. Opt. Commun. Netw.*, **4**(11):B42–B51, Nov 2012. 68

[92] Konstantinos Christodoulopoulos, I Tomkos, and EA Varvarigos. **Elastic bandwidth allocation in flexible OFDM-based optical networks**. *Journal of Lightwave Technology*, **29**(9):1354–1366, 2011. 68

[93] J. Armstrong. **OFDM for Optical Communications**. *Lightwave Technology, Journal of*, **27**(3):189–204, Feb 2009. 68

[94] A.J. Lowery, Liang Bangyuan Du, and J. Armstrong. **Performance of Optical OFDM in Ultralong-Haul WDM Lightwave Systems**. *Lightwave Technology, Journal of*, **25**(1):131–138, Jan 2007. 68

[95] M. Jinno, H. Takara, B. Kozicki, Yukio Tsukishima, Y. Sone, and S. Matsuoka. **Spectrum-efficient and scalable elastic optical path network: architecture, benefits, and enabling technologies**. *Communications Magazine, IEEE*, **47**(11):66–73, November 2009. 68

[96] Stanley Johnson, Weiyang Mo, Milorad Cvijetic, Jun He, John Wissinger, and Alan Willner. **Real-Time Software-Defined Dynamic Resource Allocation using OpenFlow for Next-Generation OFDM-based Optical Access Networks**. In *Optical Fiber Communication Conference*, page Tu2F.5. Optical Society of America, 2014. 68

[97] R. Borkowski, F. Karinou, M. Angelou, V. Arlunno, D. Zibar, D. Klonidis, N.G. Gonzalez, A. Caballero, I. Tomkos, and I.T. Monroy. **Experimental study on OSNR requirements for spectrum-flexible optical networks [Invited]**. *Optical Communications and Networking, IEEE/OSA Journal of*, **4**(11):B85–B93, Nov 2012. 68

[98] Simin Chen, Trevor Anderson, Don Hewitt, An V. Tran, Chen Zhu, Liang B. Du, Arthur J. Lowery, and Efstratios Skafidas. **Optical performance monitoring for OFDM using low bandwidth coherent receivers**. *Opt. Express*, **20**(27):28724–28733, Dec 2012. 69

[99] Calvin C. K. Chan. **Optical Performance Monitoring for Flexible Optical Networks**. In *Advanced Photonics for Communications*, page NM4D.2. Optical Society of America, 2014. 69

[100] J.M. Fabrega, P. Sevillano, M. Svaluto Moreolo, J.J. Martinez, A. Villafranca, and J. Subias. **All-optical in-band OSNR measurement in intensity-modulated direct-detection optical OFDM systems**. In *Transparent Optical Networks (ICTON), 2013 15th International Conference on*, pages 1–4, June 2013. 69

[101] Atiyah Ahsan, Michael Wang, Mohammad R. Chitgarha, Dan Kilper, Alan E. Willner, and Keren Bergman. **Autonomous OSNR Monitoring and Cross-Layer Control in a Mixed Bit-Rate and Modulation Format System Using Pilot Tones**. In *Advanced Photonics for Communications*, page NT4C.3. Optical Society of America, 2014. 75